

**Global Chassis Control
and Braking Control
using Tyre Forces Measurement**

Mathieu GERARD

Cover: Neurons under the surface.
Emilie Yane Lopes

**Global Chassis Control
and Braking Control
using Tyre Forces Measurement**

Proefschrift

ter verkrijging van de graad van doctor
aan de Technische Universiteit Delft,
op gezag van de Rector Magnificus prof.ir. K.C.A.M. Luyben,
voorzitter van het College voor Promoties,
in het openbaar te verdedigen op
maandag 28 maart 2011 om 15:00 uur
door

Mathieu Pierre GERARD

ingénieur civil électricien, Université de Liège, België,
geboren te Charleroi, België.

Dit proefschrift is goedgekeurd door de promotor:
Prof.dr.ir. M. Verhaegen

Samenstelling promotiecommissie:

Rector Magnificus
Prof.dr.ir. M. Verhaegen
Prof.dr.ir. E.G.M. Holweg
Prof.dr.ir. J. Sjöberg
Prof.dr.ir. S.M. Savaresi
Prof.dr. H. Nijmeijer
dr.ir. J.P. Maurice
dr.ir. M. Corno
Prof.dr.ir. R. Babuška

voorzitter
Technische Universiteit Delft, promotor
Technische Universiteit Delft
Chalmers University of Technology
Politecnico di Milano
Eindhoven University of Technology
TNO Automotive
Technische Universiteit Delft
Technische Universiteit Delft, reservelid



This thesis has been completed in partial fulfillment of the requirements of the Dutch Institute for Systems and Control (DISC) for graduate studies.



The research described in this thesis was supported by the Competence Centre for Automotive Research (CCAR), TNO Automotive and SKF Automotive Division.

Published and distributed by: Mathieu GERARD
E-mail: math.gerard@gmail.com

ISBN 9789491211072

Copyright © 2011 by Mathieu GERARD

All rights reserved. No part of the material protected by this copyright notice may be reproduced or utilized in any form or by any means, electronic or mechanical, including photocopying, recording or by any information storage and retrieval system, without written permission of the author.

Printed in the Netherlands

To my family



Acknowledgments

A thesis is of course a personal achievement, but all this would never have been possible without all of you; you who gave me a hand, supported me, or simply made me smile during the last 4 years. To all of you I would like to say a huge thank you.

First of all, I would like to thank my supervisor and all my colleagues within DCSC and in the Intelligent Automotive Systems group. Michel, I'm grateful for the constructive talks we had together and for the freedom you allowed me to take in my research. Edward, it was nice to work in this automotive research environment. Edwin, I really appreciated all your help regarding vehicle dynamics and lab experimentation. It was extremely valuable to have such an expert like you next door, and to feel always welcome. Matteo, the inspiration I got from our regular discussions was priceless. Your arrival in our group had a very positive impact on my research. Kitty, Ellen, Saskia, Esther, Olaf, it was always pleasant to come to you and I valued your great support. Arjan, Kees, it was nice to be able to rely on you in the lab.

Then, I would like to thank the people I've been collaborating with. William, I'm really glad we had such an interesting and productive collaboration. It was always a pleasure to work with you, to visit you in Paris and to receive you in Delft. Bernie, Vratislav, Jan-Pieter, Jeroen, Hanno, I always appreciated to have your industrial point of view on the research.

Furthermore, a very warm thank you to all my friends. Gabriel, Arturo, your friendship is priceless. I really enjoy the fun we have together and I'm grateful for your support through the difficulties of life. I'm delighted you accepted to be my paranymphs. Alberto, it was great to have you as neighbor and to feel that you are always happy to listen and to help. Ronald, Hein, Theo, Ralph, Stephan, Marcel, Bas, Patrick, let me just say RedBull. Antoine, Segi, Julien, Bishop, and all the Villersois, I'm happy we stayed in touch despite the distance. Paolo, Justin, Stefan, Ilhan, Rogier, DCSC would not have been the same without you. Emilie, I will never forget the dinners, the cocktails and singstar, and thank you for your help with the cover. Jelmer, it is really exciting to start this entrepreneurial adventure with you. Tânia, now I know what love really means.

Finally my biggest thank you goes to my family. Maman, Papa, Anne-So, Nico, vous avez toujours été là pour moi. Tant de bons moments, de vacances ensemble, de rires et de pleurs aussi. Merci de m'avoir laissé partir loin, même à contre-coeur. Mais ca reste toujours un immense bonheur de rentrer à la maison. Nous formons une famille formidable. It's my pleasure to dedicate this thesis to you.

Mathieu GERARD
Delft, March 2011

Contents

1	Introduction	1
1.1	Global Chassis Control	4
1.1.1	Approaches for Global Chassis Control	6
1.1.2	Scope of this thesis	7
1.1.3	Contributions of this thesis	7
1.2	Tyre forces measurement	8
1.2.1	Contributions of this thesis	10
1.3	Braking control	11
1.3.1	Contributions of this thesis	13
1.3.2	Tyre-in-the-loop experimental facility	13
1.4	List of publications	14
1.4.1	Journal publications	14
1.4.2	Conference publications	15
I	Global Chassis Control	17
2	Global and Local Control	19
2.1	Tyre forces	21
2.2	Actuators	25
2.2.1	Electro-hydraulic brakes	25
2.2.2	Brake-by-wire	26
2.2.3	Steer-by-wire	26
2.2.4	Active differential	26
2.2.5	In-wheel motor	26
2.3	Sensing and estimation	27
2.4	Controller structure	27
2.5	Control allocation	29
2.5.1	Constraints	29
2.5.2	Continuous optimization	30
2.6	Vehicle building blocks	31
2.6.1	Corner module	32
2.6.2	Active-steering rack with torque control	34
2.6.3	Manual steering wheel with torque control	35
2.7	Example	36

2.8	Simulation results	38
2.8.1	Vehicle model	38
2.8.2	Simulation with inactive constraints	38
2.8.3	Simulation with ABS	39
2.9	Conclusion	39
3	Hybrid Descent Method	43
3.1	Problem formulation	45
3.2	Hybrid steepest descent solution	45
3.2.1	Filippov solutions and sliding modes	46
3.2.2	Stationary points of the update law (3.2)-(3.3)	47
3.2.3	Asymptotic stability	48
3.3	Practical implementation	51
3.4	A simulation example	52
3.5	Application to Model Predictive Control	55
3.5.1	Model Predictive Control	55
3.5.2	The hybrid feedback controller	57
3.5.3	Simulation	57
3.6	Application to Control Allocation	62
3.7	Conclusion	64
II	Braking Control	67
4	ABS based on Wheel Acceleration	69
4.1	Simplified modelling	70
4.1.1	Wheel speed dynamics	70
4.1.2	Tyre force modelling	71
4.1.3	Wheel slip and wheel acceleration dynamics	71
4.2	Modelling practical phenomena	72
4.2.1	Oscillations in measurements	72
4.2.2	Wheel acceleration	73
4.2.3	Brake pressure dynamics	73
4.2.4	Brake efficiency	75
4.2.5	Relaxation length	76
4.3	The theoretical algorithm	76
4.3.1	The five-phase hybrid control strategy	76
4.3.2	Tuning of the algorithm	78
4.4	Modified algorithms	79
4.4.1	Pressure derivative profiles	79
4.4.2	Open-loop pressure steps	80
4.4.3	Closed-loop acceleration control	80
4.5	Experimental validation	81
4.5.1	Pressure derivative profiles	81
4.5.2	Open-loop pressure steps	83
4.5.3	Closed-loop acceleration control	84
4.6	Comparison with the Bosch algorithm	85

4.6.1	The original Bosch algorithm	85
4.6.2	Vehicle measurements and a modified Bosch algorithm	85
4.6.3	Comparison between the five-phase and the Bosch algorithms	88
4.7	Conclusion	89
5	ABS based on Tyre Force	91
5.1	Modelling	92
5.2	The algorithm	93
5.2.1	Switching strategy	95
5.2.2	Closed-loop control of the wheel acceleration	96
5.2.3	Bounding the trajectory for a simple model	96
5.3	Controller tuning	101
5.3.1	Tuning the controller gain	101
5.3.2	Tuning the acceleration levels	103
5.4	Single-wheel validation	103
5.4.1	Simulation	103
5.4.2	Experimental validation	105
5.4.3	Comparison with acceleration based hybrid algorithm	105
5.5	Simulation for the two-wheel vehicle	108
5.6	Conclusion	108
6	ABS using Tyre Lateral Force	111
6.1	Modelling	112
6.1.1	Single-track model	113
6.1.2	Nonlinear Tyre Model	114
6.1.3	Linear Analysis of the Single-Track Model	115
6.2	Algorithm	117
6.3	Requirement on the front axle	119
6.3.1	Simulations	120
6.4	Requirement on the rear axle	122
6.4.1	Simulations	123
6.5	Conclusion	124
7	Slip Control based on a Cascaded Approach	127
7.1	System modelling	128
7.2	Control design	128
7.2.1	An homogeneous target filter	128
7.2.2	A new time-scale	129
7.2.3	Dynamic set-point	129
7.2.4	Control law with proportional feedback	130
7.2.5	Stability of $\dot{z} = F_1(\lambda, z)$	132
7.2.6	Control law with feedforward	133
7.2.7	Feedforward with tyre uncertainties	134
7.3	Simulation results	135
7.4	Experimental validation	136
7.5	Conclusion	137

8 Conclusions and Recommendations	139
8.1 Main conclusions	140
8.2 Recommendations and directions for future research	141
8.2.1 Global Chassis Control	141
8.2.2 Braking Control	142
Bibliography	145
Summary	155
Samenvatting	157
Résumé	159
Curriculum Vitae	161

Chapter 1

Introduction

Mobility and traffic safety is a major concern in the society today. According to the World Health Organization, 1.2 million people died on the road in 2004 [123]. In 2002, The Netherlands was the 6th safest country in terms of the number of fatalities per population [38]. Still, since then, road accidents have killed 900 Dutch people per year on average [20]. An enormous human potential is so being destroyed, with also grave social and economic consequences.

Various organizations and governments are taking measures to limit this slow but continuous catastrophe. With its “Nota Mobiliteit”, the Dutch government is giving itself the objective of reducing the number of victims to less than 580 in 2020 [116]. The measures taken in the past already made the situation to improve, as seen in the constant slow decrease of the fatalities in the Dutch statistics, from 1066 in 2002 to 791 in 2007 [20]. This evolution is plotted on Figure 1.1. But more effort is still required to reach the target. Next to the improvement of the road infrastructure, the limitation of the speed and the fight against drunk drivers, the reduction of the road accidents also relies on the improvement of the safety of the vehicle itself, and in particular on active safety able to prevent accidents.

Many accidents take place because the vehicle is not following the trajectory that the driver desires. There are two reasons why this can happen. The first one is that, in its current configuration, the vehicle is physically not capable of following the trajectory. New actuation mechanisms and new control algorithms can better exploit the entire tyre potential and so extend the vehicle limits. The second reason is that the driver is not able to apply the suitable steering wheel and pedal actions that will make the vehicle follow the desired trajectory. The vehicle dynamics is changing depending on many factors like the speed or the environmental conditions. A normal driver is not able to properly control his vehicle in conditions that are not regularly encountered. The introduction of control algorithms can change the dynamics of the vehicle in those unusual conditions so that it remains predictable and easily controllable for the driver. This thesis contributes to the increase of the vehicle safety by both pushing the limits of the vehicle and facilitating the controllability for the driver.

In order to help the driver controlling his vehicle, electronic active safety systems are added. This enables the raw driver commands to be modified at the actuator level. In 1978, the Anti-lock Braking System (ABS) was introduced to assist drivers

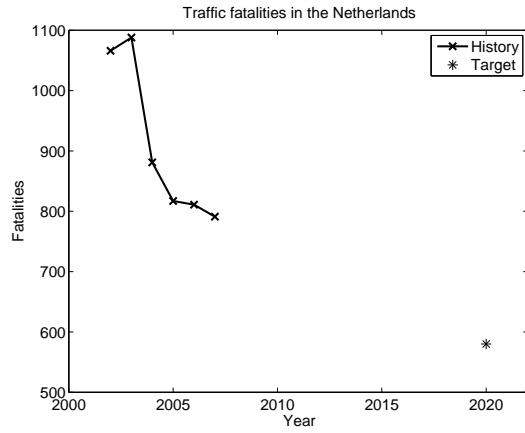


Figure 1.1: Evolution of the number of fatalities between 2002 and 2007, and target for 2020. (Source [20])

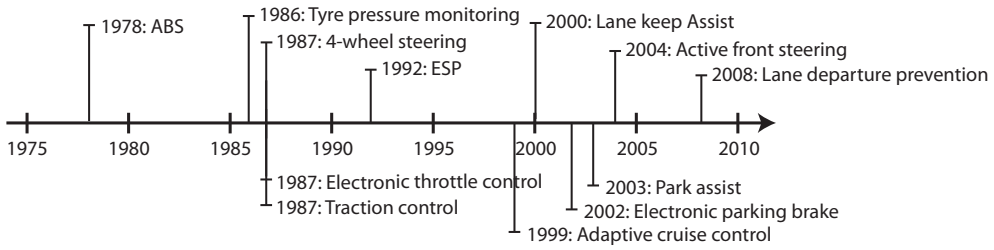


Figure 1.2: Timeline for the introduction of active safety systems in passenger cars.



Figure 1.3: Percentage of the top 50 best selling cars fitted with electronic safety equipment. (Source [20])

during heavy breaking. Since then, dozens of systems have been developed to assist drivers in all kind of tasks, as illustrated in Figure 1.2. A system like Electronic Stability Control (ESC) is capable of reducing single vehicle accidents by up to 49% [41]. Nowadays, cars can be equipped with for example: Anti-lock Brake System, Electronic Stability Control, Traction Control, Electronic Brakeforce Distribution, Active Front Steering, Adaptive Cruise Control, Lane Keeping Assist, Tire Pressure Monitoring, Emergency Brake Assist, Automatic Braking. So far, all those systems act mostly independently, with their own set of sensors and actuators. This can introduce performance limitation from un-modelled or unexpected interactions; at worse such interaction can cause instability and loss of function [54]. Furthermore, optimality is not guaranteed in the sense that the trajectory of the vehicle might not be the closest to the driver's desired one. In order to improve this, coordination between all the available systems is required.

With the increase of the amount of microcontrollers able to act on the dynamics of the vehicle, nowadays two main feedback loops can be identified for controlling the vehicle. This concept is illustrated on Figure 1.4. The first and original loop (outer-loop) is closed by the driver. He is responsible for defining the desired trajectory of the vehicle and giving instructions through the pedals and the steering wheel. The driving task can be decomposed in various ways [1]. The most well-known approach is based on the level of cognition of the task [88] where the 3 following hierarchical levels are defined:

- Strategical (route planning)
- Tactical (interaction with traffic and road)
- Operational (vehicle control through pedals and steering wheel).

Many modern Advanced Driver Assistant Systems (ADAS) can assist the driver in his driving tasks at the strategical and tactical levels [50, 1]. This thesis is about helping the driver at the operational level by making the operation of the car through pedals and steering wheel as intuitive as possible, in all driving conditions.

The same framework could be used if the vehicle is partially or totally controlled by an automatic driver. In that case, the structure makes it straightforward for the

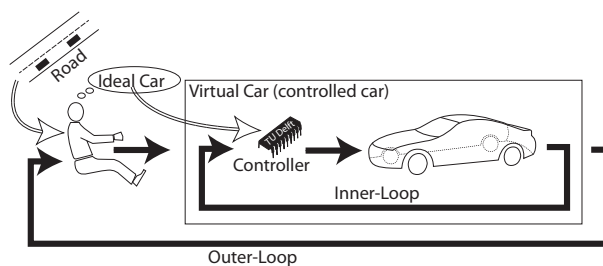


Figure 1.4: The vehicle motion is controlled via two feedback loops. The inner-loop, closed by the controller, renders the car easier to drive. The tuning is based on the image the driver has about his ideal car. The outer-loop, closed by the driver, maintains the trajectory.

high level automatic trajectory planners and decision makers to interface with the low level control of the vehicle. For all the developments of this thesis, there is no difference between having a human or electronic driver. It is therefore assumed that a human driver is controlling the vehicle for the sake of realism in the coming years.

The second loop (inner-loop) is composed by all the electronic systems acting on the vehicle dynamics. The purpose of this internal loop is to change the dynamics of (part of) the vehicle to make it easier for the driver to perform his driving task. The advances in electronics from the last decades has lead to an increasing amount of sensors, control units and actuators in vehicles, giving the inner-loop much more potential, but also making it more complex. To properly consider the coupling between the actuators, coming for example from the non-linear tyre dynamics, and to seek for a global optimum for the control of the entire vehicle, a multi-input multi-output control strategy is necessary. In automotive, this has the name of Global Chassis Control (GCC).

It should be noted that the inner-loop containing the electronics is usually at least one order of magnitude faster than the outer-loop containing the driver. Therefore, it is assumed that both loops can be separated and designed independently without risk of bad interaction. If future results establish that coupling cannot be neglected, this assumption should be reconsidered and both loops should be designed in an integrated manner.

1.1 Global Chassis Control

The literature is quite vague when it comes to giving a definition of Global Chassis Control. The only statement that could be accepted by the entire community is that Global Chassis Control involves a multi-input multi-output system, combining at least 2 traditionally independent vehicle control systems. In the following, a definition of Global Chassis Control is proposed.

Global Chassis Control is a methodology to design the inner-loop and the vehicle dynamics control systems in order to fulfill a certain number of objectives, set by the car manufacturer. Many objectives can be considered:

Stability and safety. The most important objective is to guarantee safe driving by helping the driver maintaining the desired trajectory and the stability of the vehicle. First it should be easy to transmit the desired trajectory through steering and pedal actions. Human do control objects by learning a model, a representation of how the object reacts. The simpler the model and the simpler it is to learn it and use it. In particular, research has shown that human have a larger ability at learning linear models than nonlinear ones. Further, first order systems are much simpler to control for human than second or third [87]. Simplifying the dynamics of the vehicle by rendering it linear, time-invariant and of low order will make the driver much better at controlling it's vehicle in all conditions. Secondly, the vehicle should be able to make an optimal use of the tyre potential. The main forces acting on the vehicle are generated by the tyres. The force each tyre can generate is limited, depending on the tyre state and the road conditions. Adding new actuators in the vehicle could allow to better exploit the tyre potential, as long as all the actuators around one tyre are synchronized.

Ease of development. To reduce the production costs and the time to market, it is necessary to develop a controller architecture suitable for various vehicles. The implementation on a specific vehicle should require only a very limited and methodic tuning and not a complete redesign. It has been predicted that in 2010, 13% of the production cost of a vehicle would be software, against only 4% in 2000 [56].

Feel-by-wire. Thanks to the inner-loop, the actions of the drivers are not directly translated to actuator commands anymore and the controller can change the way the vehicle reacts. In other words, it means that the feeling of the vehicle can be modified in software. This is attractive for car manufacturers as it gives the possibility to define feeling objectives at a high level, can make the tuning of the feeling faster and less expensive and allow for a change of the feeling online, depending on environment conditions or the style of the driver. More details can be found in [58], [32] and [120].

Consistent state estimation. A good control has to rely on a good measurement or estimation of the states of the vehicle. The number of sensors present in cars is increasing so that more dynamics can be observed. Today, many subsystems are still using their own sets of sensors, or they read the raw sensor signals from a bus and do not benefit from the smart processing done by other subsystems. This prevents each subsystem from using the same consistent set of measurement, which might limit performance and be critical in case of failure of a sensor. Also, it is undesirable that all the subsystems need to be reimplemented if the set of sensors is changed. For example, if the vehicle get equipped with load sensing bearings enabling the measurement of the forces close to the tyre, an update of the state estimator should be sufficient to let all the subsystems benefit from the more accurate measurement set [127, 122].

Fault tolerant. The failure of a sensor or an actuator can always happen. If nothing is done, this can lead to a dramatic change in the vehicle dynamics which the driver is unable to respond to. However, it is often possible to reconfigure the controller in order to minimize the influence of the faulty component. The state estimation algorithm can be adapted to neglect the faulty sensor and reconstruct the states from the other signals. The actuation can also be reconfigured to get the remaining actuators to do as much as possible of the action that the faulty actuator cannot perform. As two examples, let's mention the steer-by-brake [37] and the brake-by-steer [61] concepts. Controlled individual braking (brake only on one side) can make the car to follow a curvy path [37], while individual steering (both wheels either inwards or outwards) can make the vehicle to brake in straight line [61]. The way the global chassis controller is designed should allow for a clear way of changing its structure during driving if a fault is detected.

Energy efficiency. It can happen that many actuators are able to produce the same effect on the vehicle. For example, differential braking or steering can both produce a yaw moment on the chassis, or braking can be done using friction or regenerative brakes. In those cases, a choice has to be made on which combination of actuator to use. Seen the current necessity to reduce the impact of transportation on the environment, it is wise in normal driving conditions to chose for the action which is using the least energy. Still, in emergency situations, the considerations on the environments will weight less than saving lives. In that case, all the available energy should be used to maintain stability and the desired trajectory.

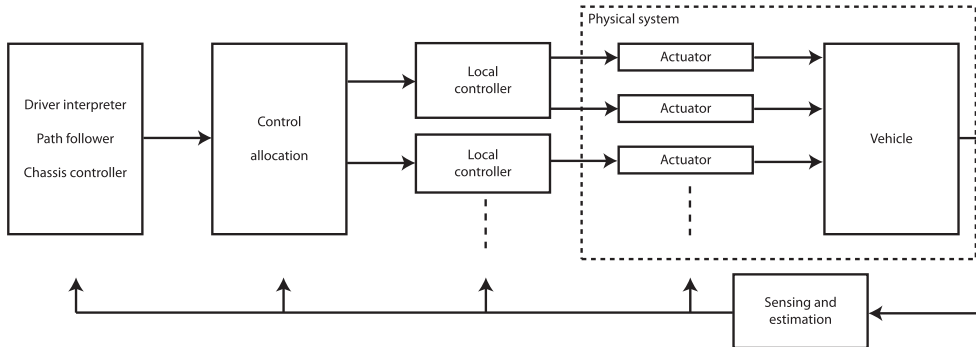


Figure 1.5: General scheme, with 2 levels, for the hierarchical approaches for Global Chassis Control.

1.1.1 Approaches for Global Chassis Control

Different approaches can be considered to design a global chassis controller. On one hand, one can argue that, since many individual systems already exist, it would be commercially more viable to keep those systems and interconnect them. This approach could also allow proprietary code from different suppliers to work together. However, it is still really unclear how such an interconnection can be implemented, and in particular how to make the architecture modular. An extensive description of the state-of-the-art in this domain and of the outstanding research problems is given in [54].

On the other hand, many researchers consider approaches with an hierarchical architecture [4, 75, 65, 72, 93, 89]. The controller can either be fully centralized or many levels of controllers can be implemented, from the high-level motion control to the low-level current control in the actuators. A general scheme is presented on Figure 1.5. Such an approach has the advantage to have a clear structure that can be analyzed. In all publications, the total forces and moment desired on the chassis constitutes the input to the control allocation block. They are defined by the driver interpreter and a path follower [4]. A common goal for defining the forces on the chassis is to render the car similar to a linear bicycle. This objective is enforced in [89] using a sliding mode controller. When the desired forces on the chassis are known, they need to be distributed to the actuators and the tyres through control allocation (see Chapter 2). For this step, two major differences are found in the literature.

- The first option is to distribute the total forces directly to the actuators using a complete nonlinear car model [4, 72, 93]. This gives a major advantage when it comes to expressing constraints on the actuators. However, the nonlinearity in the model requires the distribution to use nonlinear programming, which is complex. Workarounds are proposed, like linearizing the model at each time step [4], or like avoiding optimization by simply using a Moore-Penrose inverse matrix [93]. On Figure 1.5, this approach gives a non-convex control allocation block while the local controller blocks are empty. This class is called “direct allocation”.

- The other option is to first distribute the total forces to intermediate tyre forces in the vehicle frame [4, 75, 65, 89]. Then the tyre forces are realized at the local level using an inverse tyre model. This method has the advantage of making the distribution model linear and with no uncertain parameter, which enable the use of simpler optimization techniques. The drawback might be the expression of the constraints, especially those reducing the number of degree of freedom, called “restrictors” in [4]. On Figure 1.5, this approach gives a less complex and convex control allocation block. The local controller blocks are responsible for the tyre inversion. This class is called “indirect allocation”.

Both approaches rely on the knowledge of the tyre model. In the first case, the model appears in the equations of the control allocation. In the second case, the local transformation block need to do a tyre model inversion. This constitutes a large practical problem for two major reasons. First because the tyre model is nonlinear and cannot be inverted on its full domain; and secondly because the tyre parameters are unknown, constantly varying and impossible to estimate accurately online.

1.1.2 Scope of this thesis

This research focuses on the two first objectives of the Global Chassis Control definition: “Stability and Safety”, and “Ease of development”. In particular, the emphasis is set on exploiting the tyre potential and designing a modular architecture. Still, it is kept in mind that the proposed structure should clearly be an enabler for the other objectives. The coupling with the driver and the interpretation of his steering and pedal actions is not addressed in this research. The complexity of a driver interpreter is such that it does constitute a research on its own. It is here considered that a driver interpreter is available and delivers requirements in term of forces on the chassis. It should also be noted that mainly the dynamics in the road plane are considered (longitudinal, lateral and yaw). Experimentation on a real vehicle has not been possible during the timespan of this thesis. Validation of the developed control algorithms is done within a commercially available full vehicle simulation environment.

1.1.3 Contributions of this thesis

This thesis follows the direction of the hierarchical approach and proposes three major contributions:

- First of all, a detailed analysis of the force distribution problem, as done in Chapter 2, shows that the optimization problem has some particular characteristics: continuous optimization is required as the cost function and the constraints are constantly changing, the optimal solution does not need to be known instantly as long as an optimizing direction is found, and the computational complexity should be limited to the minimum as the implementation is done on an embedded microcontroller. From this analysis, it can be understood that traditional optimization methods might not be suitable in this case. Therefore, a new method for continuous convex optimization is developed: the Hybrid Descent Method. The method is described in Chapter 3.



Figure 1.6: Measurement wheel able to measure the forces and moments in the rim.

- Secondly, it is clear that relying on the inverse of the uncertain and nonlinear tyre model is a weak point of the current approaches. Thanks to the new sensing technologies making tyre forces measurement feasible in production vehicle, a solution more robust to tyre parameter uncertainty can be implemented. This thesis shows how local tyre controllers can exploit force measurement to realize the desired tyre forces without asking for any tyre parameter. The local controllers are discussed in Chapter 2.
- Finally, a new kind of architecture is introduced based on the concept of building blocks. All kind of vehicle with various level of actuations can be represented with the correct number of degree of freedom, which avoid the need for difficult constraints or restrictors. The advantage of this concept can be found in particular for vehicle having a partial level of actuation, between no action at all and full freedom provided by e.g. autonomous corner modules [126]. The concept is illustrated in Chapter 2.

1.2 Tyre forces measurement

A vehicle is moving thanks to the friction forces the tyres are applying on the ground. The knowledge of those forces on each tyre is precious in order to design, tune and control the vehicle.

Test vehicles, used to design new systems, and prototype vehicles are most often equipped with measurement wheels, see Figure 1.6. Such device measures the strains in the rim in order to reconstruct forces and moments in the 6 degrees of freedom. Unfortunately, such sensors are too complex, cumbersome and expensive to be installed in production vehicle. Therefore, current control systems cannot rely on the force information. The sensors available in a car today are all motion based: accelerometers, gyroscopes, encoders, etc. However, this might change in the near future.



Figure 1.7: Load sensing bearing able to measure the forces applied to the bearing in all directions. (Source: SKF)

Different initiatives are recently taking place in order to design tyre force sensors that could be inserted in production vehicle. A first option would be to keep measurement rims and make them simpler and cheaper [53]. The embedding of sensors inside the rubber of the tire is also investigated [23, 109, 108]. Still, the most promising option is to include sensors inside the hub bearing of the wheel. Different bearing manufacturers are investigating the possibility. At the moment, SKF is in a leading position with working prototypes, see Figure 1.7.

It makes sense to include force sensors in the hub bearings for different reasons. First, it is not a wear component. The bearings are now lasting long enough to accompany the vehicle during its entire life. This is clearly at the contrary of tyres and rims. Secondly, bearings are precision components, which are engineered at the micron level. Measurements in bearings therefore have the potential of being precise. Finally, force measurement in the bearing can be made on a fixed part, not rotating with the wheel. This is a serious advantage when it comes to transmitting the sensor signals.

Over the years, bearing manufacturers have developed extremely precise models of their bearings. The original purpose was to predict the deformations the bearing would undertake under a specific loading, depending on the application, see Figure 1.8. This was precious for dimensioning and predicting the wear. The idea for estimating the forces acting on the bearing is to use the model exactly the other way around. Sensors like strain gauges are fitted in the bearing to measure deformations. Then, the inverse of the model is used to reconstruct the forces and moments applied on the bearing. This inverse model is the real key component of the technology and constitutes the core of the intellectual property of the bearing manufacturer.

The current accuracy on the force measurement achieved today by SKF is already good. The RMS noise is maintained under the 2% and the bias is maximum 10% in real automotive conditions. Still, even if now only one signal is output from the sensor with force information, it is known that there are different ways of reconstructing the force signals from the raw sensors signals, which give different properties. For example, some methods could offer a larger bandwidth but give a potentially larger bias, and vice versa. One of the objectives of this research is to investigate where

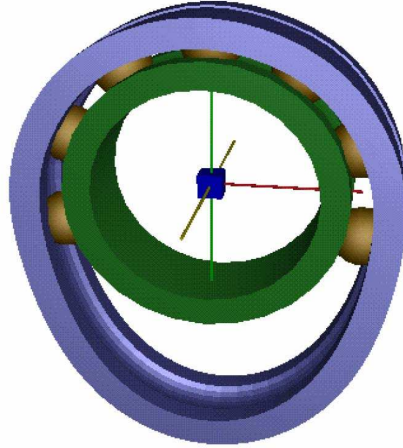


Figure 1.8: Model of the deformation of a bearing under load. (Source: SKF)

force information can provide improvements compared to the current state-of-the-art.

1.2.1 Contributions of this thesis

This thesis investigates the advantages of having force measurement for chassis control, compared to the current state-of-the-art using only motion-based sensors. Different areas are considered:

- The use of force measurement for local tyre control in the Global Chassis Control framework is discussed in Chapter 2. Thanks to force measurement, the tyre forces can be controlled in closed-loop without necessity of knowing the uncertain current tyre model. This largely improves the robustness to road conditions compared to the traditional tyre model inversion used for example in [4, 65, 72].
- The implementation of an Anti-lock Braking System (ABS) algorithms is shown to be simplified and more robust to changes in tyre characteristics when using longitudinal force measurement. A new force-based ABS algorithm is presented in Chapter 5.
- The first objective when implementing an ABS is the need for maintaining steerability and lateral stability during heavy braking. However, in current ABS implementations, only the longitudinal movement of the tyre is truly considered. Thanks to the use of lateral force measurement, a real assessment of the loss of lateral tyre potential because of braking is becoming possible. Chapter 6 discusses this issue.

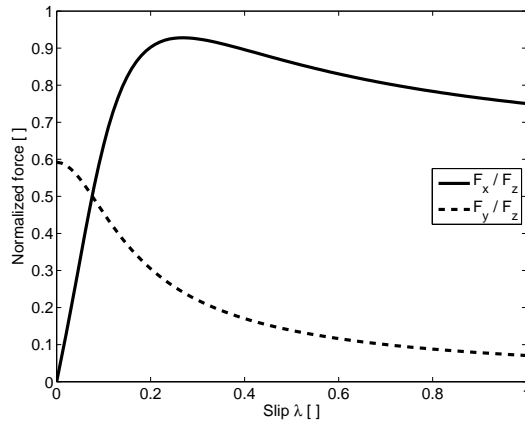


Figure 1.9: Typical longitudinal and lateral tyre curves as a function of the longitudinal slip λ , for a constant lateral slip $\alpha = 0.1$. The model used is the Magic Formula [95].

1.3 Braking control

A particularly critical problem in vehicle dynamics control is the longitudinal control of the tyre to get the desired driving or braking force. As long as the tyre remains in its stable zone, this can be done with simple linear controllers, especially if one can rely on force sensing, see Chapter 2. However, the difficulty increases when one tries to reach a force close or exceeding the maximum tyre force, as the wheel can become unstable. On the traction side, Traction Control [32, 43] is used. On the braking side, an Anti-lock Braking System (ABS) needs to be implemented. In this thesis, only the braking side is considered, especially because of the availability of lab equipment. Still, most results can be applied on the traction side.

There are originally two main reasons for implementing an ABS system in a car. The potential of the tyre to generate lateral forces is decreased when the longitudinal slip λ is increased, see Figure 1.9. The first ABS objective is therefore to limit the longitudinal slip in order to maintain steerability and lateral stability during heavy braking. Furthermore, the brake force generated by the tyre presents a peak at a moderate slip λ_0 on most surfaces, typically between 10 and 20 %, as can be seen on Figure 1.9. Maintaining the maximum brake force to reduce the brake distance is the second objective. In the GCC framework, a third objective appears, as the ABS controller needs to transmit the current tyre limit to the global controller so that unreachable forces can be redistributed.

The ABS is the most spread active safety system for road vehicles. It is now a standard equipment for all new passenger cars in the EU, the U.S. and Japan, see [103, 20] and Figure 1.3. This system has been around for more than 30 years since its introduction by Bosch in a Mercedes in 1978. Unfortunately, it is still very difficult to find details in the literature about the ABS algorithms used in practice, as the industry is really secretive. Furthermore both commercial and academic algorithms can still be improved. On one hand, commercial algorithms are often based on heuristics, which

requires a lot of tuning. No theory is available to assess stability or performance of those complex rule-based systems. On the other hand, most of the academic research about braking control is neglecting some important practical issues, such as actuation limitations and tyre dynamic behaviour, making the algorithms not suitable for implementation on a real vehicle.

In the literature, one can distinguish two main classes of ABS: those based on logic switching from wheel deceleration information (see e.g. [71, 96, 18, 79, 77, 74]), and those based on wheel slip regulation (see e.g. [64, 98, 117, 107, 33, 26, 124]).

In the class of hybrid ABS, the wheel deceleration is used to trigger the different phases of an hybrid automaton. The brake torque is increased, decreased or held depending in which phase the system is, and possibly depending on the wheel speed or acceleration. If there is a peak in the longitudinal tyre characteristic, the switching leads to a cycling around that peak, without requiring any a priori knowledge about it. During each cycle, the relative position of the peak is detected and tracked, ensuring robustness against tyre-road friction variation. However, if no peak is present in the characteristics, this class of algorithms fails to work. Those methods are not suitable to stabilize the system around an arbitrary reference λ^* . Furthermore, the vehicle speed or wheel slip, which are signals difficult to measure today, see Section 2.3, are not required. Therefore, this class of algorithms presents serious practical advantages. Some of them have been shown to work on real vehicles.

In the class of wheel slip regulation, a target wheel slip λ^* is given and the estimated slip λ is controlled around it. Those methods can work even if there is no peak in the longitudinal tyre characteristics. Their usage is nevertheless confronted to two major difficulties. Firstly, the robust measurement of the vehicle longitudinal speed, needed to compute the slip λ , remains an open problem [73, 62, 111]. Secondly, a non-optimal reference slip λ^* , obtained from an uncertain tyre characteristics, can lead to a loss of performance. Besides, most slip regulation methods comes with a theoretical background and a stability and performance analysis. However, the design of the algorithm is mainly based on linearization arguments. The nonlinear system is linearized around the desired equilibrium point, and the stability analysis is thus only valid locally (see e.g. [98] and [107]). Also, algorithms might fail to converge in the unstable region of the tyre (see e.g. [117], where the control strategy generates a limit cycle if the setpoint is in the unstable domain). And finally, the available approaches are mainly based on pure feedback, without feedforward, which limits the bandwidth of the closed-loop system.

This thesis contributes to the design, simulation, implementation and validation of ABS algorithms, both in the class of hybrid ABS and in the class of slip regulators. Furthermore this thesis investigates the benefits that tyre force measurement could bring to braking control. The precise contributions are described below.

Some of the work on the topic has been done in collaboration with CNRS/Supelec, Paris, France, and in particular with William Pasillas-Lépine. This collaboration was started in 2008 in the framework of this research with the goal of testing a particular hybrid ABS (5-phase, see [96]) and improving the algorithm to make it perform better in practice. This collaboration further lead to a good understanding of ABS issues, and to the practical implementation of a new slip regulator based on a cascaded approach.

1.3.1 Contributions of this thesis

- A tyre-in-the-loop laboratory setup for rapid prototyping and testing of ABS algorithms has been developed. The setup consists of a large drum on top of which a regular rubber tyre is rolling. Most of the mechanics was already present before the start of this project. The contribution of this thesis lies in the update of the electronics and software to make it suitable for closed-loop experiments. Details on the setup can be found in Section 1.3.2.
- When tested in practice, the theoretical 5-phase algorithm could not give the desired results. The time delay in the loop has been identified to be the main issue. Three methods to compensate delays or to improve the algorithm by making it more robust to delays have been developed and are described in Chapter 4. Thanks to those methods, a hybrid ABS algorithm based on the original 5-phase algorithm and close to the Bosch ABS has been successfully tested in practice. This work is done in collaboration with the CNRS/Supelec Paris.
- An ABS algorithm based on force measurement has been developed and is presented in Chapter 5. This new algorithm is more robust to varying road conditions, more intuitive to tune, and better performing than typical hybrid ABS algorithms only based on wheel deceleration.
- The first objective when implementing ABS is maintaining steerability and lateral stability during heaving braking. However, in current ABS implementations, only the longitudinal movement of the tyre is truly considered. Thanks to the use of lateral force measurement, a real assessment of the loss of lateral tyre potential because of braking is becoming possible. A new algorithm exploiting lateral force measurement is introduced in Chapter 6.
- The new slip controller of [97, 49] is reworked and validated experimentally in Chapter 7. The control strategy is based on both wheel slip and wheel acceleration regulation through a cascaded approach; which is proven to be globally exponentially stable in both the stable and unstable regions of the tyre. The stability conditions are relaxed and the theory is reformulated in order to better match the practical reality. Tests on the tyre-in-the-loop facility show that the slip always converges to the assigned reference. This work is done in collaboration with the CNRS/Supelec Paris.

1.3.2 Tyre-in-the-loop experimental facility

The tyre-in-the-loop experimental facility of Delft University of Technology, on which the ABS is tested, consists of a large steel drum of 2.5 meter diameter on top of which the tyre is rolling. An illustration can be seen on Figure 1.10. The setup has been used for many years for tyre modelling and identification using open-loop excitation, see [95, 125, 86]. The inertia of the drum makes it more suitable for keeping a constant speed. Recently, the electronics was upgraded in order to allow closed-loop tests to be performed and, in particular, rapid prototyping and testing of ABS strategies.

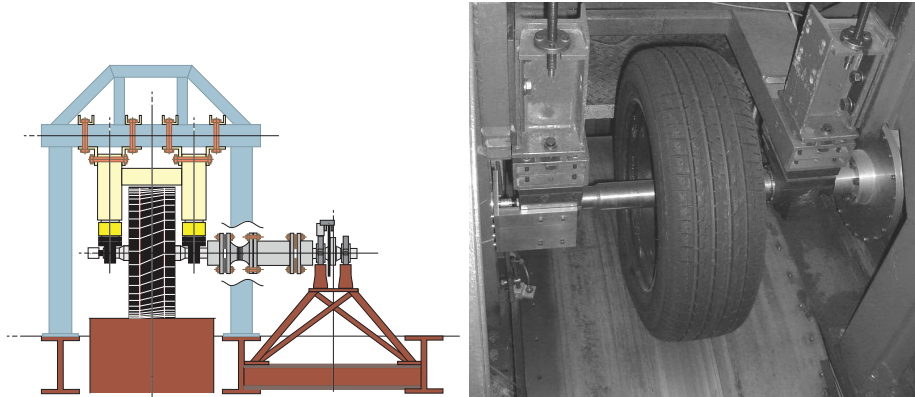


Figure 1.10: Illustration and picture of the tyre-in-the-loop experimental facility. (Source illustration: [125])

The wheel rim on which the tyre is mounted is attached to an axle with a rigidly constrained height. This axle is supported by two bearings, on both sides of the wheel. The bearing housings are connected to the fixed frame by means of piezoelectric force transducers. An hydraulic disk brake is mounted on one side of the axle. The pressure in the calliper is locally controlled by a piece of analog electronics connected to a servo-valve, in order to match the reference pressure. Both the wheel and the drum speeds can be accurately measured using encoders, which allows a precise estimation of the longitudinal slip. Currently, the wheel cannot be steered. More details about the experimental facility can be found in [35].

1.4 List of publications

This section lists the publications written in the framework of this Ph.D. research.

1.4.1 Journal publications

- Mathieu Gerard, Michel Verhaegen and Bart De Schutter. A Hybrid Steepest Descent Method for Constrained Convex Optimization. *Automatica*, vol. 45, pg 525-531. 2009.
- Mathieu Gerard, William Pasillas-Lépine, Edwin de Vries and Michel Verhaegen. Improvements to a five-phase ABS algorithm for experimental validation. Submitted to *Vehicle Systems Dynamics*.
- Mathieu Gerard, Matteo Corno, Michel Verhaegen and Edward Holweg. Hybrid ABS Control Using Force Measurement. Submitted to *IEEE Transactions on Control Systems Technology*.

1.4.2 Conference publications

- Mathieu Gerard and Michel Verhaegen. Model Predictive Control using Hybrid Feedback. Proceedings of the IFAC World Congress, Seoul, South Korea. 2008.
- Mathieu Gerard and Michel Verhaegen. Global and Local Chassis Control based on Load Sensing. Proceedings of the American Control Conference, St. Louis, MO, USA. 2009.
- Mathieu Gerard, William Pasillas-Lépine, Edwin de Vries and Michel Verhaegen. Adaptation of hybrid five-phase ABS algorithms for experimental validation. Proceedings of the IFAC Symposium Advances in Automotive Control, Munich, Germany. 2010.
- Mathieu Gerard, Matteo Corno, Michel Verhaegen and Edward Holweg. Two-Phase Antilock Braking System using Force Measurement. Proceedings of the 10th International Symposium on Advanced Vehicle Control, Loughborough, UK. 2010.
- Mathieu Gerard, Antonio Loria, William Pasillas-Lépine and Michel Verhaegen. Design and experimental validation of a cascaded wheel slip control strategy. Proceedings of the 10th International Symposium on Advanced Vehicle Control, Loughborough, UK. 2010.
- Edo de Bruijn, Mathieu Gerard, Matteo Corno, Michel Verhaegen and Edward Holweg. On the performance increase of wheel deceleration control through force sensing. Proceedings of the 2010 IEEE Multi-Conference on Systems and Control, Yokohama, Japan. 2010.
- Kimmo Eggers, Mathieu Gerard, Edwin de Vries and Michel Verhaegen. Vehicle Side-slip Angle Estimation using Sliding Mode Observers and Lateral Forces. Proceedings of IAVSD conference, Stockholm, Sweden. 2009.
- Diomidis Katzourakis, Edward Holweg, Mathieu Gerard and Riender Happee. Design Issues for Haptic Steering Force Feedback on an Automotive Simulator. Proceedings of the HAVE conference, Lecco, Italy. 2009.

CHAPTER 1. INTRODUCTION

Part I

Global Chassis Control



Chapter 2

Global and Local Control

The tyre forces in the road plane are the main forces defining the trajectory of the vehicle. Furthermore, they are the only forces controllable by the driver or by means of actuators. Other forces like gravity or air drag come as external actions that cannot be modified and that need to be compensated by the tyre forces.

Historically, the driver could modify the tyre forces mechanically using, for example, manual steering or braking. However, nowadays, more and more actuators allow for an electronic control of the tyre forces. Adding actuators has the potential to provide more freedom for modifying the tyre forces and influencing the trajectory. However, there are only 4 tyres in a car and therefore, eventually, extra actuation or control systems will overlap with each other. A global way of controlling those 4 precious tyre forces is required in order to guarantee optimal performance of the vehicle [54].

This research focuses on the problem of controlling all the actuators of a vehicle, targeted at influencing the tyre forces in the road plane, such that the forces generated at tyre level produces total forces and moment on the chassis as close as possible to the desired ones. A few solutions have been proposed in the literature. Two main classes of methods can be distinguished. In the first class, the total forces are distributed directly to the actuators [17, 118, 5, 100]. This class is called “direct allocation” and is represented on Figure 2.1. In the second class, the total forces are first distributed to intermediate forces in the vehicle frame [4]. A local control level then takes care of computing the actuators commands. This class is named “indirect allocation” and is illustrated on Figure 2.2. Four approaches in the class of direct allocation are described next.

Borrelli [17] formulates a non-linear optimization problem in the Model Predictive Control framework. The actuator commands are directly computed by the algorithm. This can be seen as an advantage since actuator constraints can be easily formulated. However, the implementability on embedded microcontrollers and scalability with respect to the number of actuators are questionable because of the computational complexity linked to the nonlinear optimization. Moreover, non-linear programming can lead to difficulties like local optima or slow convergence. Furthermore, many parameters and a tyre model have to be included in the model used in the optimization. Those are often very difficult to obtain in practice during real-time operation, see

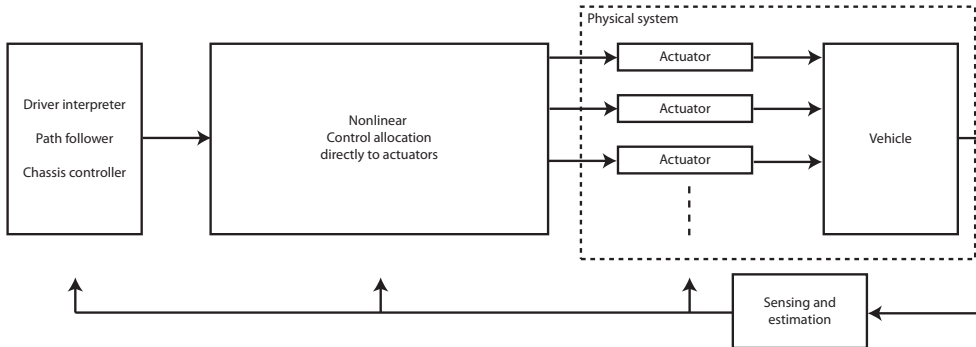


Figure 2.1: General scheme for the class of direct allocation Global Chassis Control. The computation of the actuator commands is done in 1 step.

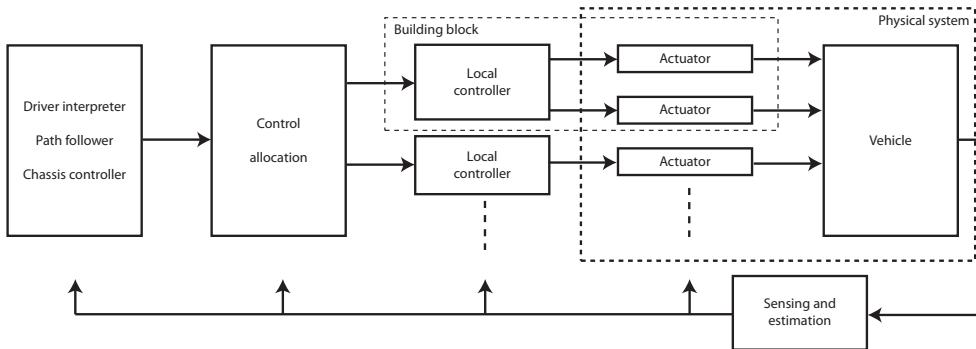


Figure 2.2: General scheme for the class of indirect allocation Global Chassis Control. The computation of the actuator commands is done in 2 steps.

Section 2.3. Methods exist to take model uncertainties into account within the MPC framework [29]. However, the computational complexity is larger than the nominal case.

To avoid solving non-linear programming problems on-line, Tøndel [118] proposes to solve the optimization off-line using multiparametric programming. Solutions are then stored in large lookup-tables. This reduces the risk of bad convergence. However, the size of the lookup-tables can become impractical if the number of variables and parameters is large, which is the case in automotive applications. Furthermore, capabilities to reconfigure the system, for example in case of fault, are frozen.

Andreasson [5] solves at each time step the optimization problem based on a linearised model. This is motivated by the fact that the dynamics of the system should not vary too much between two iterations. Unfortunately, tyres can raise difficulties since they are known to have fast dynamics and strong non-linearities. The computational complexity is decreased to the level of Quadratic Programming.

Plumlee [100] simplifies the problem by linearising the vehicle model and therefore neglecting the non-linearities. Then a variant of Quadratic Programming is used.

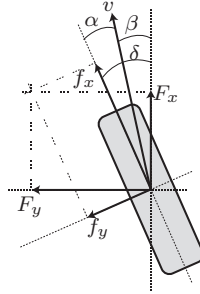


Figure 2.3: The tyre frame is oriented in the direction of the wheel while the vehicle frame is oriented towards the front of the vehicle.

In the class of indirect allocation, Andreasson [4] proposes to distribute the total forces to the tyre forces in the vehicle frame. The low-level control of the actuators is then done using a tyre model inversion. This approach does render the cost function of the allocation problem convex, which considerably reduces the complexity compared to non-linear optimization. However, if every single wheel is not completely actuated, constraints appears between the tyre forces. Such constraints called restrictors can be non-linear and depending on uncertain tyre parameters, which can kill the convexity of the problem and increase the complexity. Therefore, the total problem might not be simpler to solve than direct allocation.

This chapter proposes a new method for Global Chassis Control following the ideas of the class of indirect allocation.

Outline

Section 2.1 introduces the basics of tyre modelling. Section 2.2 focuses on the actuators that can be used to control the vehicle in the road plane. The difficulties and opportunities linked to sensing and estimation are quickly discussed in Section 2.3. The controller structure is further developed in Section 2.4. The global control allocation problem is discussed in Section 2.5 while the local building blocks are introduced in Section 2.6. Finally, an example of chassis is illustrated in Section 2.7, together with two simulations in Section 2.8.

2.1 Tyre forces

As the purpose of the Global Chassis Controller is to control the tyre forces, understanding the basics of the tyre is of prime importance. Many researches went really deep into modelling tyres [95, 115, 52, 82]. The objective here is to give a rapid overview on which we can rely to motivate choices made in the rest of the chapter. The model is based on the Magic Formula [95].

The rotational speed of the wheel ω is given by the differential equation:

$$J\dot{\omega} = T - rf_x \quad (2.1)$$

where J is the wheel inertia, T is the torque applied on the wheel, r is the wheel radius and f_x is the longitudinal tyre force.

From the state of the vehicle, the velocity vector of each wheel in the vehicle frame (V_x, V_y) can be computed [50]. The longitudinal and lateral velocities in the tyre contact patch (v_x, v_y) can be written

$$\begin{pmatrix} v_x \\ v_y \end{pmatrix} = R(\delta) \begin{pmatrix} V_x \\ V_y \end{pmatrix} \quad \text{with} \quad R(\delta) = \begin{pmatrix} \cos(\delta) & \sin(\delta) \\ -\sin(\delta) & \cos(\delta) \end{pmatrix} \quad (2.2)$$

where $R(\delta)$ is the rotation matrix, making a rotation of an angle δ around the vertical z -axis. Note that, throughout this chapter, capital letters are used for signals measured in the vehicle frame (x axis pointing towards the front of the vehicle), while minuscule letters are used for signals measured in the tyre frame (x pointing in the rolling direction of the tyre), see Figure 2.3.

The force response of the tyre to external inputs presents a lag in time. To model the transient behavior of the tyre, a first order filtering is used for computing the longitudinal and lateral slips, λ and α respectively:

$$\sigma_x \dot{\lambda} + |v_x| \lambda = r\omega - v_x \quad (2.3)$$

$$\sigma_y \dot{\alpha} + |v_x| \alpha = v_y \quad (2.4)$$

where σ_x and σ_y are parameters representing the relaxation length. In steady-state, λ and α takes the more common expression

$$\lambda = \frac{r\omega - v_x}{|v_x|} \quad (2.5)$$

$$\alpha = \frac{v_y}{|v_x|} \quad (2.6)$$

In pure slip conditions, meaning that either λ or α should be equal to zero, the longitudinal and lateral tyre forces are given by:

$$f_x^0 = f_z D_x \sin(C_x \arctan(B_x \lambda - E_x(B_x \lambda - \arctan(B_x \lambda)))) \quad (2.7)$$

$$f_y^0 = f_z D_y \sin(C_y \arctan(B_y \alpha - E_y(B_y \alpha - \arctan(B_y \alpha)))) \quad (2.8)$$

where f_z is the tyre load and

- C_x, C_y are the shape factors
- D_x, D_y are the peak factors
- E_x, E_y are the curvature factors
- $K_x = B_x C_x D_x, K_y = B_y C_y D_y$ are the stiffness factors

It should be noted that those parameters can change drastically depending on the conditions of the tyre on the road. Figure 2.4 shows a typical curve for $\frac{f_x^0}{f_z}$ or $\frac{f_y^0}{f_z}$. A peak in the curve can clearly be observed at moderate slip. In the longitudinal case, the left part of the curve with the positive slope is called the stable zone, while the right part with the negative slope is called unstable zone. This denomination comes

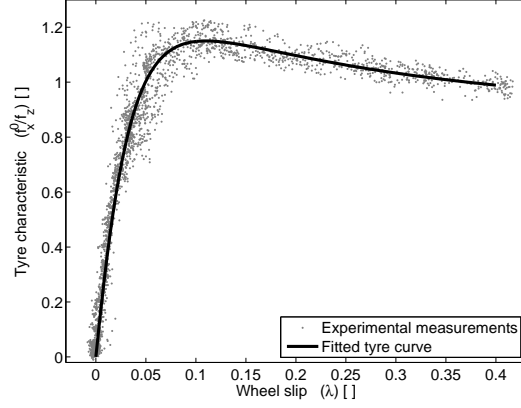


Figure 2.4: Typical tyre characteristics based on measurements from the tyre-in-the-loop facility.

from the stability analysis of the system composed of (2.1), (2.3) and (2.7). More details are given in Chapter 5.

In case of combined slip, when λ and α are both different from zero, there is an interaction between the longitudinal and the lateral forces modeled by:

$$f_x = G_x f_x^0 \quad (2.9)$$

$$G_x = \cos(\arctan(B_{gx}(\lambda)\alpha)) \quad (2.10)$$

$$B_{gx}(\lambda) = r_{x1} \cos(\arctan(r_{x2}\lambda)) \quad (2.11)$$

$$f_y = G_y f_y^0 \quad (2.12)$$

$$G_y = \cos(\arctan(B_{gy}(\alpha)\lambda)) \quad (2.13)$$

$$B_{gy}(\alpha) = r_{y1} \cos(\arctan(r_{y2}\alpha)) \quad (2.14)$$

where f_x^0 and f_y^0 are the longitudinal and lateral forces in pure slip from (2.7) and (2.8) and r_{x1} , r_{x2} , r_{y1} , r_{y2} are extra tyre parameters.

From this interaction, it can be noticed that the total force $\sqrt{f_x^2 + f_y^2}$ that can be generated by a tyre is limited. In particular, the total force has to remain inside an ellipse, called friction ellipse. This limit obviously depends on a lot of factors like, for example, the road conditions, the tyre properties and wear, and the vertical load. The ellipses are illustrated in Figure 2.5. It is clear that no actuator can make the tyre forces exceed the ellipse limit. However, having more freedom in controlling the tyre forces allows to better exploit the tyre potential. One major focus of this thesis is on the optimal use of the tyre potential up to the limit.

All tyre forces f_x and f_y combine at the chassis level in a longitudinal force F_{cx} , a lateral force F_{cy} and a yaw moment M_{cz} , acting at the center of gravity of the vehicle.

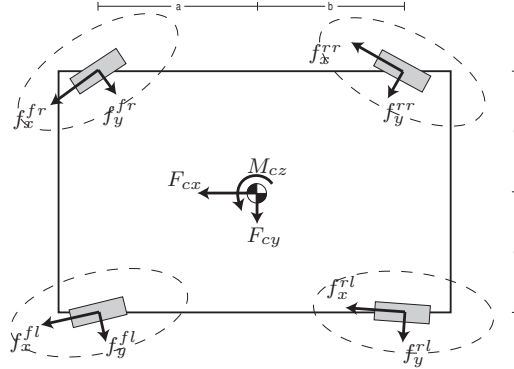


Figure 2.5: All tyre forces combine at the chassis level in a longitudinal force, a lateral force and a yaw moment, acting at the center of gravity. The total force generated at each tyre is limited by the friction ellipse.

This is illustrated on Figure 2.5. Writing down the equations we get:

$$F_{cx} = f_x^{fl} \cos \delta^{fl} + f_x^{fr} \cos \delta^{fr} + f_x^{rl} \cos \delta^{rl} + f_x^{rr} \cos \delta^{rr} - f_y^{fl} \sin \delta^{fl} - f_y^{fr} \sin \delta^{fr} - f_y^{rl} \sin \delta^{rl} - f_y^{rr} \sin \delta^{rr} \quad (2.15)$$

$$F_{cy} = f_y^{fl} \cos \delta^{fl} + f_y^{fr} \cos \delta^{fr} + f_y^{rl} \cos \delta^{rl} + f_y^{rr} \cos \delta^{rr} + f_x^{fl} \sin \delta^{fl} + f_x^{fr} \sin \delta^{fr} + f_x^{rl} \sin \delta^{rl} + f_x^{rr} \sin \delta^{rr} \quad (2.16)$$

$$M_{cz} = -c (f_x^{fl} \cos \delta^{fl} + f_x^{rl} \cos \delta^{rl} - f_y^{fl} \sin \delta^{fl} - f_y^{rl} \sin \delta^{rl}) + c (f_x^{fr} \cos \delta^{fr} + f_x^{rr} \cos \delta^{rr} - f_y^{fr} \sin \delta^{fr} - f_y^{rr} \sin \delta^{rr}) + a (f_y^{fl} \cos \delta^{fl} + f_y^{fr} \cos \delta^{fr} + f_x^{fl} \sin \delta^{fl} + f_x^{fr} \sin \delta^{fr}) - b (f_y^{rl} \cos \delta^{rl} + f_y^{rr} \cos \delta^{rr} + f_x^{rl} \sin \delta^{rl} + f_x^{rr} \sin \delta^{rr}) \quad (2.17)$$

where δ is the steering angle of the wheel and a , b and c defines the position of the center of gravity. The superscripts fl , fr , rl , rr identify the wheels front left, front right, rear left and rear right respectively. The vector F_c is defined as

$$F_c = (F_{cx}, F_{cy}, M_{cz})^T \quad (2.18)$$

The equations giving F_c from f and δ are nonlinear. Computing the solution set giving $F_c = F_c^d$, for F_c^d a given desired value for F_c , is complicated. If locally, all the forces are expressed in the vehicle frame, see Figure 2.3, using

$$\begin{pmatrix} F_x \\ F_y \end{pmatrix} = R^T(\delta) \begin{pmatrix} f_x \\ f_y \end{pmatrix} \quad (2.19)$$

then the previous equations for F_{cx} , F_{cy} and M_{cz} can be rewritten in a linear matrix

form:

$$\begin{pmatrix} F_{cx} \\ F_{cy} \\ M_{cz} \end{pmatrix} = \begin{pmatrix} 1 & 0 & 1 & 0 & 1 & 0 & 1 & 0 \\ 0 & 1 & 0 & 1 & 0 & 1 & 0 & 1 \\ -c & a & c & a & -c & -b & c & -b \end{pmatrix} \begin{pmatrix} F_x^{fl} \\ F_y^{fl} \\ F_x^{fr} \\ F_y^{fr} \\ F_x^{rl} \\ F_y^{rl} \\ F_x^{rr} \\ F_y^{rr} \end{pmatrix} \quad (2.20)$$

Solving $F_c = F_c^d$ in terms of $(F_x^{fl}, F_y^{fl}, F_x^{fr}, F_y^{fr}, F_x^{rl}, F_y^{rl}, F_x^{rr}, F_y^{rr})^T$ becomes trivial.

2.2 Actuators

Tens of actuators targeted at influencing the tyre forces in the road plane are available on the market and many more are being developed. This section gives a description of the type of actuators that are of special interest for this research. Actuators acting on the vertical dynamics of the vehicle, like active suspensions, are not considered here. Still, they should be added in future work as they can indirectly influence the longitudinal and lateral dynamics.

2.2.1 Electro-hydraulic brakes

Most cars on the road today are equipped with Electro-Hydraulic Brakes (EHB). Electrically controlled valves and a pump are added in the traditional hydraulic circuit in order to allow a modulation of the pressure in the brake caliper [18, 27]. This technology is an enabler for the implementation of ABS and ESP. The implementation of ABS in Part II is based on EHB.

The dynamics are mainly characterized by the 3 following points:

- There is an actuation delay of typically 10 to 20 ms caused by the transport of the hydraulic pressure wave in the pipes, from the valves in the control unit to the caliper. This will largely limit the performance of the torque controller.
- The brake torque is a static linear function of the brake pressure. Still, the brake efficiency, the gain between the torque and the pressure, is drastically depending on the temperature and wear.
- The pressure change rate is limited because of the limited flow in the pipes and the valve.

More details on the dynamics of the EHB can be found in Section 4.2.

The EHB is controlled by the current in the valve, which is directly related to the derivative of the brake pressure. The output is the brake torque on the wheel.

The maximal brake pressure is limited to the pressure given by the pump. Therefore the brake torque has a maximum. Still, by design, the maximum torque is taken larger than the torque needed to lock the wheel on any surface and therefore this constraint is almost never active.

2.2.2 Brake-by-wire

From a vehicle dynamics point of view, the advantages of the brake-by-wire lie in the faster and more precise torque response compared to EHB. Instead of hydraulics, the brake pads are actuated by an electro motor [22]. The delay in the actuation is much smaller than for the EHB and is often neglected. A local controller is responsible for regulating the current in the motor to get the desired brake torque.

As for the EHB, it can be considered that the brake is properly dimensioned so that the actuation limit is never reached.

2.2.3 Steer-by-wire

With a steer-by-wire system, the steering of one or more wheels is performed through an electro motor. This gives the freedom to the vehicle controller to interpret, adapt and correct driver steering actions before applying them to the wheels [22]. Steering actuators are interesting for stabilizing the vehicle as they are the most efficient way to generate yaw moment.

The steering can be implemented on any wheel, at the front or at the rear. Either the entire rack is moved or each wheel is steered individually. An internal controller is available to control the steering angle.

The steering angle is limited. It could therefore happen that the maximum tyre force could not be reached.

2.2.4 Active differential

An active differential, or torque vectoring system, is capable of actively distributing the driving torque between different driving wheels, e.g. between the left and right wheel of an axle. It is referred to literature for more details on the working principles [81].

For the applications in Global Chassis Control in this research, an active differential is always connected to a controllable engine or motor. This combination allows any driving torque to be applied on each driven wheel individually. An internal controller is assumed to control the engine and differential such that individual wheel torque commands can be given.

The active differential itself is most often not limited, and can produce any distribution ratio desired. However, the engine torque is limited, which gives constraints on the maximal torque on the wheels.

2.2.5 In-wheel motor

A tendency enabled by electric driving is the introduction of in-wheel motors. The traditional combustion engine is replaced by many decentralized small motors.

From a vehicle control point of view, any torque command can be applied on any wheel of the vehicle. This gives complete freedom in distributing longitudinal tyre forces between the 4 wheels. As a motor can also act as a generator, both a driving and braking torque can be applied. Motors are known to have a fast response and a high accuracy. However, the motor torque and the motor power are limited and are

in general not able of producing enough torque to reach the maximal tyre force on high-adherence surfaces.

2.3 Sensing and estimation

Sensors are becoming cheaper and more accurate every day. Modern cars are equipped with many sensors, and in particular sensors dedicated to measuring the movements and the conditions of the chassis. Lot of papers have been published on how to estimate state and parameters of the vehicle from the available sensors. While some time ago each subsystem would only use a few own sensors, there is now a trend towards combining all available sensors to estimate the complete state of the vehicle with large state estimators [127, 122]. The sensing and state estimation problem are out of the scope of this thesis. Still, it is important to point out some remaining difficulties and new opportunities.

Firstly, the robust measurement of the vehicle longitudinal speed, needed to compute the slip, remains a difficult problem where the use of complex state and parameter estimation techniques is required [30, 73, 62, 111]. Such complexity can lead to reliability issues and high computational load. Therefore, it should not be expected that an accurate measurement of the slip λ at each wheel is constantly available online.

Secondly, the lateral vehicle speed v_y is also difficult to estimate in real-time [9, 114, 14, 70, 3, 42]. Recent work seems to show that the use of force sensing could improve the estimation of v_y [127]. Still it is shown in [40] that lateral speed estimation using force sensing presents severe limitations when tyre parameters are assumed to be completely unknown.

Thirdly, it remains difficult to estimate the tyre parameters or the tyre-road friction on-line. Lots of research has been done on tyre-road friction estimation [48, 115, 119, 55]. But still, the presented solutions suffers from the following issues. Estimators are often based on assumptions such as unbiased sensors, known vehicle weight distribution or identical tyre characteristics at each wheel, which are difficult to meet in practice. Therefore such estimators only work in a restricted number of situations. Furthermore, only a small numbers of tyre parameters are estimated, like for example assuming linear characteristics. Unfortunately, the friction estimated during regular driving cannot properly assess how the nonlinear system will behave at the limit. Because the system is non-linear, a part of the characteristics cannot be identified as long as it is not excited.

Finally, this research relies on tyre force measurement, as explained in Section 1.2, which is new for production vehicles. This will enable a new type of control loop to be implemented, namely force-based control.

2.4 Controller structure

For the vehicle to follow a desired trajectory, a suitable total force and moment, function of time, has to act on the chassis. Such desired total force vector $F_c^d(t)$, see (2.18), can be computed by the global chassis controller and the driver interpreter

based on driver inputs, vehicle properties and other external forces like gravity and drag.

Then the objective is to produce the tyre forces which sum up in total forces and moment as close as possible to the desired ones, by using the available actuators. A few major challenges can be identified:

- the system is over-actuated in the sense that there are more actuators than degrees of freedom for the vehicle motion in the road plane,
- the system is non-linear and presents in particular saturations,
- many parameters, like the tyre-road friction at each tyre, are unknown and time varying.

In the method presented here, the computation of the actuator commands will be done in two steps, like in the class of indirect allocation [4]. This allow for designing global and local controllers to tackle simpler problems with different characteristics. At the global level, the total forces and moments desired on the chassis F_c^d needs to be distributed to the different tyres or groups of tyres. This step is called control allocation [16]. At the local level, in what we'll call the building blocks, see Section 2.6, the nonlinearities and the uncertainties of the tyre need to be deal with.

Separating the control of the chassis and of the tyre makes sense from a time constant point of view. Because of the differences in mass, the chassis dynamics are slower than the wheel dynamics, and the chassis controller can afford having a slower sampling frequency.

Like in [4], forces in the vehicle frame are used as intermediate signals. This offers advantages at both levels:

- The allocation problem is rendered convex and without any uncertain tyre parameters.
- The nonlinearities and uncertainties are confined in blocks of lower dimensions, which makes them easier to handle.

The set of intermediate signals is named S . In [4], all the 8 tyre forces in the vehicle frame are used as intermediate signals:

$$S = (F_x^{fl} \ F_y^{fl} \ F_x^{fr} \ F_y^{fr} \ F_x^{rl} \ F_y^{rl} \ F_x^{rr} \ F_y^{rr}),$$

independently of the actuator configuration. This is perfect if each wheel is completely actuated, for example using Corner Modules, see Section 2.6.1. However, if the actuation is limited, restrictors will appear in order to decrease the number of degrees of freedom. This introduces difficulties in both the global and local control. In our method, in order to avoid the restrictors, S is defined in order to match the number of degrees of freedom. In general, S will not contain all the 8 tyre forces like in [4]. The local control is not implemented per wheel anymore but inside vehicle building blocks, which can contain one or more wheels depending the coupling between them. The concept of building block is discussed in Section 2.6.

2.5 Control allocation

The purpose of control allocation is to distribute the total desired control action to a set of actuators in an over-actuated system [16]. A system is called over-actuated when many actuators can act on the same degree of freedom. For such systems, there are, in general, many ways of driving the actuators that will result in the same state trajectory. In our particular case, the objective is to get $F_c = F_c^d$, see (2.18), of dimension 3. The set S on which F_c^d needs to be distributed depends on the chassis architecture and is assumed to have a dimension between 3 and 8. Furthermore, it is assumed that F_c is affine in S :

$$F_c = GS + H \quad (2.21)$$

where G and H are matrices, possibly time-varying.

In this research, the allocation problem is formulated as an optimization problem. A cost function is used to pick the best solution out of the large feasible set. Constraints are added to take the limitations into account.

When the objective is feasible, meaning $\exists S$ s.t. $CS + D = F_c^d$, the optimization problem takes the form

$$\begin{aligned} \min_S \quad & E & (2.22) \\ \text{subject to} \quad & F_c = F_c^d \\ & \text{tyre constraints} \\ & \text{actuator constraints} \end{aligned}$$

where E is the cost function to be defined. An interesting option is to penalize the use of the actuators in order to reduce the energy consumption. Another option is to strive at maintaining the tyres as far as possible from their limits by e.g. keeping a low slip [92]. However the precise definition of such a cost function is out of the scope of this thesis. In the simulation of Section 2.8, E is taken as the 2-norm of S : $E = \|S\|_2$.

However, because of the constraints, it can happen that the objective is unfeasible. The allocation should then strive at minimizing the difference between F_c and F_c^d . The following optimization problem should be considered instead

$$\begin{aligned} \min_S \quad & \|F_c - F_c^d\|_{W_R}^2 & (2.23) \\ \text{subject to} \quad & \text{tyre constraints} \\ & \text{actuator constraints} \end{aligned}$$

where W_R is a weighting factor which can give more importance to one or the other component of F_c . As an example, more importance could be given to the lateral dynamics of the vehicle, in order to maintain stability, compared to the longitudinal dynamics.

2.5.1 Constraints

Both tyre and actuators are limited in what they can deliver. Such limitations appear in the models in term of nonlinearities. But when the controller is divided in 2 levels, it

is desirable to make abstraction of the models in the other level to reduce complexity. In our case, the complete model of the building blocks can be ignored by the global controller as long as it can be assumed that the local controller can drive the block to the desired set-point. Adding a constraint on a building block gives the allocation a measure of what can be expected from the block.

Constraints on actuators can most of the time be anticipated as they are known from the actuator specifications. For tyre constraints, it is the opposite. As discussed in Section 2.3, tyre friction parameters, and in particular the maximum achievable tyre force are extremely difficult to estimate during normal driving. In this research, we start with the principle that the maximum friction force can be detected only when reached. The detection of the maximum force is done by systems like ABS, presented in Part II, or traction control systems. Only when the ABS kicks in to maintain the tyre in its stable region, a constraint is temporarily added in the allocation at the point where the tyre currently is in term of produced forces. This point can be measured thanks to force sensing. When the ABS stops, the constraint is removed.

Because of the combined-slip effect [95], the total tyre force has to remain within an ellipse. However, the parameters of this ellipse are in practice really uncertain and no published work tackle this estimation problem in an on-line setting. Therefore, it cannot be expected that a constraint could precisely express the tyre limitations. Still, it is necessary, for the force distribution to evolve towards a feasible optimum, that the optimization is given an approximation of the tangential plane to the friction ellipse. In this work, as in [110], a rhombus is used to approximate the ellipse. While the local controller is working to maintain the tyre on the edge of its stable region, the rhombus will be scaled such that the current operating point of the tyre belongs to the border of the rhombus.

2.5.2 Continuous optimization

The allocation is formulated as a constrained convex optimization problem. Compared to traditional optimization, the allocation presents particularities:

- The desired forces on the chassis F_c^d are constantly changing based on the vehicle movement and the inputs from the driver. Therefore the force distribution needs to be continuously updated to remain optimal.
- The constraints based on the tyre limits are rapidly popping in and out, depending if the tyre is at the limit or not.
- Since the speed of the actuators is limited, it is not necessary to always compute the optimal force distribution right away. What is important is that the force distribution converges fast enough towards the optimal one.

Many methods have been presented in the literature to solve allocation problems. Good references can be found in [16] and [57]. Those methods compute the precise solution to the allocation problem at each time step. The computational cost of such techniques can be large as an optimization needs to take place at each time. Further, as the constraints will change while the force distribution is updated, the computed optimal distribution has a large chance not to be feasible.

In Chapter 3, a new Continuous Optimization method is presented, which fits perfectly the needs of this allocation application. The force distribution is not seen as a variable to be optimized over and over again, but as a variable that should be updated over time to minimize the cost function while staying in the currently acceptable region defined by the constraints. This can significantly reduce the computational complexity while a similar level of performance is maintained.

2.6 Vehicle building blocks

The main concept behind the definition of building blocks is to group coupled actuators and mask them with a set of decoupled virtual actuators so that the control allocation problem is simpler. In particular, we want to maintain the allocation between the forces and moment at the center of gravity and the virtual actuators convex. This ensures that there is a unique solution to the optimization problem, and powerful solvers are available [21].

Each building block will be assigned a desired reference and the local control loop inside each block will make sure that the reference is achieved.

Working with blocks provides a really modular architecture. A new vehicle can be created simply by connecting blocks to one another, like a big Lego. The new optimization problem is created by simply summing up the forces from all blocks and stacking all the constraints.

The precise definition of a building block is as follows. A set of actuator low-level control signals u is a building block if and only if one can define a set of virtual references U such that:

- there exists a bijection in steady-state between u and U , possibly time-varying, that can be inverted by a local controller. In mathematical terms,

$$\exists f \text{ s.t. } f(u, U, t) = 0$$

when all derivatives of u and U are equal to zero.

- all U_i from one block are independent from each other. No degree of freedom is lost in the block.
- all U_i from one block are independent from any other block or actuator in the vehicle.
- U is entering the allocation problem in a convex manner.

The first condition means that, given a reference on U , only one solution for u is allowed. In case there are many actuators to produce a similar action, a clear rule should be available on how to distribute the total action. For example, a braking torque could be generated both by a friction brake and an electro-motor [121].

From the actuators presented in Section 2.2, a few standard blocks can be composed:

- Corner Module (1 wheel, 3 actuators)

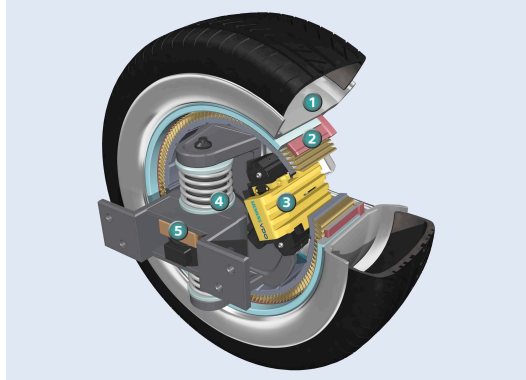


Figure 2.6: The Continental/Siemens VDO eCorner. (1) wheel rim, (2) wheel hub motor, (3) electronic wedge brake, (4) active suspension (5) electronic steering.

- Active-steering rack with active braking and torque vectoring or in-wheel motors (2 wheels, 5 actuators)
- Active-steering rack with active-braking (2 wheels, 3 actuators)
- Manual steering wheel with active-braking (1 wheel, 1 actuator)

2.6.1 Corner module

A Corner Module is composed of various actuators that act on one single wheel. The idea is that a new vehicle could be constructed by simply plugging one of those blocks at each corner. Prototypes are already available, like the Autonomous Corner Module from Volvo [126], the eCorner from Continental, see Figure 2.6, or the HY-LIGHT active wheel from Michelin. A large effort is spent on packaging to give the largest freedom to the vehicle designers.

In this research, we consider the Corner Module to be composed of an individual steering system, an in-wheel motor and a brake-by-wire. Therefore, both the longitudinal and lateral tyre force can be fully controlled. Some implementations also provides an active suspension and a camber controller, but considering those actuators falls outside the scope of this thesis.

Both the in-wheel motor and the brake-by-wire are used to produce the desired total torque. It is assumed that a distribution rule is available. The actuator signals u for the block are $u = (T, \delta)$. As noticed earlier, using u as block control input would make the allocation problem non-convex. Therefore a new set of inputs U needs to be defined.

Taking U as the longitudinal and longitudinal and lateral forces in the vehicle frame (F_x, F_y) makes the corner module to satisfy the building block definition:

- From the tyre model of Section 2.1, it can be verified that there exist a bijection between u and U as long as the tyre is in the stable zone (part of tyre characteristics with positive slope). The local ABS system prevents the tyre from entering the unstable zone.

- F_x and F_y can be fixed independently as long as the constraint is not reached.
- F_x and F_y do not depend on any other actuator in the car.
- F_x and F_y appears in a linear, and thus convex, way in the allocation problem.

Local control

The objective of each local tyre controller is to control one Corner Module via the steering system and the motor/brake such that the tyre develops the desired forces, i.e. determine the control inputs T and δ in order to drive the outputs F_x and F_y to the reference values. The approach should be as simple as possible and as robust as possible regarding the large uncertainty in tyre-road friction.

In the literature, The use of an inverse tyre model is proposed [4]. This open-loop method is interesting for implementing a feedforward path in the controller. However, seen the uncertainty on the tyre curve and the difficulty to identify the full tyre model online, the accuracy reachable with such method is questionable. Moreover, the computation of tyre slip is required, quantity which is still presently complicated to estimate accurately, see Section 2.3.

In order to improve robustness with respect to tyre uncertainty, a feedback loop is desirable. Thanks to force measurement, the implementation of such a feedback loop is possible and efficient. Still, the complexity of the model, with the nonlinear coupling between the state variables and the uncertainties, can make the control design difficult. In this research, a simple approach is used, in order to illustrate the simplicity and potential of the concept. A variation in δ will mainly affect f_y . Similarly, a variation in T will mainly affect f_x . Therefore the following double decoupled integral controller is implemented

$$\begin{pmatrix} \dot{T} \\ \dot{\delta} \end{pmatrix} = \begin{pmatrix} k_x & 0 \\ 0 & k_y \end{pmatrix} \left[R(\delta) \begin{pmatrix} F_x^d \\ F_y^d \end{pmatrix} - \begin{pmatrix} f_x \\ f_y \end{pmatrix} \right] \quad (2.24)$$

with k_x and k_y two tuning parameters. This controllers, with a straightforward tuning, gives satisfactory results in term of stability and convergence speed in the simulations of Section 2.8. Thanks to the integral action, the forces F_x and F_y always converge to their reference values, for any combination of tyre parameters.

This illustrates the simplicity of implementing a local controller thanks to force measurement. Of course, it can be expected that for a real implementation, refinement of the controller will be required to take into account the characteristics of the actuators and other practical constraints.

If a faster system response is desired, an interesting option is to add a feedforward part in the controller, for example based on partial tyre model inversion. Further, if an estimate of how the longitudinal and lateral speeds of the corner module are varying based on information about the desired trajectory of the complete vehicle is available, this could be an interesting basis to implement compensation.

Constraints

Constraints on $U = (F_x, F_y)$ are originating from the tyre limits, the limited driving torque and the limited steering angle.

Constraints from the tyre are indicated with a rhombus, as explained in Section 2.5.1. When the ABS, or the traction control, kicks in to maintain the tyre at the edge of stability, the currently maximum force is computed by summing up the measured F_x and F_y . One of the four following linear constraints is then sent to the allocation:

$$-F_{max} \leq F_x + F_y \leq F_{max} \quad (2.25)$$

$$-F_{max} \leq F_x - F_y \leq F_{max} \quad (2.26)$$

where F_{max} is defined based on current force measurement. The constraint chosen depends on the signs of F_x and F_y .

For the limit on the driving torque, a constraint of the form

$$f_x \leq f_{x_{max}} \quad (2.27)$$

is added. $f_{x_{max}}$ is based on the actuator specifications but can also be adapted depending the operating conditions. For being used in the allocation, (2.27) needs to be expressed in term of U . This gives

$$\cos(\delta)F_x + \sin(\delta)F_y < f_{x_{max}} \quad (2.28)$$

where $\cos(\delta)$ and $\sin(\delta)$ are seen as parameters, which values are continuously updated.

When the steering angle reaches the boundary, a similar constraint as (2.27) is formulated but based on f_y . The allocation constraint is therefore

$$\sin(\delta)F_x - \cos(\delta)F_y < f_{y_{max}} \quad (2.29)$$

where $f_{y_{max}}$ is based on current measurements.

2.6.2 Active-steering rack with torque control

In case the steering angle of 2 wheels is coupled through an axle, the lateral forces on both tyres cannot be fixed independently. If the lateral force of both tyres appeared in the allocation problem, it would be necessary to add a non-linear equality constraint involving uncertain tyre parameters, like in [4]. The allocation problem can be simplified if the constraint is dropped together with one degree of freedom.

Braking and driving actions on the wheels can come from actuators like active brake, in-wheel motor or active differential. To simplify the problem at this stage, those actuators are lumped in one torque actuator.

The block is composed of three actuators, two torque actuators and one steering actuator, so $u = (T_l, T_r, \delta)$. The 2 longitudinal forces on the left and on the right, F_{xl} and F_{xr} , and the total lateral force F_y in the vehicle frame is a suitable choice for U . An equivalent choice would have been to take the total longitudinal and lateral force together with the total yaw moment.

F_{xl} , F_{xr} and F_y can be written:

$$F_{xl} = f_{xl} \cos(\delta) - f_{yl} \sin(\delta) \quad (2.30)$$

$$F_{xr} = f_{xr} \cos(\delta) - f_{yr} \sin(\delta) \quad (2.31)$$

$$F_y = (f_{xl} + f_{xr}) \sin(\delta) + (f_{yl} + f_{yr}) \cos(\delta) \quad (2.32)$$

Local control

Similar to the Corner Module, a simple decoupled integral controller based on force measurement can be used to locally drive the actuators. The largest influence of the actuators, especially at large steering angles, are noticeable on the forces in the tyre frame. However, because of the steering constraint, the system is not invertible and therefore feedback is done directly on the errors computed in the vehicle frame. The controller takes the form:

$$\begin{pmatrix} \dot{T}_l \\ \dot{T}_r \\ \dot{\delta} \end{pmatrix} = \begin{pmatrix} k_x & 0 & 0 \\ 0 & k_x & 0 \\ 0 & 0 & k_y \end{pmatrix} \begin{pmatrix} F_{xl}^d - F_{xl} \\ F_{xr}^d - F_{xr} \\ F_y^d - F_y \end{pmatrix} \quad (2.33)$$

It could be expected that the controller is not robust to large steering angles. However, no problems have been observed in simulation, even during extreme driving conditions. Again, this simple controller is only used for a proof of concept.

Constraints

For this block, constraints on one single tyre cannot be formulated anymore, since the constraints have to be expressed in term of U . Still, using the same concept as in Section 2.5.1, the tangential plane to the friction ellipse can be approximated by a rhombus on F_{xl} and F_y , and on F_{xl} and F_y . Depending on which tyres are saturating, some of the following constraints can be active:

$$-F_{max} \leq F_{xl} + F_y \leq F_{max} \quad (2.34)$$

$$-F_{max} \leq F_{xl} - F_y \leq F_{max} \quad (2.35)$$

$$-F_{max} \leq F_{xr} + F_y \leq F_{max} \quad (2.36)$$

$$-F_{max} \leq F_{xr} - F_y \leq F_{max} \quad (2.37)$$

where F_{max} comes from the current measurement of the tyre forces while the tyre is maintained at the limit by the ABS.

2.6.3 Manual steering wheel with torque control

In this final case, the steering angle of the wheel is fixed by the driver and cannot be influenced by the controller. Therefore taking the longitudinal tyre force as reference $U = (f_x)$ does not destroy convexity in the allocation problem. The steering angle as well as the lateral force f_y will appear in the allocation formulation as parameters. At each time step, their values are updated with the current measurement.

Local controller

The torque that needs to be applied is simply the desired force f_x^d times the radius of the wheel. As the radius is approximately known, it is easy to implement a feed-forward. An integral controller is added to compensate for the error in the radius estimation. The simple controller, used for proof of concept, takes the form:

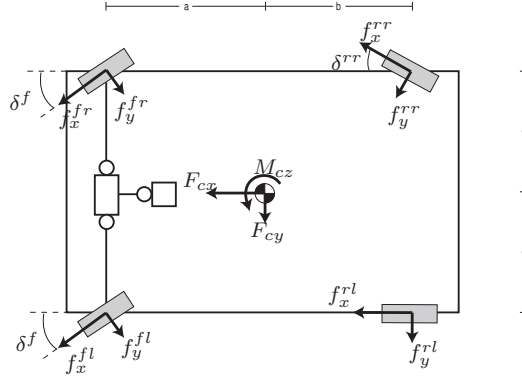


Figure 2.7: Example of chassis with an active steering + active differential front axle, steer-by-wire on the rear right wheel, in-wheel motors at the rear and brake-by-wire on each wheel.

$$T = r f_x^d + T_i \quad (2.38)$$

$$\dot{T}_i = -k_x (f_x - f_x^d) \quad (2.39)$$

Constraints

Constraints on f_x can be expressed based on tyre and actuators limitations:

$$f_{x_{min}} < f_x^d < f_{x_{max}} \quad (2.40)$$

with $f_{x_{min}}$ and $f_{x_{max}}$ parameters that can be predefined based on actuator specifications and adapted online based on detected tyre limits.

2.7 Example

The new Global Chassis Control methodology is applied to an example of chassis combining some of the actuators of Section 2.2. This example does not try to be realistic but emphasizes on the freedom available in designing new chassis.

The chassis considered is composed of 4 wheels and 10 actuators, as illustrated on Figure 2.7. The 2 front wheels are connected to an axle with steer-by-wire. The drive torque delivered by the controllable engine can be distributed freely between front left and front right using the active differential. The rear-right wheel of the vehicle is equipped with an individual steer-by-wire system and an in-wheel motor. The rear-left wheel is equipped only with an in-wheel motor, such that it can be driven but not steered. Finally, each wheel is equipped with a brake-by-wire system.

The total forces and moment generated on the chassis coming from the tyres are

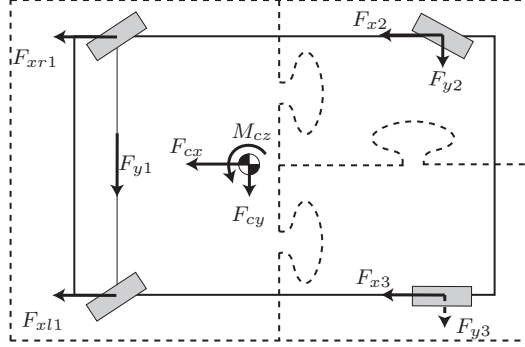


Figure 2.8: Example of chassis where the actuators are grouped into 3 building blocks.

given by:

$$F_{cx} = (f_x^{fl} + f_x^{fr}) \cos \delta^f - (f_y^{fl} + f_y^{fr}) \sin \delta^f + f_x^{rl} + f_x^{rr} \cos \delta^{rr} - f_y^{rr} \sin \delta^f \quad (2.41)$$

$$F_{cy} = (f_y^{fl} + f_y^{fr}) \cos \delta^f + (f_x^{fl} + f_x^{fr}) \sin \delta^f + f_y^{rl} + f_y^{rr} \cos \delta^{rr} + f_x^{rr} \sin \delta^f \quad (2.42)$$

$$\begin{aligned} M_{cz} = & -(f_x^{fl} \cos \delta^f - f_y^{fl} \sin \delta^f)c + (f_x^{fr} \cos \delta^f - f_y^{fr} \sin \delta^f)c + f_x^{rl}c \\ & - (f_x^{rr} \cos \delta^{rr} - f_y^{rr} \sin \delta^{rr})c + ((f_y^{fl} + f_y^{fr}) \cos \delta^f + (f_x^{fl} + f_x^{fr}) \sin \delta^f) a \\ & - (f_y^{rl} + f_y^{rr} \cos \delta^{rr} + f_x^{rr} \sin \delta^{rr})b \end{aligned} \quad (2.43)$$

This chassis can be organized into building blocks. The front axle is an “Active-steering rack with torque control”, the rear right wheel is a “Corner Module” and the rear left wheel is a “Manual steering wheel with torque control” with the steering angle always equal to zero. Figure 2.8 illustrates the chassis with the building blocks and the new intermediate signals S for the allocation.

The inputs for the building blocks are

$$S = (F_{xl1} \quad F_{xr1} \quad F_{y1} \quad F_{x2} \quad F_{y2} \quad f_{x3})$$

The lateral force on the rear left wheel is not controllable and is taken as a measurable disturbance.

The total forces and moment on the chassis can be easily computed from the forces in the blocks with a linear matrix multiplication

$$\underbrace{\begin{pmatrix} F_{cx} \\ F_{cy} \\ M_{cz} \end{pmatrix}}_{F_c} = \underbrace{\begin{pmatrix} 1 & 1 & 0 & 1 & 0 & 1 \\ 0 & 0 & 1 & 0 & 1 & 0 \\ -c & c & a & c & -b & -c \end{pmatrix}}_G \underbrace{\begin{pmatrix} F_{xl1} \\ F_{xr1} \\ F_{y1} \\ F_{x2} \\ F_{y2} \\ F_{x3} \end{pmatrix}}_S + \underbrace{\begin{pmatrix} 0 \\ 1 \\ -b \end{pmatrix}}_H (F_{y3})$$

where the underbrace notation refers to (2.21).

The allocation problem is convex and the continuous methodology of Chapter 3 can be used. The constraints in the allocation comes from the 3 building blocks.

Depending which tyre or actuator is saturating, constraints on the form (2.25)-(2.26), (2.28), (2.29), (2.34)-(2.37), or (2.40) are temporarily added.

2.8 Simulation results

Two simulations are performed to illustrate the Global Chassis Controller. In the first one, a reference maneuver is followed, for which the constraints are not hit. This shows how the desired total forces and moment are achieved using the allocation and the local control. In the second simulation, the vehicle is asked to brake in a split-mu situation, where the left side of the road is more slippery than the right. The maximum tyre force is reached on the rear-left wheel and the ABS gets activated. The steerable wheels are used to maintain the desired trajectory after redistribution of the control action.

2.8.1 Vehicle model

The vehicle model is build in Modelica/Dymola [25, 46] using the Vehicle Dynamics Library [6]. This commercial library provides modular complex vehicle models based on the Modelica Multi-Body framework [94]. The standard components of the library are extended with multi-body models of the different building blocks constituting the example chassis.

The simulated model has 57 states and about 10000 variables. The movement of the chassis, as well as the wheels are considered in 6 degrees of freedom. A complex tyre model is taken from the library, which includes tyre relaxation, combined-slip and vertical dynamics.

2.8.2 Simulation with inactive constraints

In this first simulation, the objective is to let the vehicle follow a desired trajectory, defined by the total longitudinal and lateral forces on the chassis with a side-slip angle constantly equal to zero. A simple PD controller is used to compute the desired yaw moment required to maintain the side-slip at zero. The controller has the form

$$M_z = kv_y + k_d\dot{v}_y \quad (2.44)$$

where v_y is the lateral speed and k and k_d are tuning parameters. In the simulations, the parameters are given the values $k = 2000$ and $k_d = 500$. Such controller is easy to implement in simulation but would be much more involved in practice, seen the difficulty to measure or estimate v_y , see Section 2.3.

The reference total forces on the chassis can be seen on the left plot of Figure 2.9. On the same plot, the allocated forces and achieved forces are also visible. Both steps in the control will introduce some errors and delay, but it can still be concluded that the achieved forces precisely follow the desired ones.

The control allocation is implemented using the Hybrid Descent Method of Chapter 3. In this simulation, the constraints are not hit and therefore no constraint handling is required. The left plot of Figure 2.9 shows the forces produced by each block.

A local controller is implemented in each building block. The same values are taken for the controller parameters in each block: $k_x = 10$, $k_y = 0.001$. From the left plot of Figure 2.9, where the desired and achieved forces are very close together, it can be concluded that the local controllers are able to properly control the actuators. This confirms that a simple force-based linear control can deal with a complex and uncertain tyre model.

2.8.3 Simulation with ABS

In this second simulation, the vehicle is asked to brake in straight-line on a split-mu road. The right side of the road has a friction coefficient of 1, while the left side is more slippery with a friction coefficient of only 0.5. The desired total brake force is set to 6000N, for a car of 1100kg. The total lateral force is set to zero. The total yaw moment is controlled, with the same PD controller as in the previous situation, in order to maintain the lateral speed at zero. At the local level, the ABS controller presented in Chapter 5 is implemented. The results are shown on Figure 2.10.

At the beginning of the simulation, the tyre characteristics are still unknown and no constraint is present in the allocation. While the desired brake force on the wheels is increasing, the maximum tyre force is reached at the rear-left wheel. This is logical as the rear wheels are the least loaded and the left wheels have a road with less grip. The ABS gets activated to maintain the wheel at the limit of stability and a constraint is added in the allocation at the currently measured tyre forces. The optimization method in the allocation takes the constraint into account and redistribute the total forces. Lateral forces are requested on the steerable wheels in order to compensate for the uneven brake force between left and right. With the constraint, the desired brake force on the rear-left wheel F_{x3}^d eventually becomes small enough for the ABS to stop. At that moment, the constraint is removed and, with the objective of using the actuators as less as possible, F_{x3}^d increases again.

2.9 Conclusion

In this chapter, a framework for Global Chassis Control is presented. This framework extends the class of indirect allocation where the total desired forces and moment on the chassis are first distributed to a set of intermediate forces in the vehicle frame, before being translated into actuator commands. The architecture, based on the concept of building blocks, allows vehicles with various levels of actuation to be represented with the correct number of degrees of freedom. This avoids the need for difficult constraints or restrictors. Thanks to the 2 control levels, the allocation problem is maintained convex and independent from uncertain parameters, and the tyre nonlinearities and uncertainties can be dealt with in blocks of smaller dimensions. This decreases the overall complexity compared to previously published methods.

From the analysis of the allocation problem, it can be concluded that there is a need for a continuous optimization technique. An optimization method targeted to this problem is developed in Chapter 3.

At the local level, it is shown that force feedback enables decoupled linear integral controllers to track the desired reference well while being robust with respect to tyre

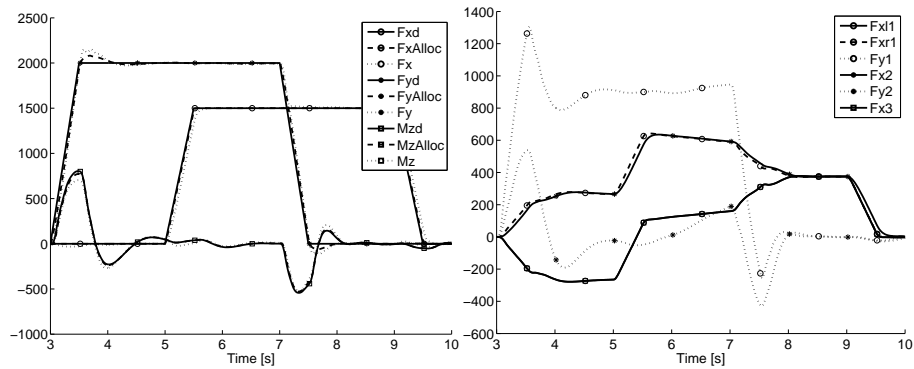


Figure 2.9: Simulation of a maneuver where the tyre constraints are not hit.

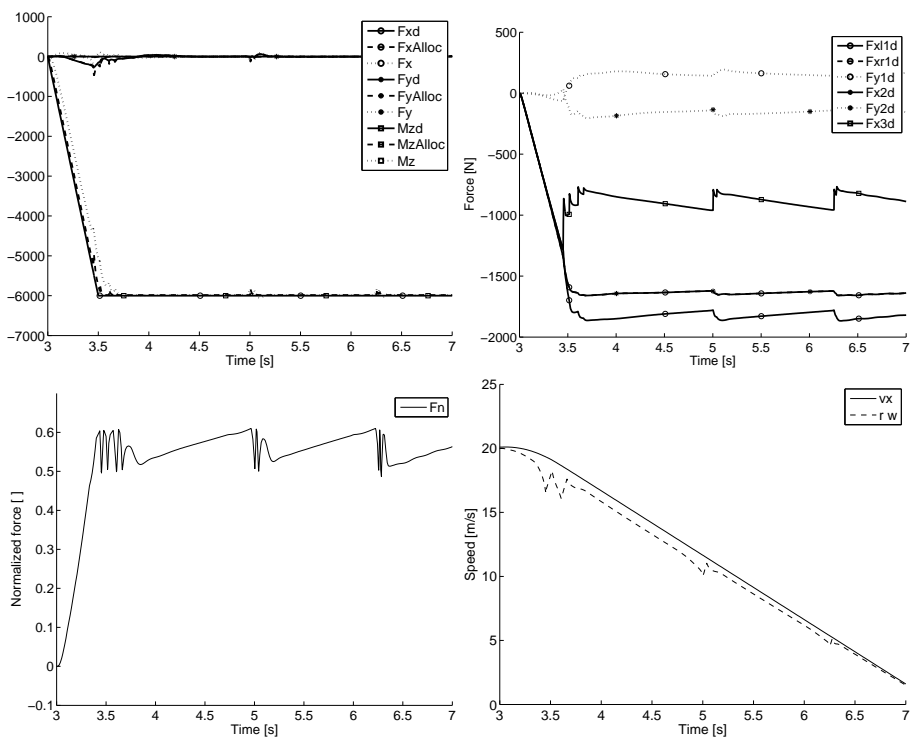


Figure 2.10: Simulation of a braking on split-mu. The rear-left wheel is not able to deliver the initial force asked by the allocation and the ABS is activated. The temporary addition of a constraint changes the allocation and the steerable wheels are used to maintain a straight trajectory. When the ABS is not active anymore, the desired braking force on the rear-left wheel is increased until the maximum is reached again.

characteristics.

Simulations with a complex and realistic vehicle model confirms that this approach can be suitable for practical implementation. This method can deal with the limits of the vehicle. When the limit of a tyre is reached, the local ABS controller is activated and a constraint is temporarily added in the allocation. The forces are redistributed and the demand on the saturating tyre is decreased.

So far, the framework has been developed focusing on two main Global Chassis Control objectives, see Section 1.1: “stability and Safety”, with the handling of the tyre limits, and “Ease of development”, with the modular architecture. Still, it can be expected that the framework is suitable for implementing a fault-tolerant control, with an online reconfiguration of the architecture, and adding energy efficiency objectives, for example by improving the allocation cost function.



Chapter 3

Hybrid Descent Method

Optimization problems play a role of increasing importance in many engineering domains, and specially in control theory. While some design procedures require finding the optimum of a complex problem only once, other real-time control techniques want to track the optimum of a time-varying cost function with time-varying constraints. Some applications based on continuous optimization are the following:

- **Model Predictive Control** [84, 47]. The cost function measures the error between the predicted outputs of the controlled plant and the desired outputs, over a prediction horizon. The desired outputs can be changed in real-time, for example by a human operator, which makes the optimization problem time-varying. The variables to be continuously optimized are the future control inputs to the plant over a control horizon.
- **Control Allocation** [16, 57, 63]. Here the task is to optimally distribute some desired control input to a set of actuators, based on actuator cost and constraints. The changing character of the generic control input makes the problem time-varying.
- **Lyapunov-based control**. Stabilization is performed by making a Lyapunov function or an objective function to decrease over time down to a minimum. A good summary of such methods applied to the field of motion coordination can be found in [85].
- **Model Reference Adaptive Control** [7, 105, 60]. The objective is to adapt the controller parameters so that the controlled plant behaves like the reference one. The time-varying cost function is computed from the output error between the controlled and the reference plants.

In the literature, one can distinguish 3 main approaches to deal with these problems:

- **Repeated Optimization** [84] where the new optimization problem is solved at each time step;

- **Precomputed Optimization** [11] where all the possible problems are solved off-line and stored in a look-up table, which can become very large;
- **Update Laws** [7] where the optimization variables are taken as states of a dynamical system and are given a certain dynamics.

In the field of optimization, many efficient techniques exist to solve constrained convex optimization problems [21]. They are designed to output, after several iterations, an accurate value of the optimum. Therefore they are very well suited for off-line optimization, where a problem should be solved accurately once. However, the iterative character and the complexity of the algorithm do not always make it suitable for on-line implementation. This is probably why those techniques are not often, and very cautiously, integrated into embedded controllers.

On the other hand, update laws are very easy to implement and require very few computation power. Since many years, research on this topic has been going on within the field of adaptive control [7, 105, 60]. For example, one interesting method to adapt the parameters on-line in Model Reference Adaptive Control is to use a gradient descent method for a cost function defined as the square of the output error between the controlled real plant and the reference. This technique works well in the unconstrained case.

However, when it comes to adding constraints, solutions in the control field are much more limited. One possible method found in [105] and [60] is the gradient method with projection. The idea is to project the gradient on the active constraints when the state is on the boundary of the feasible set. In that way, the descent direction is always such that the state stays in the feasible set. This method works in continuous time but the discrete-time implementation is more intricate, especially in the case of nonlinear constraints. Moreover, the way to compute the projection is not obvious and can be complex. Therefore it is only worked out and used for very simple cases.

In case of discrete-time implementation, which is always the case when using digital controllers, the only currently available method, proposed in [60], uses scaling to project back any new value of the state into the feasible set if necessary. However, the idea is worked out only in case of a very simple feasible set (a ball centered at the origin) and no proof of convergence is given.

This chapter bridges those two worlds of control and optimization by developing an update law to deal with the general case of a convex cost function and convex constraints while enabling easy integration into traditional controllers. Moreover, the method is simple, which allows good insight, has low computational cost and is easily discretizable for discrete-time implementation.

The proposed technique takes the form of a traditional ordinary differential equation

$$\dot{x} = f(x)$$

In [24], they are designed to sort lists and to diagonalize matrices. References [67] and [15] present plenty of examples where methods coming from the control area can be used to synthesise and analyse numerical algorithms. In this thesis, the vector field f will be designed to solve constrained convex optimization problems. If the optimization problem is time-varying, f can obviously be expected to also depend

on time. However, the rest of the chapter will focus on an invariant problem for simplicity.

Outline

The formal requirements are described in Section 3.1. The proposed system is described and analyzed in Section 3.2. Section 3.3 shows that the technique can still be used after a simple discretization. Furthermore, a simulation example is presented in Section 3.4. Finally, the use of the method is illustrated for two applications: Model Predictive Control in Section 3.5, and Control Allocation in Section 3.6.

3.1 Problem formulation

Let us consider the convex optimization problem

$$\begin{aligned} \min_x \quad & q(x) \\ \text{subject to} \quad & g(x) \leq 0 \end{aligned} \tag{3.1}$$

with $x \in \mathbb{R}^n$, $q : \mathbb{R}^n \rightarrow \mathbb{R}$ a differentiable convex function and $g : \mathbb{R}^n \rightarrow \mathbb{R}^m$ such that each g_i is a differentiable convex function for $i = 1, \dots, m$. The constraint $g(x) \leq 0$ defines a convex set that we will call the feasible set, for consistency with the optimization terminology. Its complement is called the infeasible set. The two following assumptions are made:

Assumption 1 The feasible set is not empty, i.e. $\exists x_f$ s.t. $g(x_f) \leq 0$.

The optimal value of the cost function in the feasible set is then denoted q^* , i.e. $q^* = \min_x \{q(x) | g(x) \leq 0\}$

Assumption 2 q^* is finite

The objective is to find a vector function $f : \mathbb{R}^n \rightarrow \mathbb{R}^n$ such that the dynamical system

$$\dot{x}(t) = f(x(t)) \tag{3.2}$$

has the following properties:

- for $x(\bar{t})$ outside the feasible set at some time \bar{t} , the trajectory $x(t)$ enters into the feasible set, i.e. $\exists t_f > \bar{t}$ s.t. $g(x(t_f)) \leq 0$.
- the trajectory $x(t)$ remains in the feasible set as soon as $x(t_f)$ is in the set, i.e. $g(x(t)) \leq 0 \quad \forall t > t_f$ s.t. $g(x(t_f)) \leq 0$,
- for $x(t_f)$ in the feasible set, the trajectory $x(t)$ decreases the cost function $q(x(t))$ at all time until $q(x(t)) = q^*$, i.e. $q(x(t_1)) > q(x(t_2)) \quad \forall (t_1, t_2)$ with $t_f \leq t_1 < t_2$ s.t. $q(x(t_1)) > q^*$, and $\lim_{t \rightarrow \infty} q(x(t)) = q^*$.

3.2 Hybrid steepest descent solution

One efficient way to decrease an unconstrained cost function is to use a gradient descent method, as used traditionally in adaptive control [105]. Therefore the basis

of this method is similar. It can also be noted that the gradient of a function is not its only descent direction. Other directions have been proposed in the literature, like Newton's direction [21]. The investigation of alternative directions to improve the convergence while limiting the increase of computation complexity is left for future work.

The original idea of the method is based on the way the constraints are considered. Because of the computational complexity, a direct projection of the gradient on the constraints is discarded. But on the other hand, each constraint is seen as a kind of barrier. More precisely, each constraint which would not be satisfied at a certain time instant will push the trajectory toward the feasible set. In that way, the trajectory will never leave the feasible set. Furthermore, if $x(t)$ is on the boundary of the feasible set, it will be pushed alternatively by both the gradient and the constraint. If they are pushing in opposite directions, $x(t)$ will naturally slide along the border and the projection will appear indirectly. Compared to interior point methods, this technique has the advantage to have descent directions defined outside the feasible set, which can be useful in case of time-varying constraints.

The proposed hybrid feedback law is therefore:

$$f(x) = \begin{cases} -\nabla q(x) & \text{if } g_j(x) \leq 0 \quad \forall j \\ -\sum_{i \in L(x)} \nabla g_i(x) & \text{if } \exists j : g_j(x) > 0 \end{cases} \quad (3.3)$$

with $L(x) = \{l : g_l(x) \geq 0\}$.

The rest of this section is dedicated to the analysis of the behavior of this system using hybrid systems techniques and Lyapunov arguments.

3.2.1 Filippov solutions and sliding modes

The vector field $f(x)$ is measurable and essentially locally bounded but discontinuous. Therefore the study of the solution of the vector differential equation $\dot{x}(t) = f(x(t))$ requires the use of a particular solution concept. We make use of the Filippov solution concept [44, 112, 78] recalled in the following definition:

Definition (Filippov) A vector function $x(\cdot)$ is called a solution of (3.2) on $[t_1, t_2]$ if $x(\cdot)$ is absolutely continuous on $[t_1, t_2]$ and for almost all $t \in [t_1, t_2]$: $\dot{x} \in K[f](x)$, where $K[f](x)$ is the convex hull of the limits of $f(y)$ for $y \rightarrow x$ while y stays out of a set of zero Lebesgue measure where f is not defined [44, 112].

At a point x around which $f(x)$ is continuous, $K[f](x)$ reduces to $f(x)$. However, on a switching surface, $K[f](x)$ will contain a set of possible values for \dot{x} .

So, at all time, \dot{x} has the following form:

$$\dot{x} = -\gamma_0(x)\nabla q(x) - \sum_{i=1}^m \gamma_i(x)\nabla g_i(x) \quad (3.4)$$

for some $\gamma_j(x) \geq 0, j \in \{0, \dots, m\}$. Depending the situation, the values of the $\gamma_j(x)$ will be different:

- for x strictly in the feasible set, $\gamma_0 = 1$ and $\gamma_i = 0 \forall i$,
- for x in the infeasible set, $\gamma_j = 1 \forall j \in L(x)$ and 0 otherwise (so $\gamma_0 = 0$),

- for x on a boundary, the values of the γ_j will depend on a possible sliding motion as defined by the Filippov solution concept.

Following the Filippov solution concept, for x on the switching surface between the feasible and infeasible sets, either a sliding motion can take place, i.e. a motion along the switching surface, or a motion toward one of the sets [44]. Since the $-\nabla g_i(x)$ are always pointing toward the feasible region, a sliding mode will appear only if $-\nabla q(x)$ is pointing toward the infeasible region. In that case, the sliding motion will require $\gamma_0(x) > 0$ in (3.4). In case there is no sliding motion, then due to (3.3), we have $f(x) = -\nabla q(x)$ and $\gamma_0(x) = 1$ in (3.4). In conclusion, $\gamma_0(x) > 0$ on the boundary between the feasible and infeasible sets.

3.2.2 Stationary points of the update law (3.2)-(3.3)

The most interesting property of the update law (3.2)-(3.3) is that the globally stable equilibria of the dynamical system precisely coincide with the optimal points of the constrained optimization problem. First it will be shown that the stationary points of the systems are optimal, and vice versa. The stability of those points is proved in the next subsection.

Definition [44] A point $x = p$ is called stationary if it is a trajectory, that is, if $x(t) \equiv p$ is a solution of (3.2).

Following the definition, it can be concluded that a point p is stationary if and only if $0 \in K[f](p)$, [44]. Further, a point will be called an equilibrium if it is stationary and stable.

Theorem 3.1 below states that, if the convex optimization problem is feasible, the stationary points lie in the feasible set. The “optimality” of the stationary points is considered in Theorem 3.2. Further, the next section demonstrates the asymptotic stability.

Theorem 3.1. *If the functions $g_i(x) : \mathfrak{R}^n \rightarrow \mathfrak{R}$ are convex ($i = 1, \dots, m$) and if there exists an x_f such that $g_i(x_f) \leq 0 \ \forall i \in \{1, \dots, m\}$ then*

$$\sum_{i \in L} \nabla g_i(\bar{x}) \neq 0$$

for any subset L of $\{1, \dots, m\}$ and any \bar{x} such that $g_i(\bar{x}) > 0$ for some $i \in L$.

Proof. Let us define $T_{\bar{x}}^{g_i}(x)$ the tangent hyperplane to the function g_i at \bar{x} :

$$T_{\bar{x}}^{g_i}(x) = \nabla g_i^T(\bar{x})(x - \bar{x}) + g_i(\bar{x}) \triangleq G_i(\bar{x})x - h_i(\bar{x}) \quad (3.5)$$

where $G_i(\bar{x}) = \nabla g_i^T(\bar{x})$ and $h_i(\bar{x}) = \nabla g_i^T(\bar{x})\bar{x} - g_i(\bar{x})$. Due to the convexity of g_i , we know that

$$g_i(x) \geq T_{\bar{x}}^{g_i}(x) \quad \forall \bar{x}, \forall x \quad (3.6)$$

The proof is done by contradiction. Assume there exist a point \bar{x} and a set L such that

$$\begin{cases} g_i(\bar{x}) = G_i(\bar{x})\bar{x} - h_i(\bar{x}) > 0 \quad \forall i \in L \\ \sum_{i \in L} G_i(\bar{x}) = 0 \end{cases} \quad (3.7)$$

This directly leads to

$$0 = \sum_{i \in L} G_i(\bar{x})\bar{x} > \sum_{i \in L} h_i(\bar{x}) \quad (3.8)$$

Furthermore, by the hypothesis of the theorem, there exists an x_f such that $g_i(x_f) \leq 0 \quad \forall i \in L$ and therefore by (3.5) and (3.6)

$$0 \geq \sum_{i \in L} g_i(x_f) \geq \sum_{i \in L} (G_i(\bar{x})x_f - h_i(\bar{x})) = - \sum_{i \in L} h_i(\bar{x}) \quad (3.9)$$

Equations (3.8) and (3.9) clearly lead to a contradiction. It can therefore be concluded that a combination (\bar{x}, L) does not exist, which proves the theorem. \square

Using this result, the “optimality” of the stationary points can be assessed.

Theorem 3.2. *If (3.1) is feasible then a point p is a stationary point of (3.2)-(3.3) if and only if it is an optimal point of (3.1).*

Proof. Due to Theorem 3.1, it can be concluded that $f(x)$ is always different from 0 for x in the infeasible set and therefore the stationary points lie in the feasible set.

For any feasible x , the dynamics takes the form of equation (3.4) with $\gamma_0(x) > 0$. If there exists a stationary point p such that $\dot{x}(p) = 0$, and by defining

$$\lambda_i = \frac{\gamma_i(p)}{\gamma_0(p)} \quad (3.10)$$

it is easy to check that the following set of equations is satisfied:

$$\begin{aligned} g_i(p) &\leq 0 \quad \forall i \\ \lambda_i &\geq 0 \quad \forall i \\ \lambda_i g_i(p) &= 0 \quad \forall i \\ \nabla q(p) + \sum_{i=1}^m \lambda_i \nabla g_i(p) &= 0 \end{aligned}$$

These equations are the well-known *Karush-Kuhn-Tucker* (KKT) conditions, which prove that the stationary point p is an optimal solution of the convex problem (3.1) while the λ 's are the Lagrange multipliers [21, 13].

Moreover, if p is optimal, it satisfies the KKT conditions. The Lagrange multipliers λ will define a suitable dynamics of the form (3.4), which belongs to $K[f](p)$. Therefore, 0 belongs to $K[f](p)$ and, following the definition, p is a stationary point. \square

By Assumptions 1 and 2, there always exists at least one such stationary point p . Furthermore, $q(p) = q^*$.

3.2.3 Asymptotic stability

Finally, it can be shown that (3.2)-(3.3) is asymptotically stable and converges toward one of the stationary points found above. In view of the structure of (3.3), we propose the following Lyapunov function:

$$V(x) = \max(q(x), q^*) - q^* + \beta \sum_{i=1}^m \max(g_i(x), 0) \quad (3.11)$$

with β a strictly positive parameter.

It is obvious that this Lyapunov function is strictly positive everywhere except at stationary points where $V(p) = 0$:

- in the infeasible set, we have $V(x) > 0$ since at least one $g_i(x) > 0$
- in the feasible set (or at the boundary), we have $V(x) > 0$ since $q(x) > q^*$, except at the stationary points where $q(x) = q^*$

Unfortunately, this Lyapunov function is not differentiable everywhere. To handle this case, the theory developed in [112] will be used. The main stability theorem is recalled below. But first, to go more smoothly through the technicalities, let us recall some definitions.

Definition [59] A function $f(x)$ is said to be essentially bounded on X if the function is unbounded only on a set of measure zero, i.e. $\mu\{x \in X : |f(x)| > a\} = 0$ for some real number $a \geq 0$ where μ is the Lebesgue measure.

Definition [31] A function $V(x)$ is said to be regular when the usual directional derivative exists in any direction. Examples of regular functions include smooth functions, convex Lipschitz functions, and functions that can be written as the pointwise maximum of a set of smooth functions.

Therefore it can be concluded that $V(x)$ is regular.

Definition [69] A continuous function $\alpha : [0, a) \rightarrow [0, \infty)$ is said to belong to class \mathcal{K} if it is strictly increasing and $\alpha(0) = 0$.

Definition [31] The Clarke's generalized gradient $\partial V(x)$ of a locally Lipschitz function $V(x)$ is the convex hull of the limits of the gradients of the function around the points where the gradient of V is not defined.

$$\partial V(x) = \text{co}\left\{ \lim_{y \rightarrow x, y \notin \Omega_V} \nabla V(y) \right\} \quad (3.12)$$

for Ω_V a set of measure zero where the gradient of V is not defined.

Definition [112] The set $\dot{V}(x)$, which is proved in [112] to contain $\frac{d}{dt}V(x(t))$, when this last quantity exists, is defined as

$$\dot{V}(x) \triangleq \bigcap_{\xi \in \partial V(x)} \xi^T K[f](x) \quad (3.13)$$

In the smooth case, where all the functions involved are differentiable, $\dot{V}(x)$ reduces to the time derivative of the function $V(x(t))$: $\dot{V}(x) = \nabla V^T \dot{x}$.

Definition A set S is said to be negative if all the elements of the set are negative: $S < 0 \Leftrightarrow s < 0 \forall s \in S$

Theorem 3.3. [112] Let $\dot{x} = f(x)$ be essentially locally bounded in a region $Q \supset \{x \in \mathbb{R}^n \mid \|x - p\| < r\}$ for some real number r and $0 \in K[f](p)$. Also let $V : \mathbb{R}^n \rightarrow \mathbb{R}$ be a regular function satisfying $V(p) = 0$ and $0 < V_1(\|x - p\|) \leq V(x) \leq V_2(\|x - p\|)$ for $x \neq p$ in Q for some $V_1, V_2 \in \text{class } \mathcal{K}$. Then

1. $\dot{V}(x) \leq 0$ in Q implies that $x(t) \equiv p$ is a uniform stable function.

2. If in addition, there exists a class \mathcal{K} function $w(\cdot)$ in Q with the property $\dot{V}(x) \leq -w(x) < 0$ for $x \neq p$ then the solution $x(t) \equiv p$ is uniformly asymptotically stable.

Now Theorem 3.3 is used to prove the stability of (3.2)-(3.3).

Theorem 3.4. *The system defined by (3.2)-(3.3) is uniformly asymptotically stable if it has one unique finite stationary point.*

Proof. The vector field f (3.3) satisfies the requirements of Theorem 3.3 for any set Q of the form $\{x \in \mathbb{R}^n \mid \|x - p\| < r\}$ with a finite r and $0 \in K[f](p)$. Moreover, the Lyapunov function V (3.11) is continuous, since it is the sum of continuous functions; regular and convex, since it can be written as the pointwise maximum of a set of smooth convex functions; and positive. Then due to the convexity of the functions and the unique finite stationary point p such that $V(p) = 0$, V can be bounded from below by the function $V_1(\|x - p\|)$ with V_1 of class \mathcal{K} . With the same arguments, V can also be bounded from above by a function $V_2(\|x - p\|)$ with V_2 of class \mathcal{K} .

The stability conclusion coming from Theorem 3.3 now depends on the values of the generalized time derivative of V . The 3 main regions are first considered before going to a more general case including the boundaries.

- For x in the feasible set we have: $V(x) = q(x) - q^*$, $\nabla V = \nabla q$, $\dot{x} = -\nabla q$ and therefore

$$\dot{V}(x) = -\nabla q(x)^T \nabla q(x) \leq 0 \quad (3.14)$$

which is always negative as long as $\nabla q(x) \neq 0$, and this can only happen at the stationary point. Moreover, as we move away from the optimal point in the feasible set, the norm of $\nabla q(x)$ cannot decrease, because of the convexity of $q(x)$, and therefore $\dot{V}(x)$ cannot increase. This will be important when showing that $\dot{V}(x)$ can be bounded from below and from above by class \mathcal{K} functions.

- For x in the infeasible set for $q(x) < q^*$ we have: $V(x) = \beta \sum_{i \in L} g_i(x)$, $\nabla V = \sum_{i \in L} \nabla g_i(x)$, $\dot{x} = -\sum_{i \in L} \nabla g_i(x)$ and therefore

$$\dot{V}(x) = -\beta \left\| \sum_{i \in L} \nabla g_i(x) \right\|^2 < 0 \quad (3.15)$$

which is always strictly negative and never increasing as we move away from the stationary point by the same convexity arguments as before.

- For x in the infeasible set for $q(x) \geq q^*$ we have: $V(x) = q(x) - q^* + \beta \sum_{i \in L} g_i(x)$, $\nabla V = \nabla q + \sum_{i \in L} \nabla g_i(x)$, $\dot{x} = -\sum_{i \in L} \nabla g_i(x)$ and therefore

$$\dot{V}(x) = -\nabla q(x)^T \left(\sum_{i \in L} \nabla g_i(x) \right) - \beta \left\| \sum_{i \in L} \nabla g_i(x) \right\|^2 < 0 \quad (3.16)$$

Since $\sum_{i \in L} \nabla g_i(x) \neq 0$ (see Theorem 3.1), it is always possible to find a β large enough such that $\dot{V}(x)$ is strictly negative. Moreover, again thanks to convexity,

the norm of $\nabla g_i(x)$ cannot decrease as we move away from the stationary point in the infeasible set. Therefore, a large enough β can also render $\dot{V}(x)$ non-increasing. The interpretation of β is here to create a large enough barrier such that the constraints dominate the cost function in the infeasible set.

- In the general case, $\dot{V}(x)$ is not anymore a number but a set of values for each x . To show that $\dot{V}(x) < 0$, the fact that a subset of a negative set is also a negative set will be used twice.

Since $K[f](x)$ is a subset of the “headless” cone

$$\bar{X} = \{-\varphi_0 \nabla q(x) - \sum_{i \in L(x)} \varphi_i \nabla g_i(x) \mid \varphi_j \geq 0, \sum_j \varphi_j > 0\}$$

and since ∂V contains

$$\bar{V} = \{\nabla q(x) + \beta \sum_{i \in L(x)} \gamma_i \nabla g_i(x) \mid \gamma_j \geq 0, \sum_j \gamma_j \leq 1\}$$

$\dot{V}(x)$ is included in the set $\bar{W} = \{\bigcap_{\xi \in \bar{V}} \xi^T \bar{X}\}$. So if \bar{W} is negative, then \dot{V} is negative as well.

If $K[f](x)$ does not contain 0, i.e. if x is not the stationary point, then 0 is not in the convex “headless” cone \bar{X} neither and the entire set is situated in a half-space defined by the separating hyperplane passing through 0 and with normal vector v . Such hyperplane is not unique and therefore a normal vector v can be chosen such that v belongs to \bar{X} with $\varphi_0 > 0$ and $\sum_j \varphi_j = 1$. Then it is obvious that the vector $-\frac{1}{\varphi_0}v$ belongs to \bar{V} for $\beta \geq \frac{1}{\varphi_0}$. Therefore, there exists a vector $\xi = -\frac{1}{\varphi_0}v$ belonging to \bar{V} such that $\xi^T \bar{X} < 0$, which implies $\bar{W} < 0$ and finally $\dot{V}(x) < 0$. In case $K[f](p)$ contains zero, the stationary point is reached and the value of the Lyapunov function will remain zero.

Finally, Theorem 3.3 holds which proves the theorem. □

In the case where the system (3.2)-(3.3) has many stationary points (for a convex optimization problem they will represent a convex set : a sublevel set of a convex function [21]), the equivalent of LaSalle’s theorem for non-smooth systems presented in [112] can be used to show that the system (3.2)-(3.3) will converge to a point in the largest invariant set of $\{x \mid 0 \in \dot{V}(x)\}$, which in our case is the complete set of optimal points.

3.3 Practical implementation

Because of the sliding mode, i.e. the infinite number of switches, the dynamical system cannot be simulated directly. Two methods can be considered for practical implementation. The first method is to sample the system at a given sampling frequency [8].

In that way, the computation can easily be scheduled on time-driven microcontrollers and the number of switches is limited to one every period. Obviously, because of the sampling, the accuracy of the system is going to be reduced. Two main drawbacks can be foreseen, whatever the sampling technique used:

- during a sliding mode, the trajectory will not stay perfectly on the boundary but will meander slightly around it. The amplitudes of the oscillations will depend on the sampling period and on the norms of the gradients $\nabla q(x)$ and $\nabla g_i(x)$.
- the trajectory will not precisely converge toward the precise optimal point but will oscillate around it.

In this research, the sampling is done by approximating the derivative by a forward difference, i.e. Euler's method. For a sampling time Δt , the difference equation is given by

$$x_{k+1} = x_k + f(x_k)\Delta t \quad (3.17)$$

The investigation of other sampling methods as well as the precise influence of the sampling time on the performance is left for future work. Results from [78] can be used to ensure that the trajectory of the discretized system remains close to the one of the original system.

In the second method, the simulation remains in continuous-time and smooth transitions are implemented between the feasible and the infeasible set [39]. In practice, the gradient of the constraints are weighted based on the value of the constraint via a smoothed step s , for example:

$$s(g(x)) = \frac{1}{\pi} \operatorname{atan}\left(\frac{g(x)}{\epsilon}\right) + 0.5 \quad (3.18)$$

where ϵ is a tuning parameter which should be small. Then the gradient of the cost function is weighted by a complementary function. Finally, the smooth version of f is given by

$$f_s = - \left(1 - \frac{1}{m} \sum_{i=1}^m s(g_i(x)) \right) \nabla q(x) - \sum_{i=1}^m s(g_i(x)) \nabla g_i(x) \quad (3.19)$$

In the simulations of Chapter 2, the Hybrid Descent Method is implemented in continuous-time using smooth transitions. The discretization method is illustrated in the next section.

3.4 A simulation example

To illustrate the essence of the developed method, we consider a simple convex optimization problem in 2 dimensions. The cost function and one of the constraints are chosen to be linear while the second constraint is taken nonlinear, although convex.

Let us consider the following optimization problem for $x = (x_1 \ x_2)^T$:

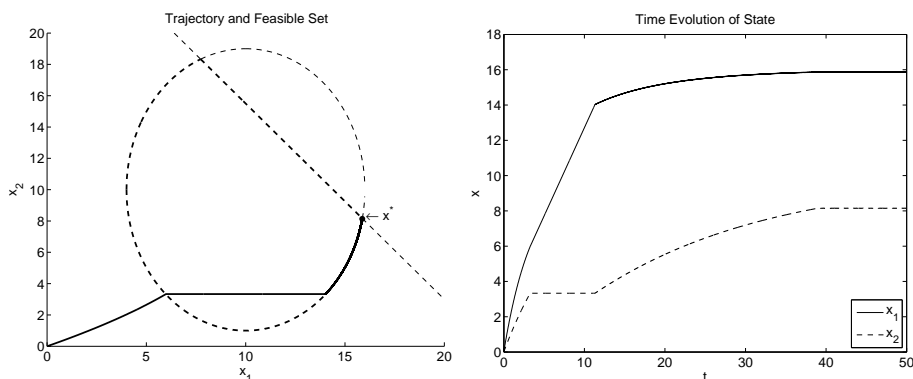


Figure 3.1: Simulation with sampling time $\Delta t = 0.01$. The oscillations in the sliding mode are not visible and the trajectory converges toward the optimal point. Just after $t = 3$ the trajectory reaches the feasible set; after $t = 11$ the trajectory starts sliding along the nonlinear constraint; and at $t = 40$ the optimal point is reached.

$$\begin{aligned} \min_x \quad & -x_1 & (3.20) \\ \text{subject to} \quad & \frac{(x_1 - 10)^2}{36} + \frac{(x_2 - 10)^2}{81} - 1 \leq 0 \\ & \frac{10}{8}x_1 + x_2 - 28 \leq 0 \end{aligned}$$

We have:

$$\nabla q(x) = \begin{pmatrix} -1 & 0 \end{pmatrix}^T \quad (3.21)$$

$$\nabla g_1(x) = \begin{pmatrix} \frac{1}{18}(x_1 - 10) & \frac{2}{81}(x_2 - 10) \end{pmatrix}^T \quad (3.22)$$

$$\nabla g_2(x) = \begin{pmatrix} \frac{10}{8} & 1 \end{pmatrix}^T \quad (3.23)$$

Figure 3.1 presents the results of the simulation for a small sampling time $\Delta t = 0.01$ and initial condition $x_0 = (0 \ 0)^T$. While x is outside the feasible set (until $t = 3$), the trajectory converges toward it. Then the gradient of the cost function is followed until reaching a constraint at $t = 11$. Afterwards, the trajectory slides along the constraint to the optimal point, which is reached at $t = 40$. Thanks to the small sampling time, the oscillations in the sliding mode are hardly visible. It can be checked that the Lyapunov function (with $\beta = 3$) always decreases over time. Note that on the trajectory picture, the dashed curves represent the zero level-sets of the constraints and therefore the interior of the bold dashed curve is the feasible set.

Figure 3.2 presents the same results for a larger sampling time $\Delta t = 0.5$. Here the oscillations are very large but the trajectory is still evolving in the right direction.

In order to reduce the oscillations induced by the sliding mode, smooth transitions are implemented between the feasible and infeasible sets. The results are shown on Figure 3.3. The oscillations are completely removed, unfortunately at a cost of a decrease of the accuracy.

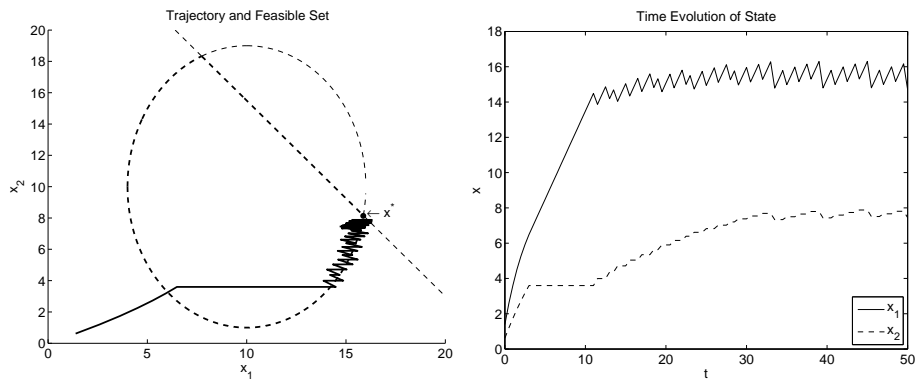


Figure 3.2: Simulation with sampling time $\Delta t = 0.5$. The oscillations in the sliding mode are now visible but the trajectory still evolves in the right direction until oscillating around the optimal point.

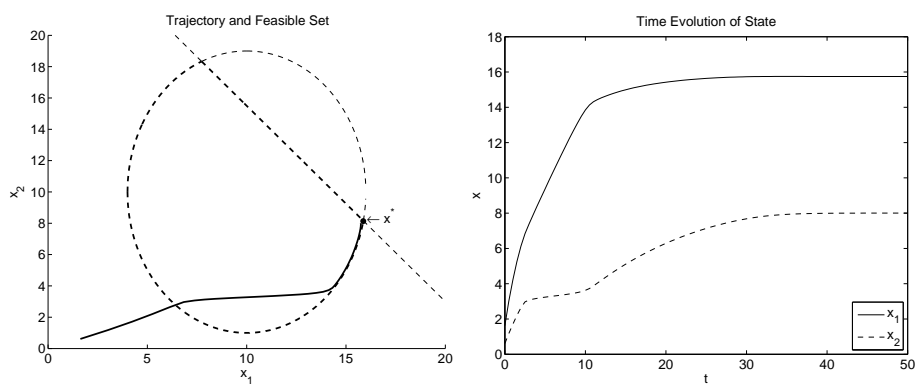


Figure 3.3: Simulation with sampling time $\Delta t = 0.5$ and smooth transitions. The oscillations in the sliding mode are completely removed.

3.5 Application to Model Predictive Control

A very interesting modern control method is Model Predictive Control (MPC) [28, 10, 102]. Thanks to an internal model of the plant, the controller is able to predict its expected future outputs and therefore optimize the current input accordingly. The main advantages of MPC are the following:

- It can handle multi-input multi-output processes, processes with large time-delay, non-minimum phase processes, and unstable processes;
- It can take constraints into account in a natural manner: input constraints as well as output constraints or state constraints;
- It can be reconfigured by changing the internal model, for example in case of fault detection.

MPC is formulated as an optimization problem on a receding horizon. At all time, a cost function penalizing the difference between the desired and expected outputs should be minimized under the constraints. Many publications already studied properties and tuning of MPC cost functions and constraints, see for example [84, 47, 104] and references therein.

Typically, most implementations of MPC are done using discrete-time controllers and a discrete-time model of the plant is used as an internal model. Continuous-time models could also be used like in Receding Horizon Control, see [101]. MPC based on discrete-time internal models are considered here.

Papers in the literature often rely on on-line optimization, where a repeated optimization method is used and the exact value of the optimum is computed at each time step, see [84]. Other approaches compute a multiparametric optimal solution beforehand (off-line) and store the results for on-line use, see [12]. In the first case, such an on-line optimization can be computationally expensive and therefore too demanding for small embedded microcontrollers. In the second case, the amount of data to be stored can become extremely large if many parameters or constraints appear in the problem formulation. Thus, real-time implementation of MPC is not an easy task and this is probably one reason why it is cautiously used in embedded controllers dealing with fast dynamics processes.

By applying the Hybrid Descent Method, it becomes possible to implement a MPC-like controller using a hybrid dynamical system.

3.5.1 Model Predictive Control

In MPC, the future evolution of the system on a certain time interval is considered. An internal model of the process to be controlled is used to compute the predictions. To limit the number of variables and simplify the computation, a discrete-time internal model is used with a sampling time ΔT . Therefore, if the noise-free process has the state-space model

$$\begin{cases} \dot{x}(t) &= Ax(t) + Bu(t) \\ y(t) &= Cx(t) \end{cases} \quad (3.24)$$

then the equivalent internal model takes the form

$$\begin{cases} x_{k+1} &= \tilde{A}x_k + \tilde{B}u_k \\ y_k &= \tilde{C}x_k \end{cases} \quad (3.25)$$

Using a prediction horizon N_p , the prediction covers the time interval $[t, t + N_p \Delta T]$; and the cost function is based on the value of the output at the N_p next sampling time instants. The variables to be optimized in the procedure are the input u at the following N_u sampling time instants. In the following, t is the measurement time; therefore time before t has already been measured and is known, while time after t is expected by the controller. Using the following variables:

$$\tilde{u}(t) = \begin{pmatrix} u(t) \\ u(t + \Delta T) \\ \vdots \\ u(t + (N_u - 1)\Delta T) \end{pmatrix} \quad (3.26)$$

$$\tilde{x}(t) = \begin{pmatrix} x(t + \Delta T) \\ x(t + 2\Delta T) \\ \vdots \\ x(t + N_u \Delta T) \end{pmatrix} = \begin{pmatrix} \tilde{A}x(t) + \tilde{B}u(t) \\ \tilde{A}x(t + \Delta T) + \tilde{B}u(t + \Delta T) \\ \vdots \\ \tilde{A}x(t + (N_u - 1)\Delta T) + \tilde{B}u(t + (N_u - 1)\Delta T) \end{pmatrix} \quad (3.27)$$

$$\tilde{y}(t) = \begin{pmatrix} y(t + \Delta T) \\ y(t + 2\Delta T) \\ \vdots \\ y(t + N_u \Delta T) \end{pmatrix} = \begin{pmatrix} \tilde{C}x(t + \Delta T) \\ \tilde{C}x(t + 2\Delta T) \\ \vdots \\ \tilde{C}x(t + N_u \Delta T) \end{pmatrix} \quad (3.28)$$

the traditional MPC cost function q is

$$q(\tilde{u}(t), x(t), \tilde{y}_{ref}(t)) = \|\tilde{y} - \tilde{y}_{ref}\|_{Q_y}^2 + \|\Delta\tilde{u}\|_{Q_u}^2 \quad (3.29)$$

where \tilde{y}_{ref} is the desired output at the N_p next sampling time instants, $\Delta\tilde{u}$ contains the value of the signal $u(t) - u(t - \Delta T)$ at the next N_u sampling time instants and Q_y and Q_u are weighting matrices.

This cost function can be rewritten in a standard quadratic form

$$q(\tilde{u}(t), x(t), \tilde{y}_{ref}(t)) = \frac{1}{2}\tilde{u}^T Q \tilde{u} + x^T R^T \tilde{u} + \tilde{y}_{ref}^T S^T \tilde{u} + c(x, \tilde{y}_{ref}) \quad (3.30)$$

where c does not depend on \tilde{u} and Q , R and S are time-independent matrices. Note that the cost function depends on the future values of u and y_{ref} , which are embedded in \tilde{u} and \tilde{y}_{ref} respectively; while it is parametrized by the value of x only at the current time t which is the “initial state” of the current horizon. For concision, the explicit dependency on t is omitted.

The gradient is therefore

$$\nabla_{\tilde{u}} q = \frac{\partial q}{\partial \tilde{u}} = Q\tilde{u} + Rx + S\tilde{y}_{ref} \quad (3.31)$$

A set of constraints can be defined. Constraints on the control input can directly be expressed while constraints on state or outputs require the use of the internal

model. Here, the constraint set, also called feasible set, is restricted to the smooth convex case described by

$$g_i(\tilde{u}, x) \leq 0 \quad i = 1 \dots m \quad (3.32)$$

where $g_i : \mathfrak{R}^n \rightarrow \mathfrak{R}$ is a differentiable convex function. Obviously, if the internal model is used to express constraints, the functions g_i will also depend on the state x .

Furthermore, rate constraints can be expressed on the control inputs. The general form of those constraints are the following:

$$|\dot{u}(t)| < \dot{u}_{max} \quad \forall t \quad (3.33)$$

This constraint is expressed in continuous time for the continuous system (3.24) and directly used in the continuous implementation of the controller (3.35).

In traditional implementation, to give time for the optimization to be performed, the MPC controller is implemented in discrete time. Here, we will first have a look at the continuous-time case.

3.5.2 The hybrid feedback controller

By using the Hybrid Descent Method as continuous optimization technique, the MPC controller can be implemented as a hybrid dynamical system. The controller scheme is represented on Figure 3.4. The future inputs \tilde{u} are driven by a differential equation on the form

$$\dot{\tilde{u}}(t) = f(\tilde{u}(t), x(t), \tilde{y}_{ref}(t)) \quad (3.34)$$

where f is designed according to (3.3). The cost function q is given by (3.29) and only the constraints (3.32) are considered.

To include the rate constraints (3.33), a variation of the update law can be considered. The dynamical system takes the form

$$\dot{\tilde{u}}(t) = \text{sat}[\alpha f(\tilde{u}(t), x(t), \tilde{y}_{ref}(t)), \dot{u}_{max}] \quad (3.35)$$

where sat is the traditional saturation function that limits the value of $\alpha f(\cdot)_i$ to $+$ or $- \dot{u}_{max_i}$ and α is a tuning parameter that scales the descent direction. To fully exploit the capabilities of the actuators in terms of rate of change, a large enough α should be used. However, a too large α will lead to a too reactive controller that could be difficult to discretize, as will be seen later on.

For practical implementation, as discussed in Section 3.3, the control system can be implemented either in continuous-time with smooth transitions, or in discrete-time with for example an Euler discretization of period Δt . It should be noted that the sampling frequency of the controller does not need to be related to the sampling frequency of the internal model. Two different notations are used.

3.5.3 Simulation

Some simulations are used to show that the method is working and to analyse the influence of the parameters Δt and α . The first simulations focus on input constraints while the last one introduces output constraints. A random stable non-minimum phase linear system is taken as process to be controlled. The transfer function contains

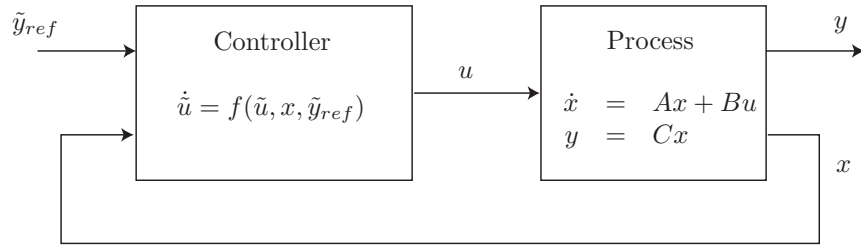


Figure 3.4: Controller scheme

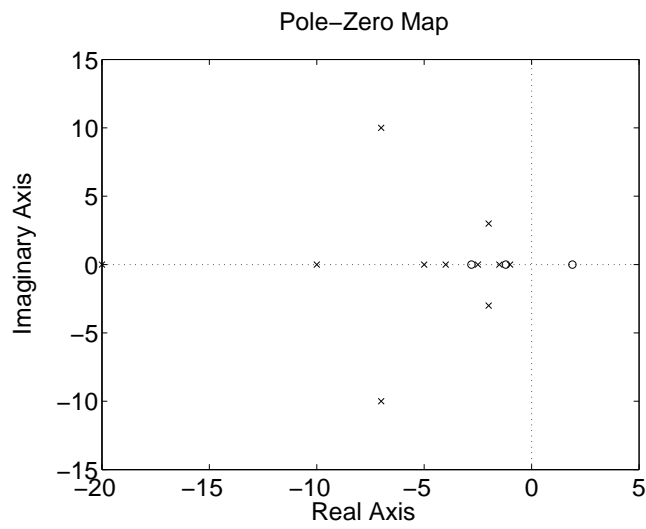


Figure 3.5: Pole-zero map of the process to be controlled.

3.5. APPLICATION TO MODEL PREDICTIVE CONTROL

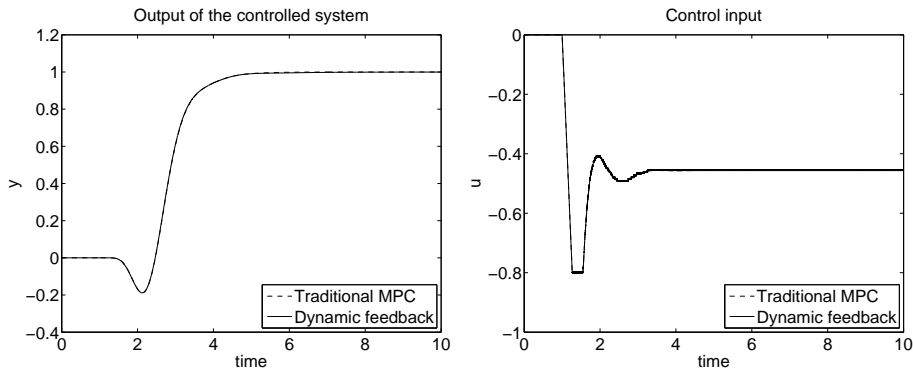


Figure 3.6: Simulation of the dynamic feedback Model Predictive Controller discretized with a very high sampling frequency. α is also chosen large. For comparison, an implementation of a traditional MPC is shown as dotted line.

11 poles and 2 zeros in the left half plane, and one zero in the right half plane. The pole-zero map is shown in Figure 3.5.

For use as internal model in the MPC, the model should be discretized and transformed to a state-space form. The sampling time is here taken as $\Delta T = 0.1$.

The control input is constrained by both a range and a rate limit, which apply for each component of \tilde{u} :

$$\begin{aligned} u_{max} &= 0.8 \\ \dot{u}_{max} &= 3 \end{aligned} \tag{3.36}$$

The tuning of the MPC is not the primary objective of this Section. Moreover, it might be of interest to show that the controller is able to deal with large horizons. So the following parameters are taken: control horizon $N_u = 20$, prediction horizon $N_p = 40$, and identity matrices for Q_y and Q_u .

In the simulation, the initial state of the process is $x_0 = [0, 0]$ and a step output reference is asked after 1 second. Note that in this setup, the controller is not aware of the change in set-point before it actually takes place. This precisely happen when a human operator set in real-time the reference of the controller.

For comparison purpose, the MPC is implemented both using traditional optimization techniques and the new hybrid feedback. The traditional version relies on the solver QuadProg in Matlab. The response is given by the dotted lines. The feedback system (3.35) is tuned using first a large and then a small α . In the case of the large α , 3 sampling frequencies are compared.

The first simulation gives a case that should be very close to the continuous version. To this end, the sampling frequency is taken very high: $\Delta t = 0.001$. In order to make sure that the controller will be reactive enough to fully exploit the actuators, a large value is taken for α : $\alpha = 100$. The results are shown in Figure 3.6. The results are extremely close compared to the traditional MPC. The desired steady-state is reached in the same time and the constraints are perfectly respected. This seems really promising.

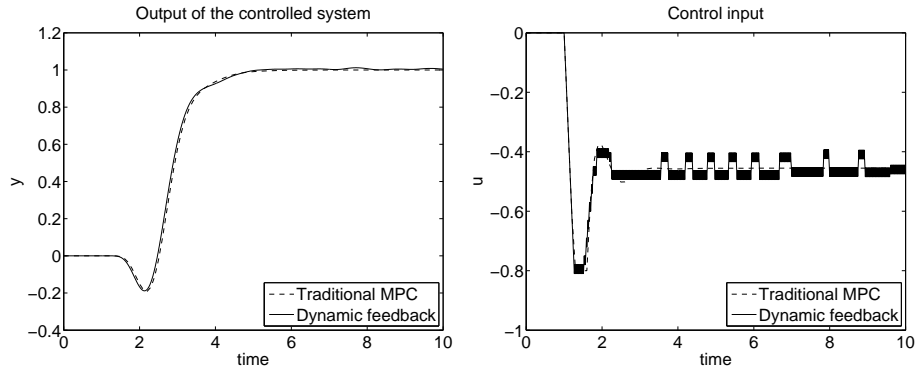


Figure 3.7: Simulation of the dynamic feedback Model Predictive Controller discretized with a 10 times longer sampling period. α is still large. Oscillations appears when a constraint is reached and near the steady-state.

Then the sampling frequency of the controller is decreased and a 10 times larger sampling period is taken $\Delta t = 0.01$. The plots are displayed in Figure 3.7. As it was expected, oscillations appears in the control input during a sliding mode, i.e. when a constraint is reached, and when the minimum of the cost function is reached, i.e. near the steady-state. However, the global behaviour is still close to the traditional optimization.

To investigate further the influence of the sampling frequency of the controller, the sampling time is again multiplied by 10 to reach $\Delta t = 0.1$. As can be seen in Figure 3.8, the oscillations are larger; which had to be expected. A small steady state error appears because the oscillations are not symmetric compared to the steady-state control input. But the trajectory remains close to the desired one. So it can be concluded that the sampling time influences the oscillations and the steady-state value, while it also directly influences the computation complexity.

From the equation defining the controller (3.35), it can be understood that α has a large influence on the size of the oscillations. To show this, the same simulation with a large sampling period $\Delta t = 0.1$ is repeated with an α much smaller: $\alpha = 0.01$. Figure 3.9 show the results. It can be noticed that the oscillations have been completely removed and that the steady-state error has completely disappeared; but at a cost of a slower response. Therefore, a good tuning of α or even an adapting value could improve largely the method.

Furthermore this method allows, similarly to traditional MPC, the expression of output constraints. This is done by including the internal model in the computation of the constraint set. For linear systems, the predicted outputs \tilde{y} can be computed using two time-invariant prediction matrices P_x and P_u and the equation

$$\tilde{y}(t) = P_x x(t) + P_u \tilde{u}(t) \quad (3.37)$$

It is then possible to guarantee that y will stay above a minimum value y_{min} by

3.5. APPLICATION TO MODEL PREDICTIVE CONTROL

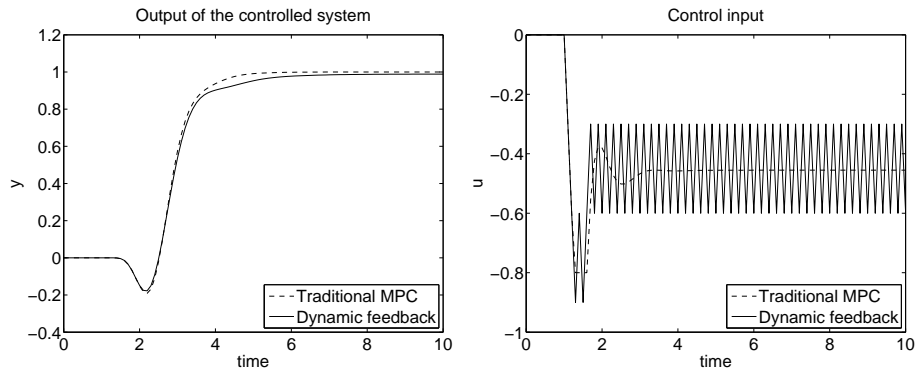


Figure 3.8: Simulation of the dynamic feedback Model Predictive Controller discretized with an again 10 times longer sampling period. α is still large. The oscillations becomes even larger and a steady-state error appears but the behaviour of the system is still globally correct.

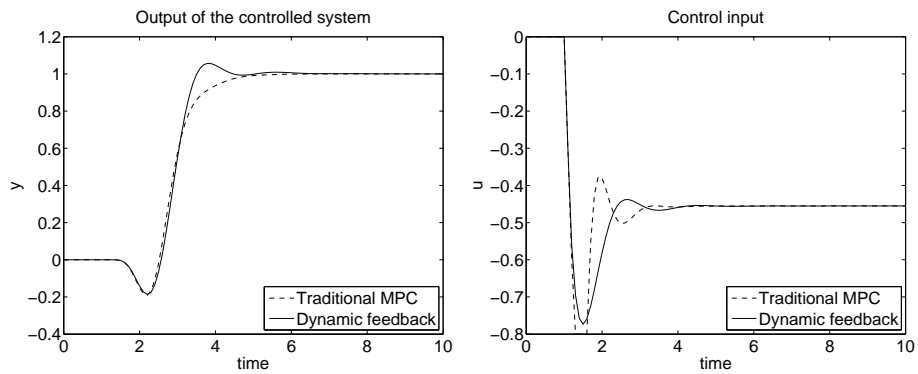


Figure 3.9: Simulation of the dynamic feedback Model Predictive Controller discretized with the same long sampling period; but α is now chosen very small. Oscillations and steady-state error completely disappear but the response is slower.

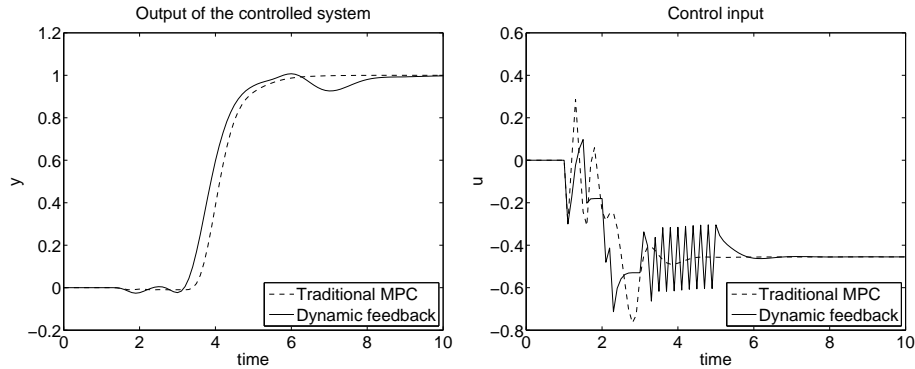


Figure 3.10: Simulation of the dynamic feedback Model Predictive Controller with output constraints $y_{min} = -0.01$. The controller is discretized with a long sampling period $\Delta t = 0.1$. α has been chosen large at the beginning to rapidly steer the system and respect the constraint; and is decreased after 5 seconds to cancel out the large oscillations. The constraint is well respected and the global behaviour is really good compared to a traditional MPC.

using the state-dependent constraints

$$g(\tilde{u}, x) = -P_u \tilde{u} - P_x x + y_{min} \leq 0 \quad (3.38)$$

For the same system described by the pole-zero map of Figure 3.5, the output constraint $y_{min} = -0.01$ is added to the previous input constraints (3.36). The results of the simulation are shown on Figure 3.10. It can be seen that the undershoot is removed. With a good tuning of α , the results are comparable to traditional MPC. However, the choice of α seems to be more critical than before. In case of a too low α , the controller is not reactive enough to steer the system properly at the beginning to respect the constraint. On the other hand, a too large α induces large oscillations near the steady-state. In this simulation, the value of α is decreased after 5 seconds so that both fast response and small oscillations are achieved. This shows the need for an adaptive scheme for α , which is left for future work. So it has been shown that output constraints can be handled by this control method.

3.6 Application to Control Allocation

In many applications, like Global Chassis Control or Flight Control, many actuators can act on the same degree of freedom. Such systems are called over-actuated. If the linear state-space system

$$\dot{x} = Ax + Bu \quad (3.39)$$

$$y = Cx \quad (3.40)$$

is considered, over-actuation means that B is not full-rank. In other words, there are many input $u(t)$ that gives the same state trajectory $x(t)$.

Traditional control methods usually have difficulties to deal with over-actuated systems. First because of the impossibility to invert the system. And secondly because over-actuated systems often come with tight actuation constraints, which justifies the large number of parallel actuators. Traditional control methods are easier to apply to a system with a limited number of virtual inputs v rendering the new virtual input matrix B_v full rank.

The problem of finding the real control input u that matches the virtual input v :

$$Bu = B_v v \tag{3.41}$$

is called Control Allocation [16, 57].

Many methods have been presented in the literature to mathematically formulate and solve control allocation problems. Good references can be found in [16] and [57]. An interesting way of formulating the problem is to write it in the form of an optimization [21] with a cost function q weighting the use of each actuator, and constraints representing the actuator limitations. Most of the optimization based allocation techniques are computing the precise solution at each time step. This can easily be implemented using traditional optimization techniques. However, this might not be the most suitable for this kind of problems.

As described in Section 2.5.2, allocation present particularities compared to traditional optimization:

- The desired virtual input v is constantly changing, which requires u to be continuously updated.
- Constraints might rapidly pop in and out depending on the detected limitations.
- Since the speed of the actuators is limited, it is not necessary to know the final optimum as long as the system is converging at maximal speed towards it.

Therefore, u could be seen, not as a variable to be optimized over and over again, but as a variable continuously updated over time. This can significantly reduce the computational complexity while a high level of performance is maintained.

The Hybrid Descent Method is suitable for implementing such continuous optimization. Another comparable method has been developed by Johansen [63]. The methods differ in the way they handle the constraints. The Hybrid Descent Method introduces the equality constraints in the cost function and uses the inequality constraints to define the feasible set, while [63] does the opposite: the inequality constraints are included in the cost function using barriers while the equality constraints define the acceptable region. Furthermore, in [63] the Lagrange multipliers are computed explicitly and need to be adapted on-line, while in the Hybrid Descent Method they are not computed but come as a by-product of the sliding mode. Both methods have stability and convergence proofs available.

When using the Hybrid Descent Method for control allocation, the controlled

system keeps a state-space form:

$$\dot{x} = Ax + Bu \tag{3.42}$$

$$y = Cx \tag{3.43}$$

$$\dot{x}_c = A_c x_c + B_c y \tag{3.44}$$

$$v = C_c x_c + D_c y \tag{3.45}$$

$$\dot{u} = f(u, v, u_{max}) \tag{3.46}$$

where (3.42)-(3.43) is the original system, (3.44)-(3.45) is the controller providing the virtual input v and (3.46) is the allocation controlling the real input u . The notation u_{max} is used as a generic way to express the constraints.

As in the case of MPC, see section 3.5.2, the actuator output and rate constraints are handled in a different way. Output constraints are used to define the feasible set in f , which generates switching. Rate constraints are used to saturate f .

The Hybrid Descent Method is used to implement the control allocation in the Global Chassis Control example and simulation in Chapter 2.

3.7 Conclusion

A hybrid system implementing a convex optimization algorithm has been presented. The main idea is to follow the steepest descent direction of the objective function in the feasible set and of the constraints in the infeasible set. The continuous hybrid system guarantees that its trajectory enters the feasible set of the related optimization problem and next converges asymptotically to the set of optimal points. Furthermore, practical implementation, using smooth transitions or discretization, has been discussed. Smooth transitions can slightly decrease the accuracy while discretization introduced chattering.

In this chapter, global asymptotic convergence has been proven for the class of time-invariant convex problems. In case of non-convex problems, the convergence can still be assured towards a local optimum. However, nothing guarantees that the global optimum is attained. In case of time-varying optimization problems, it can be expected that the trajectory asymptotically tracks the time-varying optimal point. This is confirmed in the simulations of Chapter 2.

It can also be noted that the gradient of a function is not its only descent direction. Other directions have been proposed in the literature, like Newton's direction [21]. The investigation of alternative directions to improve the convergence while limiting the increase of computation complexity is left for future work. Furthermore, various way of handling constraints exist in optimization algorithms. While interior point methods are suitable for providing very accurate solution using logarithmic barriers, this method has the advantage to have descent directions also defined outside the feasible set. This is particularly useful if constraints are allowed to change over time.

The scope of application of this kind of method will not be in the off-line optimization arena. However, in particular for on-line applications, this method is of interest. This is because of its implementation as a dynamical system, its simplicity, its low computation cost, and its capacity to be implemented in discrete-time. In particular,

3.7. CONCLUSION

the method has been applied to Model Predictive Control and Control Allocation. Possible domains where the method could also be applied include Iterative Learning Control, Adaptive Control, on-line System Identification, and all other domains where cost functions have to be continuously minimized under constraints.

Part II

Braking Control



Chapter 4

ABS based on Wheel Acceleration

In collaboration with CNRS/Supelec, Paris, France.

In this chapter, the 5-phase hybrid ABS algorithm presented in [96] is improved and validated in tyre-in-the-loop experiments. This algorithm belongs to the class of hybrid ABS, see Section 1.3. In previous work, the algorithm was theoretically studied using a basic wheel model, and the theoretical limit cycle was analyzed. Conclusions could be drawn on how to tune the algorithm to achieve the best limit cycle and on the resulting performances.

Unfortunately, the original algorithm is not robust to the actuation delay present in practice and fails the experimental validation. In this work, three methods to deal with delays are developed and validated.

The most common ABS algorithm running on production vehicles is commercialized by Bosch [18]. This algorithm also belongs to the class of hybrid ABS based on wheel acceleration and is comparable to the 5-phase ABS. As the exact commercial algorithm is secret, a precise comparison is impossible. However, this chapter strives at illustrating resemblances and differences.

Outline

The simplified model used in [96] is presented in Section 4.1. The modelling of the relevant phenomena for experimental implementation is described in Section 4.2. The theoretical algorithm derived in [96] is recalled in Section 4.3 and the systematic tuning is addressed. The influence of the time delay on the brake actuation being very important, the theoretical algorithm had to be adapted and three possible modifications are described in Section 4.4. Results from the experimental validation are analysed in Section 4.5, where limit cycles close to the ones expected from theory and simulation are obtained. In Section 4.6, the algorithm is compared to the commercial ABS implemented by Bosch.

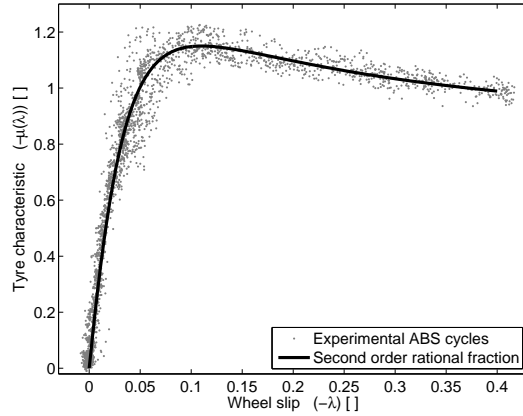


Figure 4.1: Measurement and fitting of the nondimensional tyre characteristic $\mu(\cdot)$ for the tyre-in-the-loop facility. The maximum braking force is achieved with a longitudinal slip of 10%.

4.1 Simplified modelling

The development of the five-phase algorithm presented in Section 4.3 is based on a simplified single-wheel model. Only the longitudinal dynamics of a single loaded wheel is considered. Even though weight transfer and combined slip are ignored, all the basic phenomena related to ABS already appear in this very simple model. Moreover, the limit cycles predicted by this model (Figure 4.7) are already quite close to those obtained with more realistic models (Figure 4.8) or in experiments (Figures 4.9 and 4.10).

4.1.1 Wheel speed dynamics

The angular velocity ω of the wheel has the following dynamics:

$$I\dot{\omega} = -RF_x + T, \quad (4.1)$$

where I denotes the inertia of the wheel, R its radius, F_x the longitudinal tyre force, and T the torque applied to the wheel.

The torque $T = T_e - T_b$ is composed of the engine torque T_e and the brake torque T_b . We will assume that during ABS braking the clutch is open and thus neglect the engine torque. Moreover, we will assume that the brake torque is given by

$$T_b = \gamma_b P_b, \quad (4.2)$$

where P_b denotes the brake pressure and γ_b the brake efficiency, see Section 4.2.4.

4.1.2 Tyre force modelling

The longitudinal tyre force F_x is often modelled by a relation

$$F_x(\lambda, F_z) = \mu(\lambda)F_z. \quad (4.3)$$

That is, by a function that depends linearly on vertical load $F_z > 0$ and nonlinearly on wheel slip λ

$$\lambda = \frac{R\omega - v_x}{v_x}, \quad (4.4)$$

where v_x is the longitudinal speed of the vehicle. Note that the slip is positive when driving and negative when braking. Wheel lock corresponds to a slip $\lambda = -1$. It can be observed that this definition of slip shows a singularity at zero vehicle speed. Other ways of defining the slip allow to deal with this issue, see Section 4.2.5.

The nondimensional tyre characteristic $\mu(\cdot)$ is an odd function such that $\mu(0) = 0$ and $\mu'(0) > 0$ (see Figure 4.1). It is important to stress that this curve presents a peak at $\lambda = \lambda^*$ so that $\mu'(\lambda^*) = 0$. The part of the curve $|\lambda| < \lambda^*$ with a positive slope $\mu' > 0$ is called the “stable zone” of the tyre while the other side of the peak with $|\lambda| > \lambda^*$ and $\mu' < 0$ is called the “unstable zone”. This denomination comes from the stability analysis of the single-wheel model.

Several mathematical formulas have been used to describe this curve. Trigonometric functions are used in [95], exponentials in [27], and second order rational fractions in both [71] and [96]:

$$\mu(\lambda) = \frac{a_1\lambda - a_2\lambda^2}{1 - a_3\lambda + a_4\lambda^2}, \quad \text{for } \lambda \leq 0. \quad (4.5)$$

The important point is that all this mathematical formulas use coefficients that depend on tyre characteristics, road conditions, tyre pressure, temperature, etc. However, in order to be robust, the ABS algorithm cannot assume these coefficients to be a priori known. Formulas on how to relate the a_i coefficients of (4.5) to more common features like the slope at the origin or the position of the peak can be found in [96]. The particular tyre characteristic identified on the test bench and used in simulation is parametrized as follows: $a_1 = 36$, $a_2 = 217$, $a_3 = 13$ and $a_4 = 271$. Figure 4.1 shows the measurements and the fitted curve.

One advantage of using rational fractions to model the tyre characteristics is that its slope can easily be computed analytically. In particular, we have

$$\mu'(\lambda) = \frac{d\mu}{d\lambda} = \frac{a_1 - 2a_2\lambda + (a_2a_3 - a_1a_4)\lambda^2}{(1 - a_3\lambda + a_4\lambda^2)^2} \quad (4.6)$$

4.1.3 Wheel slip and wheel acceleration dynamics

In this subsection, the equations describing the evolution of wheel slip and wheel acceleration are derived. It should be noted that other wheel deceleration models have been proposed in the literature [90, 91, 117].

The vehicle is supposed to brake with the maximal constant deceleration a_x^* allowed by road conditions, which is $a_x^* = -\mu(\lambda^*)g$. In other words

$$\dot{v}_x = a_x^*. \quad (4.7)$$

Moreover, the tyre load F_z will be assumed to be constant.

If we define the wheel slip offset and the wheel acceleration offset by

$$\begin{aligned}x_1 &= \lambda - \lambda^* \\x_2 &= R\dot{\omega} - a_x^*,\end{aligned}$$

we obtain the following system:

$$\dot{x}_1 = \frac{1}{v_x} (x_2 - (\lambda^* + x_1)a_x^*) \quad (4.8)$$

$$\dot{x}_2 = -\frac{a}{v_x} \bar{\mu}'(x_1) (x_2 - (\lambda^* + x_1)a_x^*) + u, \quad (4.9)$$

where

$$a = \frac{R^2}{I} F_z \quad \text{and} \quad u = \frac{R}{I} \dot{T}. \quad (4.10)$$

The function $\bar{\mu}(\cdot)$ is defined as

$$\bar{\mu}(x) = \mu(\lambda^* + x) - \mu(\lambda^*), \quad (4.11)$$

and thus represents the tyre characteristics with the peak at the origin.

4.2 Modelling practical phenomena

The simplified model, presented in Section 4.1, is not sufficient to explain the behavior observed during experiments. The modelling of five additional effects is required and treated in the following subsections. Since the experimental validation has been carried out on a laboratory test rig, see Section 1.3.2, the detailed modelling focusses on the test rig phenomena. Nevertheless, it is important to stress that most issues appearing on the experimental setup also appear on a real vehicle.

4.2.1 Oscillations in measurements

When the tyre is rolling, oscillations can be seen in all measured signals. Longitudinal and vertical forces, as well as wheel speed and wheel acceleration are perturbed. In our lab, such oscillations are periodic, with a period of one wheel rotation, which can be seen on Figure 4.2. One plausible explanation originates from the difference in tyre properties along its circumference. Possible variations in wheel diameter, rubber carcass/belt-stiffness, tread wear, etc. can lead to load variations. This will have a direct impact on the longitudinal and lateral forces generated in the contact patch, and therefore indirectly on the wheel speed and the wheel acceleration. On a real vehicle, the road irregularity will also contribute to the load variations, resulting in a more random pattern of oscillations. Such oscillations need to be taken into account since they can trigger control intervention at inappropriate moments. Those disturbing oscillations will not often introduce noise in the cycle and prevent the appearance of a constant limit cycle. Still, a surprising conclusion is that a constant ABS cycle can appear in case of periodic disturbing oscillations. This phenomenon is visible both in simulation and in practice and will be theoretically studied in a future work.

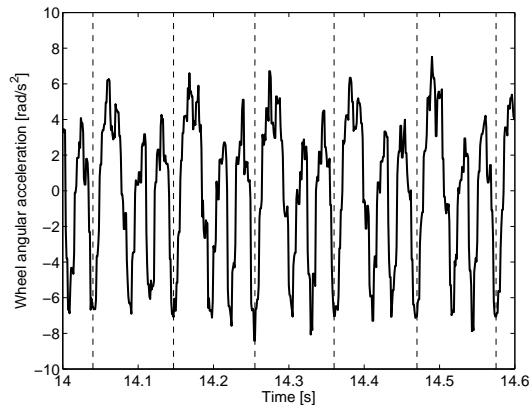


Figure 4.2: Oscillations measured on the wheel acceleration signal during free rolling at about 18m/s. The vertical lines indicate one wheel rotation and a clear periodicity can be concluded.

4.2.2 Wheel acceleration

The wheel acceleration signal is not directly available and should be computed from the wheel angular encoder. The encoder signal is composed of a series of pulses sent when one of the teeth of the encoder passes in front of the hall sensor.

It is common to reconstruct the wheel speed from the encoder signal. Two methods are often used [113, 32]. At low rotational speed, the best technique is to measure the time difference between two pulses. At high speed, it becomes more accurate to count the number of pulses received within a small time interval. The speed at which one should switch from one method to the other depends on the speed of the internal clock of the electronics used to measure the time difference, the sampling rate, and the number of teeth on the encoder.

It is well known that taking the time derivative of a noisy signal considerably amplifies its noise level. Therefore, computing the wheel acceleration by differentiating the reconstructed speed signal amplifies high frequency noise and should be avoided.

Instead of taking a time derivative, we use a linear regression on the raw encoder pulsed signal in order to fit a parabola to the time/displacement measurements (see Figure 4.3). The second time derivative can then be calculated analytically, introducing less noise than with numerical differentiation [34].

4.2.3 Brake pressure dynamics

The hydraulic line and the servo-valve used to control the pressure in the disk brake limit the performance of the actuation. In a first approximation, the controlled valve will introduce a second-order dynamics and a flow rate limit, and the hydraulic line a transport time delay between the desired and the actual brake pressure. Taking those effects into account is of first importance for designing a working ABS system.

A rough identification of the characteristics gives: a pure time delay $\Delta t = 7 \text{ ms}$,

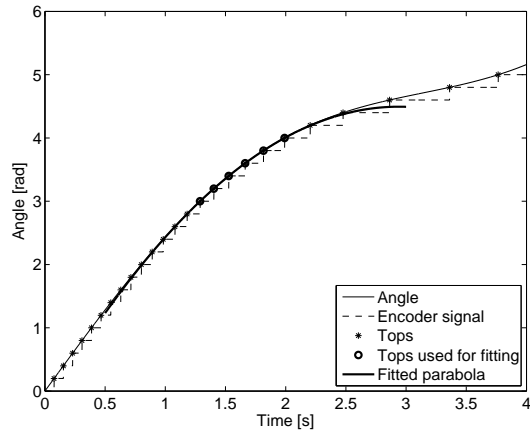


Figure 4.3: Linear regression on the wheel encoder pulsed signal. Pulses are sent at constant displacement and the incoming time is measured. Fitting a line provides speed information while fitting a parabola also provides average acceleration.

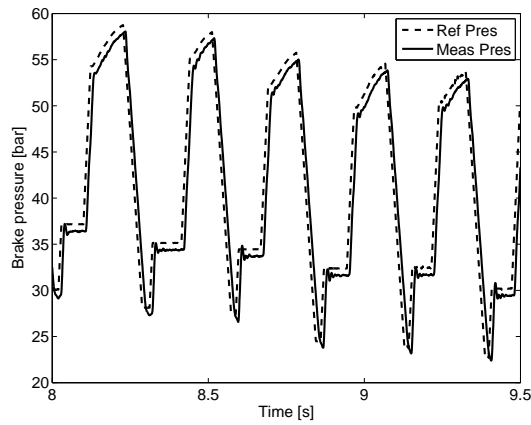


Figure 4.4: The measured brake pressure follows the reference pressure with a delay and a second order dynamics.

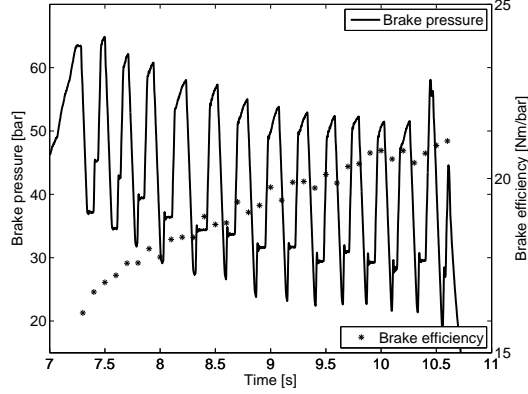


Figure 4.5: Variation of the brake pressure and brake efficiency during braking. The efficiency increases by about 30 % because of the temperature changes. ABS controllers need to be robust to this effect.

a pressure rate limit between $r_{max} = +750 \text{ bar/s}$ and $r_{min} = -500 \text{ bar/s}$, and a second-order dynamics with a cut-off frequency of 60 Hz ($\omega = 120\pi$) and a damping factor $\xi = 0.33$. Therefore (assuming that $P_{act}(0) = 0$ and $\dot{P}_{act}(0) = 0$), the actual pressure P_{act} is driven by the following differential equation

$$\dot{P}_{act}(t) = \max \left(\min \left(\omega^2 \int_0^t (P_{ref}(t - \Delta t) - P_{act}(t)) dt - 2\xi\omega P_{act}(t), r_{max} \right), r_{min} \right). \quad (4.12)$$

If, for simplicity, one imposes to model the brake pressure dynamics with only a single pure time delay then the best equivalent time delay is 10 ms . The difference between the reference and the actual brake pressure is shown on Figure 4.4. The small constant offset between these two variables comes from the drift in the piezoelectric pressure sensor and from the analog pressure control.

4.2.4 Brake efficiency

The brake efficiency γ_b in Equation (4.2) is changing during braking depending on the brake temperature. In general, the efficiency increases with the temperature, up to a certain level where fading starts and friction drops rapidly. This means that the ABS algorithm needs to be robust to changes in the brake properties. During a heavy braking on the test bench, the gain γ_b will typically increase by 30 % in only 4 seconds. Figure 4.5 illustrates the evolution of the brake pressure and the brake efficiency during one test where the brake torque is kept within the same range. It can be noticed that the pressure required decreases over time while the brake efficiency increases by 30 %.

4.2.5 Relaxation length

Work on tyre identification like [95] and [125] has shown that the force response of the tyre to various external inputs shows a lag in time. Since hybrid ABS controllers specify very abrupt references to brakes actuators, and thus generate a highly dynamic tyre response, such an effect must necessarily be taken into account.

The fact that tyre deflections (of side walls, carcass and rubber tread) have to build up before the force is created calls for a model containing carcass compliance. A convenient method for modelling the transient tyre behavior [125, 86] is to filter the wheel slip

$$\sigma(\lambda)\dot{\lambda} + |v_x|\lambda = R\omega - v_x.$$

In [125], the relaxation length σ is found to decrease with the tyre slip λ , to finally reach zero at the top of the tyre characteristics. Due to the open-loop testing of tyre slip curves, Zegelaar obtained his results in the stable zone only.

The typical manifestation of the tyre relaxation effect can be seen on the last plot of Figure 4.9. For the tyre in the stable zone ($\lambda < \lambda^* = 0.1$), the slip-force trajectory is not the same when increasing or decreasing the force. In particular, the force response describes an hysteresis loop: a steeper force slope can be observed during slip decrease and a more gradual slope for slip increase. In this work, the relaxation length at zero slip is roughly $\sigma(0) = 0.1$ m, which is a standard value for the moderate load applied on the test rig.

4.3 The theoretical algorithm

For ABS regulation of (4.8)-(4.9), the control objective is to keep the unmeasured variable x_1 in a small neighborhood of zero, with a control u only based on the wheel deceleration $\dot{\omega}$ or an equivalent signal.

Theoretically, in the phase plane, the origin $(0, 0)$ is optimal for having the shortest braking distance and good steerability, as $x_1 = 0$ gives the peak of the tyre characteristics. With the cycling, the objective is to stay as close as possible to $(0, 0)$. Any variation in x_1 will make the average brake force to decrease, while variations in x_2 will require a heavier work from the brake actuator. Therefore, the size of the limit cycle is a measure for performance. Still, to robustly detect the position of the peak and reject measurement noise, the size of the limit cycle can never be reduced to zero.

4.3.1 The five-phase hybrid control strategy

When a hybrid control law (based on a discrete state) is used in order to control a continuous dynamical system, the closed-loop system results in a hybrid automaton. We refer the reader to [83] for a general introduction to hybrid systems; and to [96] for a detailed analysis of the particular case of ABS hybrid automata.

The hybrid automaton of the ABS regulation logic, similar to the one in [96] and [2], is described on Figure 4.6. All parameters ϵ_i and u_i in the automaton are positive. Each of the five phases of the algorithm defines the control action T_b that should be applied to the brake. Events based on the measure of wheel acceleration

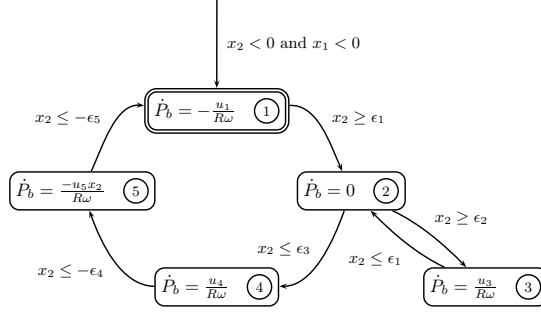


Figure 4.6: The five-phase ABS automaton.

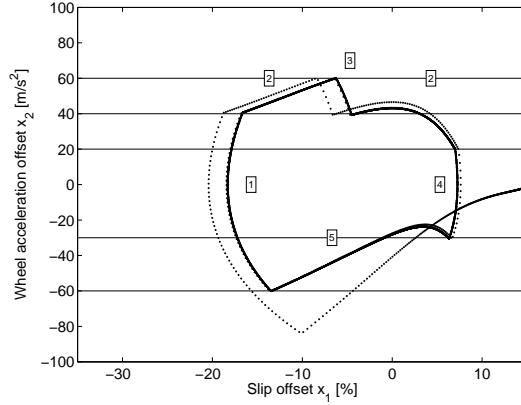


Figure 4.7: Limit cycle obtained when the theoretical five-phase algorithm of Section 4.3 is applied to the simplified model of Section 4.1. The numbers refers to the different phases of the automaton of Figure 4.6.

trigger phase switches. The cycling between the different phases generates a repetitive trajectory. If the tuning parameters are chosen properly, on a simplified model, this repetitive trajectory will be a non-smooth limit cycle, like the one presented in Figure 4.7.

A general interpretation of the algorithm is as follows. When the tyre enters the unstable zone ($x_1 < 0$), the resulting force drop will cause the wheel to start locking. When the acceleration crosses $-\epsilon_5$, phase 1 is triggered. During phase 1, the pressure is quickly reduced to change the sign of the wheel acceleration and let the wheel spin again. Phase 1 is so short that both the wheel slip and the tyre force can be considered to remain constant, so the change in acceleration is only determined by the change in brake torque. When the pressure has been decreased enough to make $\dot{x}_1 > 0$, phase 2 is triggered. During phase 2, the torque is kept constant so that the wheel acceleration is only influenced by the changes in brake force. With $\dot{x}_1 > 0$, the force

will first increase, go over the maximum at $x_1 = 0$ and then decrease again. This last decrease forces the acceleration to cross ϵ_3 which marks the return of the tyre in the stable zone. To make sure that the acceleration will never get too large and exceed ϵ_2 , phase 3 can be shortly triggered to increase the brake pressure a bit and reset the acceleration to ϵ_1 . When the tyre is back in the stable zone, the brake pressure should be increased, otherwise the brake force would remain far below the maximum. This is the purpose of phase 4, which is the opposite of phase 1. When the acceleration is less than $-\epsilon_4$, which ensures $\dot{x}_1 < 0$, phase 5 is triggered and the torque is kept constant until wheel lock tendency is detected. Phase 1 is then triggered again and the cycle starts over. Note that to enable the detection of wheel lock at a lower slip, the torque can be increased slowly during phase 5 instead of being kept constant [2].

It should be pointed out that the control law does not require the knowledge of λ^* or the tyre parameters a_i to be implemented. Furthermore, it is possible to observe x_2 in practice by estimating a_x^* online based on accelerometer signal and average brake pressure. The robustness towards uncertainties on a_x^* can be improved by increasing the thresholds ϵ_i .

4.3.2 Tuning of the algorithm

In order to tune the five-phase ABS algorithm, nine parameters need to be chosen: the wheel deceleration thresholds ϵ_i and the brake pressure derivatives u_i . The theoretical study of the limit cycles performed in [96] gives a good basis and clear rules to get an initial parameter set. The modelling of the experimental phenomena in Section 4.2 also allows for a systematic tuning.

Theoretically, the first choice is taking symmetric thresholds: $\epsilon_5 = \epsilon_1$ and $\epsilon_4 = \epsilon_3$. Nevertheless, in practice, several phenomena related to the delays impose taking slightly asymmetric thresholds in order to improve performance. The oscillations in the measurements discussed in Section 4.2.1 can trigger control intervention at inappropriate moments. There are two ways to deal with these oscillations in our algorithm: the first is to choose large enough thresholds so that only significant variations in the acceleration signal are detected; the second is to filter the acceleration signal to remove undesired high frequent noise. During testing, a compromise was chosen between both methods. The acceleration signal is averaged on 1/10 of the wheel rotation. At 18 m/s , the delay introduced due to filtering is about 5 ms . With this filtering, peak to peak oscillations of 4 m/s^2 can still be observed. Therefore, the thresholds ϵ_i are separated by 20 m/s^2 to avoid mistriggering. In the experiments, the values $\epsilon_1 = 40$, $\epsilon_2 = 60$, $\epsilon_3 = 20$, $\epsilon_4 = 30$ and $\epsilon_5 = 60$ m/s^2 were set.

Ideally, the brake pressure variations should be as quick as possible in order to produce the smallest possible limit cycle. Therefore, the maximum brake pressure derivatives allowed by the brake actuator were taken for the rates u_i . That is, we took $u_1/R\omega = 500$ bar/sec and $u_i/R\omega = 750$ bar/sec for u_3 and u_4 , which is coherent with the actuator parameters given in Section 4.2.3.

The choice of u_5 is more delicate. If too small values of u_5 are taken, the cycle amplitudes are quite big and thus the performance is bad. If too big values of u_5 are taken, the algorithm becomes quite sensitive with respect to delays and the wheel might lock or remain trapped in the stable zone of the tyre. A good compromise

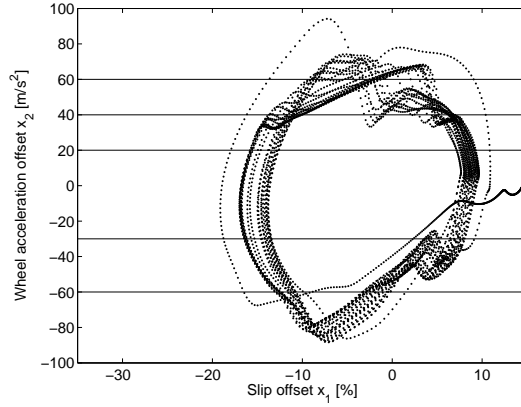


Figure 4.8: Limit cycle obtained when the modified algorithm of Section 4.4.2 is applied to a model that reproduces the issues of Section 4.2.

seems to be $-u_5 x_2 / (R\omega) = 50 \text{ bar/sec}$, typically one order of magnitude less than quick pressure variations.

The limit cycle obtained with this specific tuning, when the five-phase algorithm is applied to the simplified model of Section 4.1 is shown on Figure 4.7.

4.4 Modified algorithms

When implemented on the test bench, the theoretical version of the five-phase algorithm presented in Section 4.3 fails to cycle and remains blocked in an arbitrary phase. The delays, due to measurement filtering, tyre dynamics, and actuator limitations, have been identified to be the main cause of failure. Therefore, the theoretical algorithm needs to be improved to become more robust with respect to delays. Three methods are proposed, analyzed and validated. All delays are lumped in a single global actuation delay.

4.4.1 Pressure derivative profiles

In order to reduce the influence of delays, a first approach is to slow down the pressure increase or decrease of phases 1, 3 and 4 before the wheel acceleration x_2 actually reaches the switching threshold ϵ_i .

Many pressure derivative profiles could be used to this end. The following sigmoid is proposed:

$$\dot{P}_i(x_2) = \frac{1}{2}(\dot{P}_i^a + \dot{P}_i^b) + \frac{1}{2}(\dot{P}_i^b - \dot{P}_i^a) \tanh(k_i(x_2 - \bar{\epsilon}_i)), \quad (4.13)$$

where \dot{P}_i^a and \dot{P}_i^b are the brake pressure derivatives at the beginning and end of the phase and $\bar{\epsilon}_i$ is the transition point. This sigmoid allows for a fast response of the system at the beginning of the phase, since the maximum pressure rate allowed by the

brake is used, while having a smooth transition at the end, since a smaller pressure rate is used.

Theoretically, with a well chosen $\bar{\epsilon}_i$, it could be possible to take $\dot{P}_i^b = 0$, which would completely compensate the influence of the delay. Such a choice might, however, harm the robustness of the algorithm, since the regulations could remain blocked in one phase. In practice, keeping \dot{P}_i^b slightly positive or negative is a more robust choice.

The main advantage of this approach, based on pressure derivative profiles, is that it can compensate delays while remaining robust with respect to other effects like changes in brake efficiency. The main disadvantage is that this modified algorithm is more difficult to tune because it involves more parameters, which depend on the value of the delays and on the vehicle velocity.

4.4.2 Open-loop pressure steps

A different approach, that also reduces the influence of delays, is to pre-compute (using the wheel acceleration model) the discontinuous brake pressure variation that will make the wheel evolve from the current acceleration to the desired one. Theoretically, in order to obtain an acceleration step of magnitude

$$\Delta x_2 = x_2(t_0^+) - x_2(t_0^-) \quad \text{at } t_0,$$

a brake pressure step of magnitude

$$\Delta P = \frac{I}{R\gamma_b} \Delta x_2 \quad (4.14)$$

should be applied to the system, where γ_b is the brake efficiency defined in Equation (4.2).

But, in practice, real brake actuators are not able to follow such a discontinuous brake pressure variation and a rate limit must be added. Moreover, asymmetry in the brake torque response requires small adjustments on ΔP .

The main advantages of this method is that it is intrinsically robust with respect to time delays and that it gives limit cycles that are close to those predicted by the theoretical algorithm. The cycles given by this controller, when practical phenomena are simulated, are shown on Figure 4.8. The main disadvantage of the method is that it requires a good internal model, which makes it less robust with respect to model uncertainties, like brake efficiency variations and other changes of brake actuator parameters.

It is important to stress that this method is better suited for brake actuators that follow a pressure or a torque reference (instead of a pressure rate); and that it might be cumbersome to implement it on vehicles equipped with hydraulic brakes without using brake pressure sensors.

4.4.3 Closed-loop acceleration control

A third approach is to manage the jumps, from the current wheel acceleration to the desired one, in closed-loop. During phases 1, 3 and 4, the torque is modified in

order to obtain a wheel acceleration that reaches smoothly its target value ϵ_i , which enables the algorithm to switch to the next phase. During these phases, the closed-loop control operates around a precomputed trajectory x_2^{ref} . Phases 2 and 5 are left untouched.

The reference trajectory x_2^{ref} is made such that it goes as fast as possible from the current wheel acceleration x_2 to the next switching threshold ϵ_i , but with a limited rate that changes with x_2 . There are two reasons to limit \dot{x}_2^{ref} . Firstly, it is important to have a reference that remains within the physical limitations of the brake actuator described in Section 4.2.3. Secondly, the sensitivity to the delay is proportional to the rate of change of x_2 at the end of the phase. Therefore, it is natural to reduce \dot{x}_2^{ref} to zero when x_2^{ref} approaches ϵ_i , in order to minimize this sensitivity.

Inspired by the velocity profiles used for servo-drives [76], we will take a reference trajectory x_2^{ref} such that

$$\dot{x}_2^{ref} = \begin{cases} -\text{sign}(e)\sqrt{2u_0|e|} & \text{if } \sqrt{2u_0|e|} < v_0 \\ -\text{sign}(e)v_0 & \text{if } \sqrt{2u_0|e|} \geq v_0 \end{cases} \quad (4.15)$$

with $e = x_2^{ref} - \epsilon_i$. The constant v_0 is the maximal first derivative for x_2^{ref} and u_0 its maximal second derivative.

Once the reference x_2^{ref} fixed, the controller is made of a simple proportional feedback

$$\dot{P}_b = K(x_2^{ref} - x_2).$$

The gain K should be taken big enough in order to track correctly the reference, but is limited by the delay margin of the system.

The main advantage of this method is that only a limited number of parameters need to be tuned. Furthermore, the parameters do not need to be scheduled with the vehicle speed. Also, the same trajectory generator and controller can be used in all phases, with the same parameters. Thanks to the feedback, the method is robust to any change in the environment. The authors believe that, among the three methods they have tested, this last method is the most interesting one if we compare practical implementation issues.

4.5 Experimental validation

The three methods rendering the algorithm more robust to time delays presented above have been tested on the tyre-in-the-loop test facility of Section 1.3.2 and give the expected satisfying results. Thanks to the precise modelling of the test bench phenomena, the experimental tests are very similar to the simulations. As optimal performance was not the final aim, only a reasonable effort was put on optimizing the tuning, and all tests were done at a constant vehicle speed. To limit the thermal load on the brake system, the experiments were deliberately performed with a small vertical load of 3000 N.

4.5.1 Pressure derivative profiles

Experimental testing shows that the ABS controller based on pressure derivative profiles works well in practice. Measurements are plotted on Figure 4.9. It can be

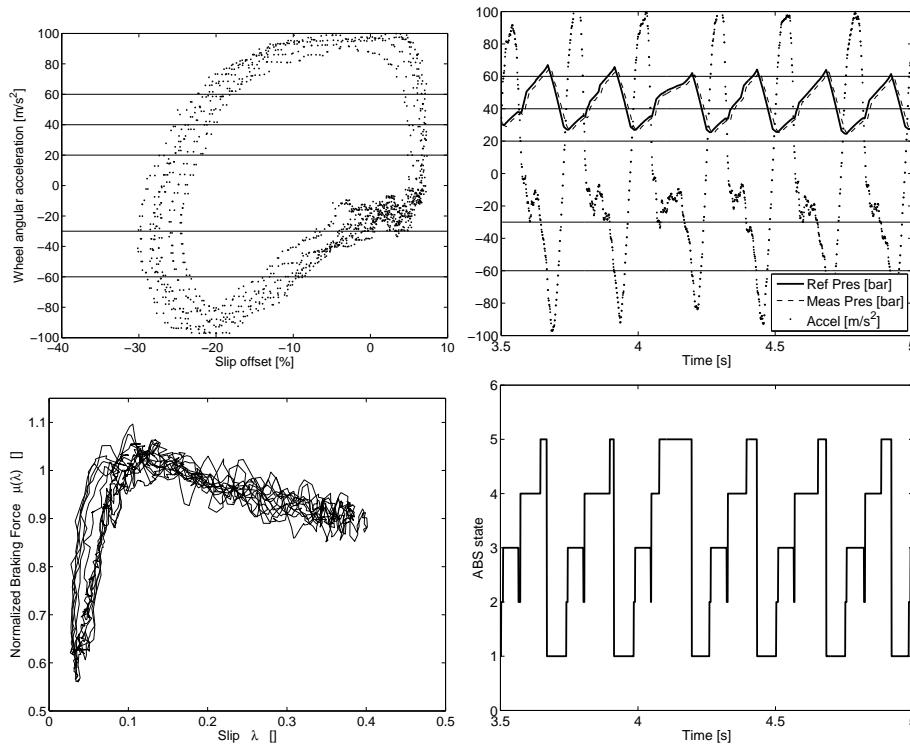


Figure 4.9: Experimental results for the ABS algorithm based on pressure derivative profiles.

noticed that, even with the large disturbance on the brake force and acceleration, the controlled system reaches and maintains a consistent limit cycle, encircling the optimal point $(0, 0)$.

Because the reduction of the pressure derivative, when approaching the switching threshold, is probably not big enough yet, the time delay is still causing the acceleration to go far outside the predefined thresholds. Various tests have shown that experiencing a larger positive acceleration results in a larger excursion into the stable zone. The difficulty to maintain the acceleration within the bounds is therefore responsible for the moderate performance of this algorithm regarding the predicted brake distance. Of course, a more precise tuning of the pressure derivative profile could solve this issue.

The longitudinal slip oscillates between 5 and 40 percent, which is good. It could be desired to have an even smaller excursion in order to maintain even more lateral stability and decrease brake distance. However, with this type of ABS methods based on wheel acceleration, the slip excursion needed to activate the phases is not directly controlled and depends heavily on the shape of the tyre curve. The larger the slopes of the tyre characteristic and the smaller the slip variation. In the particular case of the tyre-in-the-loop setup, the relatively small load on the wheel gives a tendency for

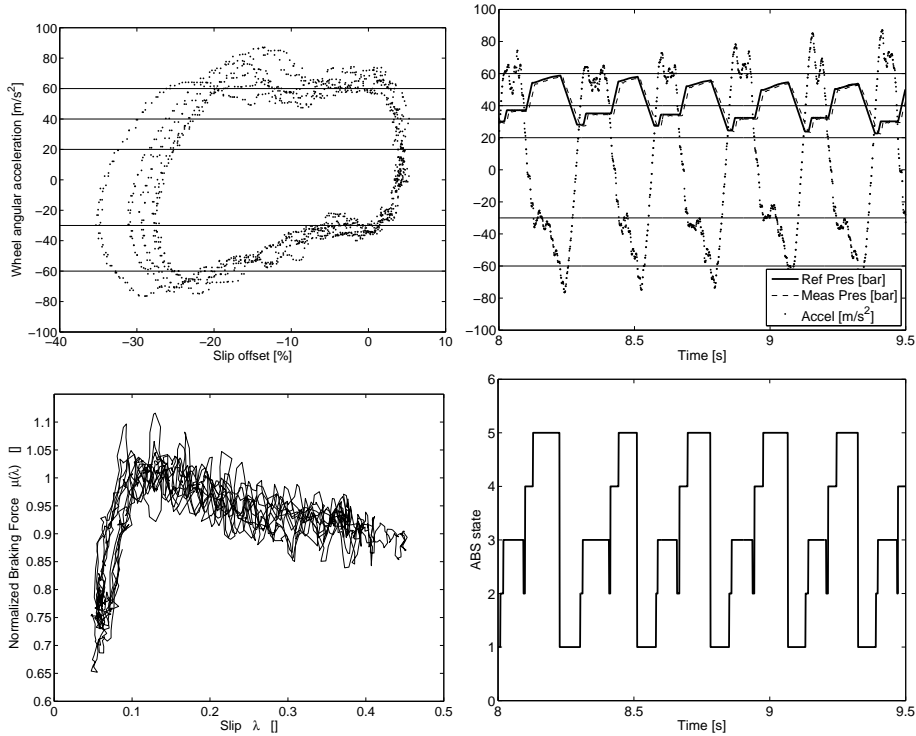


Figure 4.10: Experimental results for the ABS algorithm based on open-loop pressure references.

having large slip oscillations.

The tuning of this algorithm is quite robust. Small changes in the parameters or in the system do not affect the general shape of the limit cycle. Because the pressure is always kept decreasing or increasing respectively in phases 1 and 4, the acceleration will cycle more robustly between positive and negative and influences from vehicle speed or brake efficiency are minimized.

4.5.2 Open-loop pressure steps

The ABS controller based on open-loop pressure reference has also been successfully tested in practice. The measurements are plotted in Figure 4.10. Also in this case, the limit cycles are clearly visible and reproducible despite the disturbance.

This method is much better at maintaining the acceleration within the predefined thresholds. Intrinsically, the robustness with respect to time delays is larger. Thanks to the maximum acceleration maintained at a lower positive value, the force drop in the stable zone is smaller and the corresponding brake distance would also be reduced.

Unfortunately, since the pressure commands are given in open-loop, the algorithm has difficulties to react to system changes. In particular the tuning is quite sensitive

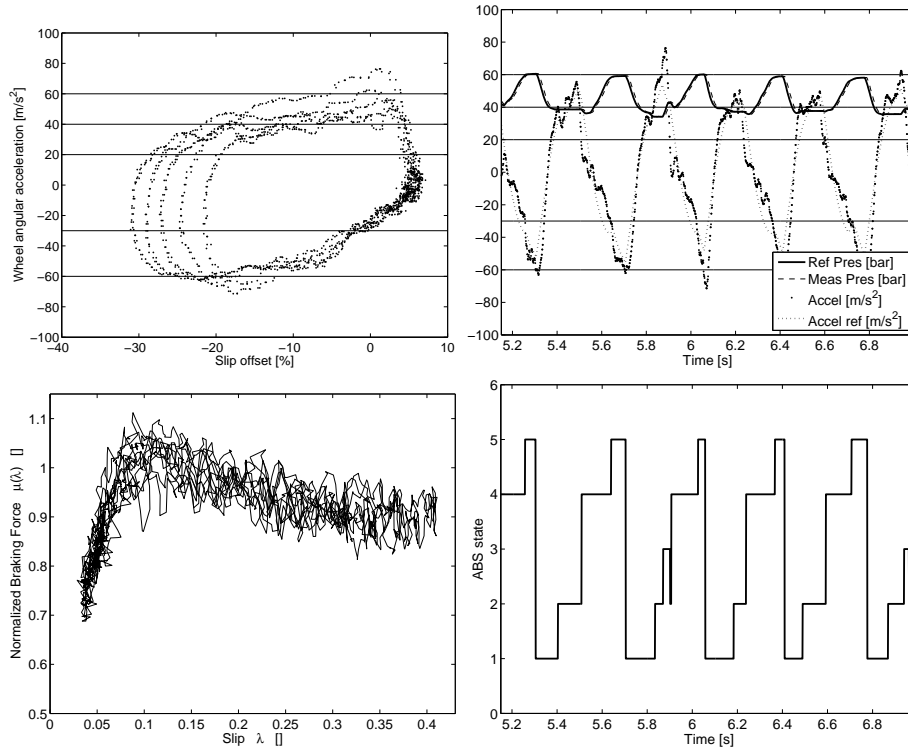


Figure 4.11: Experimental results for the ABS algorithm based on closed-loop acceleration control.

with respect to the brake efficiency γ_b . An overestimation of γ_b could prevent from triggering the next phase, while an underestimation of γ_b would make the acceleration to go far outside the thresholds, thus reducing the performance. Furthermore, the tuning of the phases 1 and 4 need to be different in practice, compared to simulation, in order to cope with the encountered asymmetry in the brake reaction when increasing or decreasing the pressure. The robustness gained against the time delay seems to harm the robustness against other phenomena.

4.5.3 Closed-loop acceleration control

The version of the ABS with closed-loop acceleration control is the last one to be successfully validated. The results of the experimental tests are plotted on Figure 4.11. The target acceleration is visible on the second plot. In phase 4 of the algorithm, the acceleration needs some time to reach the target value since the tyre has to go from its unstable region to its stable region. During the other phases, the acceleration and the reference remains very close.

Based on simulations, the feedback gain was chosen to be $K = 3$ and the rate limitations fixed to $v_0 = 2000$ and $u_0 = 100000$. Moreover, like for the two other

methods, the switching thresholds ϵ_i are those of Section 4.3.2.

This method is the easiest to tune and gives the best performances. The acceleration is maintained within the desired bounds. The force drop in the stable zone is limited to 0.7 which is similar to the method of Section 4.5.2. Finally, the slip offset x_2 is maintained between 20 and 30%, which is similar to the method of Section 4.5.1. The system is cycling around the top of the tyre characteristics. Further, the control is robust to all changes like brake efficiency or actuation delay.

4.6 Comparison with the Bosch algorithm

The ABS algorithm proposed in this chapter can be compared with the commercial one implemented by Bosch and described in [18]. Both algorithms are based on a hybrid logic and use the wheel acceleration as their only measurement. In this section, some of the similarities and the differences are highlighted. Throughout this section, the notation Bosch ABS will refer to the algorithm of [18] and Subsection 4.6.1; while five-phase ABS will refer to the algorithm of Section 4.3.

4.6.1 The original Bosch algorithm

The algorithm described by Bosch [18] is first recalled. When the phase of idleness is omitted, the algorithm is composed of six phases, as illustrated on Figure 4.12(a). On this figure, in order to facilitate the comparison between both algorithms, the phases of the Bosch algorithm are renamed to better match the phases of the five-phase algorithm of Figure 4.12(b). Phases similar to 1, 2 and 4 with either large torque variations or constant torque can be found and are matched. Further, it can be noticed that a phase similar to phase 3 is not present in the Bosch ABS, while phase 5 is split in two different phases.

The jumps between the different phases are triggered by wheel acceleration thresholds. Three thresholds can be identified: “ $-a$ ”, “ $+a$ ”, and “ $+A$ ”. This notation is kept here to improve coherence with the original reference [18]. It should be noted, however, that the three thresholds have values independent of each other and “ $-a$ ” is not the opposite of “ $+a$ ”. On Figure 4.12(a), the threshold for the transition between phases 1 and 2 is denoted by b . In the original version of the Bosch ABS, the constant b is equal to the parameter “ $-a$ ”.

4.6.2 Vehicle measurements and a modified Bosch algorithm

Measurements performed on a BMW 5 series equipped with an ABS system from Bosch are presented in Figure 4.13. Similar measurements originating from a Peugeot 307 also equipped with ABS system from Bosch were also analyzed and exhibited a characteristic behavior that was similar to that of the BMW vehicle.

The data of Figure 4.13 come from the front-left wheel and the manoeuvre is a heavy braking on a straight line, performed on a high adherence surface. The vehicle speed during the measurement varies from 25 to 6 m/s and it can be observed that, even if the tuning of the algorithm is adapted, the cycles are larger at a lower speed. The wheel deceleration thresholds $+A$, $+a$ and $-a$ can be identified to be 50, 20

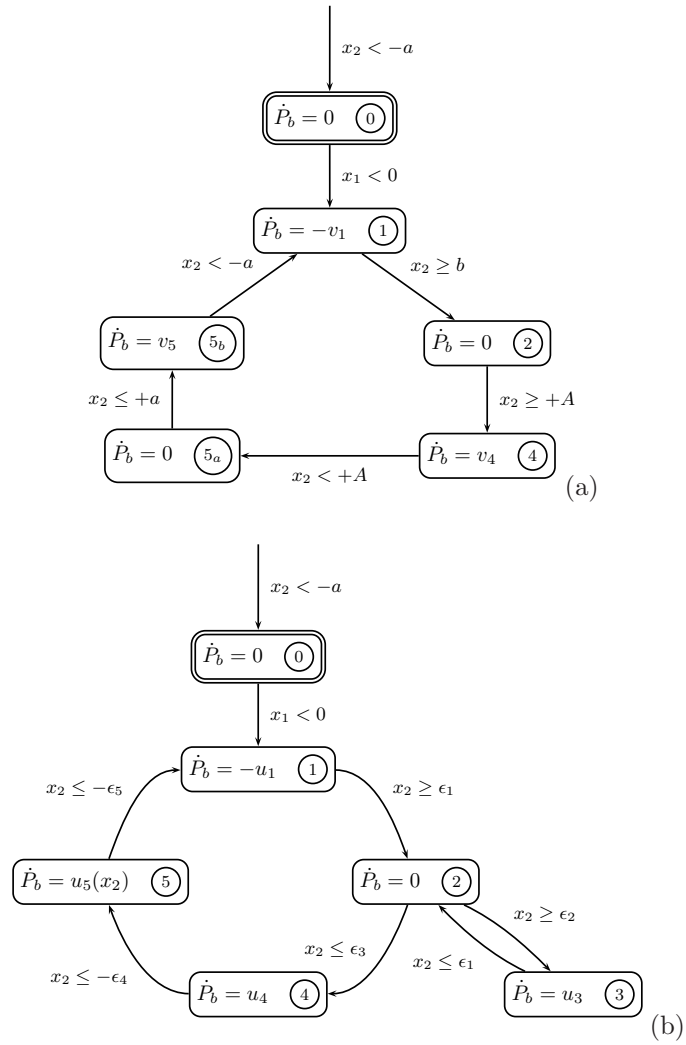


Figure 4.12: (a) The hybrid automaton associated to the Bosch algorithm. (b) A simplified version of the five-phase algorithm, considered at a constant speed.

4.6. COMPARISON WITH THE BOSCH ALGORITHM

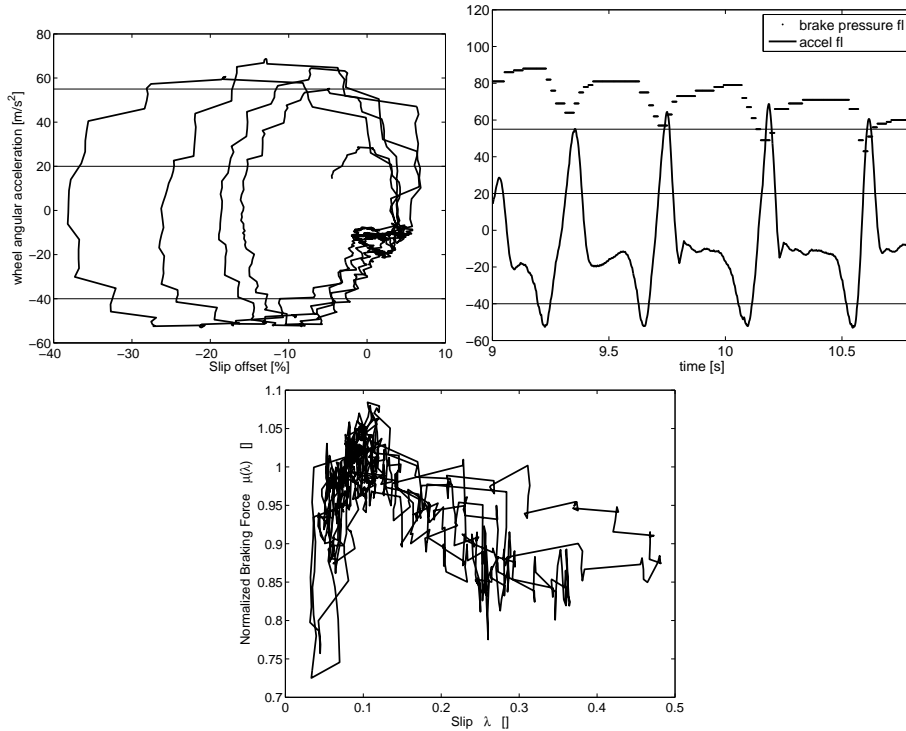


Figure 4.13: Measurements for the Bosch ABS on a BMW car, front-left wheel, straight braking on high μ .

and $-40 m/s^2$, and are indicated as straight lines on the plots. The brake pressure variation rates are difficult to measure precisely because of the limited accuracy of the sensors and are varying with the vehicle speed. The following average estimates can be made: $v_1 = -275 bar/s$, $v_4 = 275 bar/s$ and $v_5 = 15 bar/s$. The brake efficiency is varying a lot during the braking manoeuvre because of thermal phenomena, from $20 Nm/bar$ at the beginning to $40 Nm/bar$ at the end.

One major difference between the Bosch algorithm of [18] and the vehicle measurements lies at the transition between phases 1 and 2. According to the official description of the algorithm [18], the threshold b should be “ $-a$ ”. On the vehicle data it appears, however, that the value of b seems to be much closer to “ $+a$ ”. During implementation of the original Bosch algorithm, with $b = “-a”$, the logics could not be made properly functional neither in simulation nor on the test bench. Switching from phase 1 to phase 2 when the wheel acceleration is still negative, at “ $-a$ ”, is too early and does not allow the wheel to spin up again. Therefore, in order to have a working algorithm, the Bosch algorithm was modified to have a threshold b that is positive. This modification is based on the vehicle measurements and on the theoretical study of the first integrals of the simplified model [96]. Observe that the stability of the five-phase algorithm is guaranteed by stopping the pressure decrease

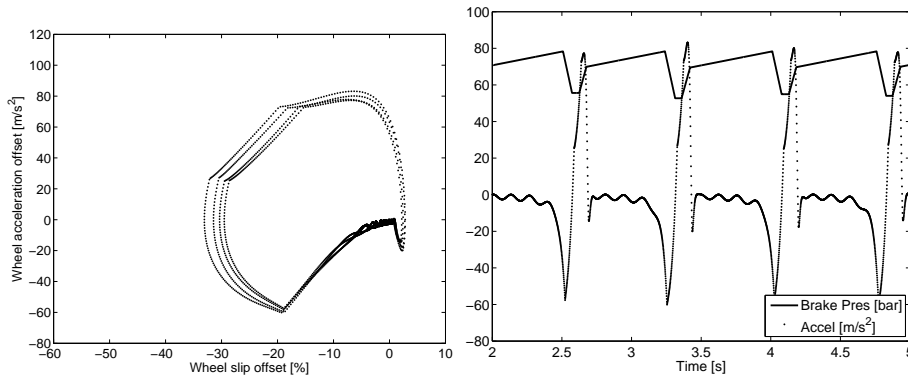


Figure 4.14: Simulation results for the Bosch algorithm. The wheel acceleration thresholds are $+A = 50 \text{ m/s}^2$, $+a = 20 \text{ m/s}^2$, and $-a = -40 \text{ m/s}^2$. The brake pressure variation rates are $v_1 = -350 \text{ bar/s}$, $v_4 = 275 \text{ bar/s}$ and $v_5 = 15 \text{ bar/s}$.

when the wheel acceleration is positive.

The Bosch ABS is simulated with the objective to match the general behavior observed in the measurements. The results are shown on Figure 4.14. When possible, the parameter values identified from the BMW are used. However, the brake pressure variation rate v_1 needed to be increased in order to have a better match of the limit cycles. Reproducing in simulation the limit cycle observed on the vehicle is extremely difficult, firstly because of the difficulty to tune all the tyre and vehicle parameters to fit the reality, secondly because of the differences between the algorithms implemented on the car and in the simulation, and thirdly because of the measurement inaccuracy and noise.

4.6.3 Comparison between the five-phase and the Bosch ABS algorithms

The five-phase ABS and the Bosch ABS can now be compared. The comparison focuses on the core of the algorithms, considered at a constant speed.

A first interesting difference between the algorithms is that the Bosch ABS requires a large delay in the system, coming for example from the hydraulic actuation. If a more ideal brake system without delay is simulated, like a brake-by-wire system or an in-wheel motor, the algorithm will not work properly. The reason behind this specific point is that, in the Bosch ABS, the same threshold “+A” is used to jump from phase 2 to phase 4, and from phase 4 to phase 5a. Without delay, the algorithm will jump to phase 5a with a too small pressure increase. The modification required to improve the situation is to decrease the threshold between phases 4 and 5a.

A clear advantage of the five-phase ABS is its mathematical basis. A consequence of this theoretical background is that it is easier to predict how the five-phase logic will react in different situations and adapt it if necessary, for example in the case of different actuator characteristics (like those of hydraulic, electromechanical, and

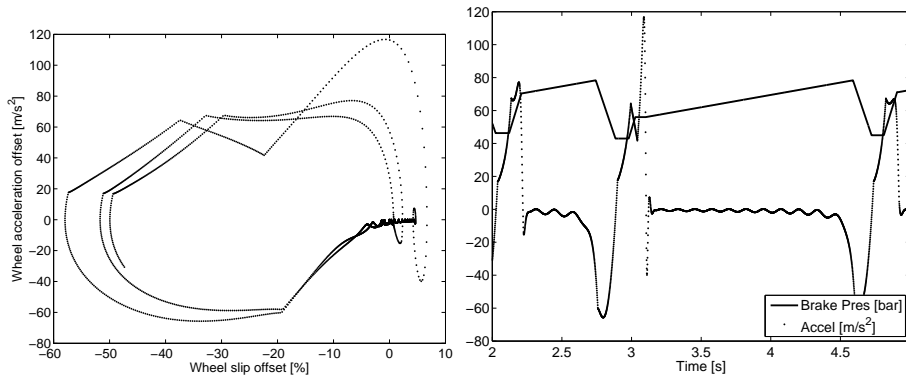


Figure 4.15: Simulation results for the Bosch algorithm. The wheel acceleration thresholds are $+A = 50 \text{ m/s}^2$, $+a = 20 \text{ m/s}^2$, and $-a = -40 \text{ m/s}^2$. The brake pressure variation rates are $v_1 = -250 \text{ bar/s}$, $v_4 = 275 \text{ bar/s}$ and $v_5 = 15 \text{ bar/s}$.

electric brakes). The Bosch algorithm, with its heuristic conception and its set of unprecise descriptions given in the literature, remains obscure. Tuning this algorithm properly and making modifications on it remains delicate.

It is also important to note that the Bosch algorithm does not contain a phase comparable to the third phase of the five-phase ABS. Such a phase is useful to limit the amplitude of the wheel-slip excursion into the stable zone, after a pressure release. The absence of this phase can lead to cycles that are longer than normal and to a decrease of performance, when particular initial conditions are encountered. Figure 4.15 shows a simulation where this kind of performance decrease is exhibited, in the case of the Bosch algorithm. Therefore, the presence of phase 3 is an advantage of the five-phase strategy.

Finally, it can be concluded that, for the specific conditions available in the laboratory, the level of performance achieved is comparable: the size of the limit cycles and the average brake force are similar. Of course, the Bosch ABS has many extra rules next to the core in order to cope with a large number of specific situations, but this falls outside the scope of this comparison.

4.7 Conclusion

In this chapter, the five-phase algorithm proposed in [96] was extended with three methods to deal with time delays. Time delays in measurement and actuation were found to be the main reasons why the theoretical five-phase algorithm fails in experiments.

The use of pressure derivative profiles reduces the influence of delays, but does not perfectly compensate for them. This method is difficult to tune because of the large number of parameters involved, but maintains a good level of robustness with respect to other phenomena, like changes in brake efficiency.

Giving pressure reference steps in open-loop offers a good resistance with respect

to time delays and makes the algorithm remain closer to the original theoretical framework. But the robustness of this approach, with respect to system changes, appears to be small. And, in particular, a good estimation of the brake efficiency is required.

By using closed-loop acceleration control, the advantages of both previous methods are combined. A high level of robustness is achieved with respect to all practical issues considered in Section 4.2. Moreover, the acceleration remains close to the desired trajectory ensuring a tight limit cycle.

These three techniques give limit cycles encircling the optimal braking point at the top of the tyre characteristic, without any need of estimating the parameters of this curve. Only the wheel acceleration measurement is used to implement the control logic. The proposed simulation model, including five important practical phenomena, is capable of reproducing the same results as in the experiments and is therefore suitable for testing ABS strategies. Thanks to the tyre-in-the-loop testing, it can be expected that the algorithms can rapidly be installed in a complete vehicle.

Considering the descriptions of the Bosch ABS available in the literature and the experimental measurements, it can be concluded that the core of the five-phase ABS presents some advantages compared to its commercial analogue. Not only the five-phase ABS is supported by a theoretical foundation, but it also gives more flexibility to handle long and short delays. Furthermore, the presence of phase 3 better maintains regular cycles with a smaller force drop during the pressure release. The performance regarding the size of the limit cycles are similar in the specific conditions used for the study. One step further has been made towards the objective of having an open ABS algorithm comparable to the Bosch ABS. However, the commercially available Bosch ABS comes with many extra rules to cope with all kind of situations, which are still far from being openly available.

Chapter 5

ABS based on Tyre Force

The Anti-lock Braking System (ABS) is the most famous active safety system for road vehicles, see Section 1.3. This system has been around for more than 30 years but, in general, ABS algorithms can still be improved. First they can be made simpler, hence easier to understand and tune, while keeping the same performance. Moreover, their performance can be enhanced in terms of reducing the slip variations and decreasing the brake distance. Finally, the robustness against tyre-road friction characteristic can be improved and new algorithms should be able to handle rapid changes in friction without complex logic. This chapter introduces a force-based ABS that brings improvements in those 3 directions.

A few publications about ABS algorithms exploiting tyre force measurements can be found in the literature. Kamada [66] investigates the correlation between slip derivative and force derivative. This technique works fine in simulation but has shown severe limitations when implemented in practice because of the noise level. Botero [19] implements a slip regulator (see Section 1.3) using sliding mode control where the force estimation is required to enforce sliding. De Bruijn [36] uses force measurement to define the upper and lower torque levels between which the controller is switching. The algorithm developed in this chapter extends the class of hybrid ABS (see Section 1.3).

Two limitations are inherent to the family of hybrid ABS: the brake force cannot always be at its maximum since a force drop is needed to switch phase, and problems are encountered when the tyre-road friction characteristics does not present a clear maximum at a limited slip, like on snow or gravel. The same limitations will be found in this new force-based ABS.

In traditional hybrid algorithms based on wheel acceleration, the acceleration is used both for detection and control. First, the acceleration is used to detect when the tyre has passed the maximum of its characteristics, by indirectly observing the tyre force when the brake torque remains constant. Secondly, the acceleration needs to be controlled to drive the tyre to a limit cycle, by varying the brake torque. Those two utilizations are conflicting with each other. This often requires complicated logics with many states and the alternance between phases where the brake torque is changing quickly or kept constant; which can make the tuning more difficult and can affect the performances.

Thanks to direct tyre force measurement, the above limitations can be alleviated, the detection of the friction peak can be made more sensitive and the acceleration can permanently be controlled to provide a tight limit cycle. Possibilities for implementing tyre force measurement on production vehicles, in particular using force sensing bearings, are discussed in Section 1.2.

In this chapter, a new ABS algorithm using force and acceleration measurements is developed. The algorithm is simpler than other approaches in the literature as it contains only 2 states and 3 tuning parameters, and does not require parameter scheduling. The stability is proven and the analysis provides tuning tools. The algorithm is validated experimentally on a tyre-in-the-loop test bench and is shown to perform better than the deceleration hybrid algorithm of Chapter 4. No knowledge of the tyre-road characteristics is needed for control.

Outline

The wheel and vehicle models are introduced in Section 5.1. In Section 5.2, the algorithm is described and the stability proven. The tuning is discussed in Section 5.3. Section 5.4 concentrates on the single wheel model with simulation results, experimental validation and comparison. Finally, in Section 5.5, simulations are performed using a two-wheel model.

5.1 Modelling

The study of the ABS system will be done in two stages, using vehicle models with different level of complexity. The wheel and tyre model remain the same throughout this chapter while the chassis model will go from a one-wheel model to a single-track two-wheel model.

In the first stage, only the longitudinal dynamics of a single loaded wheel is considered. In particular, the relaxation length of the tyre and the actuation delay are taken into account. Even though weight transfer and combined slip are ignored, all the basic phenomena related to ABS already appear in this simple model. Also, this level of detail is suitable to model the tyre-in-the-loop experimental setup.

In the second stage, the weight transfer from the rear to the front during braking is added. A single-track two-wheel vehicle model is used where the longitudinal as well as the vertical dynamics of the wheels and the chassis are considered. This model is now suitable for representing a real car braking in straight line.

The model of each wheel is as follows:

$$J\dot{\omega} = rF_b - T_b \quad (5.1)$$

$$\tau\dot{F}_b = -F_b + F_z f(\lambda, \mu, \alpha, \dots) \quad (5.2)$$

$$\lambda = \frac{v - r\omega}{v} = 1 - \frac{r\omega}{v} \quad (5.3)$$

$$\dot{T}_b = -\gamma u(t - \Delta t) \quad (5.4)$$

where s is the Laplace variable, J and r are the inertia and radius of the wheel, F_b the tyre brake force, T_b the brake torque, v the vehicle speed, τ the relaxation length,

F_z the vertical load on the tyre, f the non-linear tyre characteristics expressed for example by the magic formula, see [95], λ the tyre slip during braking, w the speed of the wheel, γ the brake efficiency, Δt the total delay, and u the brake pressure derivative control input. The partial derivative of f with respect to λ is

$$f'(\lambda) = \frac{\partial f}{\partial \lambda}(\lambda) \quad (5.5)$$

The vehicle speed as well as the tyre loads are given by the vehicle model. For the single-wheel model, the following simple equations are added to (5.1)-(5.4):

$$\dot{v} = -\frac{1}{m}F_b \quad (5.6)$$

$$F_z = mg \quad (5.7)$$

where g is the gravity acceleration.

For the two-wheel model, following an approach similar to [106], 4 states are added: the height of the vehicle center of gravity z , the pitch angle of the vehicle p and the height of the wheel hubs at the front and at the rear z_t^f and z_t^r . The upper indices f and r are used to distinguish the front from the rear of the vehicle. The equations added to (5.1)-(5.4) are the following:

$$\dot{v} = -\frac{1}{m}(F_b^f + F_b^r) \quad (5.8)$$

$$\ddot{z} = \frac{1}{m}(F_s^f + F_s^r) - g \quad (5.9)$$

$$J_c \ddot{p} = -aF_s^f + bF_s^r + (F_b^f + F_b^r)z \quad (5.10)$$

$$F_s^f = -k^f(z_s^f - z_{s0}^f - z_t^f) - d^f \dot{z}_s^f \quad (5.11)$$

$$F_s^r = -k^r(z_s^r - z_{s0}^r - z_t^r) - d^r \dot{z}_s^r \quad (5.12)$$

$$z_s^f = z - h - a \sin(p) \quad (5.13)$$

$$z_s^r = z - h + b \sin(p) \quad (5.14)$$

$$m_t \ddot{z}_t^f = -F_s^f + F_z^f \quad (5.15)$$

$$m_t \ddot{z}_t^r = -F_s^r + F_z^r \quad (5.16)$$

$$F_z^f = -k_t(z_t^f - z_{t0}^f) \quad (5.17)$$

$$F_z^r = -k_t(z_t^r - z_{t0}^r) \quad (5.18)$$

where J_c is the inertia of the chassis around the lateral direction, F_s is the vertical force in the suspension, z_s is the vertical displacement of the suspension, h is the height of the center of gravity, a and b the distances between the center of gravity and the front or respectively the rear of the vehicle, k and d are stiffnesses and damping coefficient.

5.2 The algorithm

Each wheel of the vehicle is controlled separately. Therefore, the description and analysis of the algorithm will be done for one wheel only, according to the single-wheel model (5.1)-(5.7).

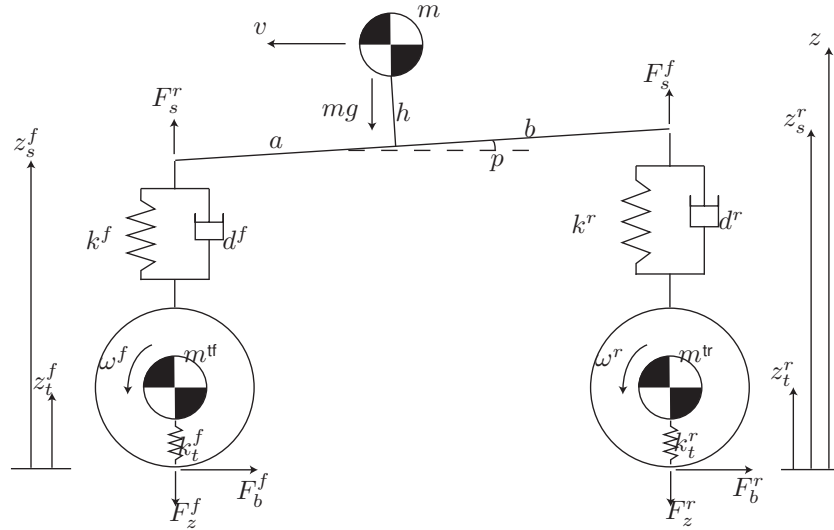


Figure 5.1: Illustration of the single-track two-wheel vehicle model.

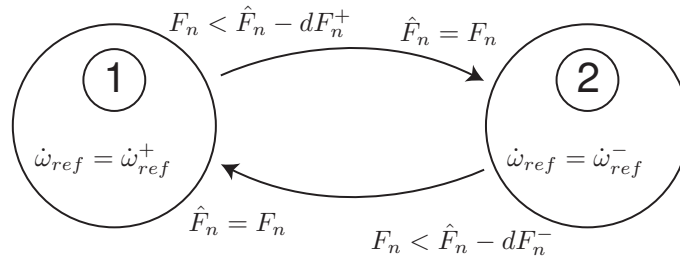


Figure 5.2: Hybrid Automaton of the ABS algorithm. In each phase, the acceleration is controlled in closed-loop at the desired level $\dot{\omega}_{ref}$. The switching is based on force measurement, with F_n the normalized braking force, \hat{F}_n the local maximum over time of F_n and dF_n^+ and dF_n^- two tuning parameters. The inequalities at the beginning of the arrows indicate the switching condition; the equalities at the end indicate the reset assignments.

The algorithm consists of 2 phases and a switching mechanism, as depicted on Figure 5.2. During phase 1, the control action will be such that the slip will decrease ($\dot{\lambda} < 0$). During phase 2, it is the opposite ($\dot{\lambda} > 0$). The switching will take place after the tyre slip λ crosses λ^* , meaning that after some increase, the brake force is decreasing again. This back and forth process will ensure that the system is cycling around the optimal slip λ^* .

To ensure that the slip increases or decreases during respectively phase 2 or 1, the wheel angular acceleration is controlled in closed loop. This method makes the control robust to changes in brake efficiency or tyre radius. It is also suited for hydraulic braking since the pressure or torque do not need to be measured. However, the large delay in the loop coming from the measurement and the actuation limits

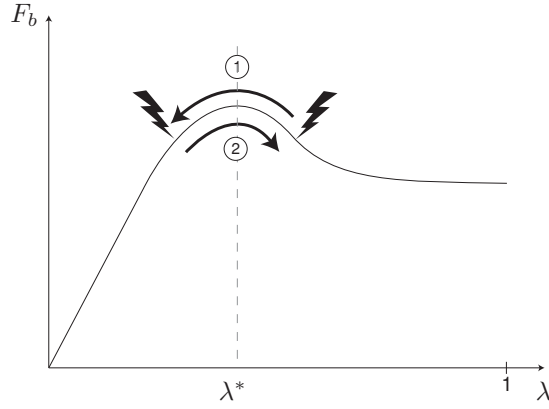


Figure 5.3: General trajectory of a hybrid two-phase ABS algorithm visualized on the tyre friction curve.

the performance of the control.

The switching mechanism is implemented looking at the brake force measurement. If the switching takes place after the tyre slip λ crosses λ^* , meaning that after some increase the brake force is decreasing again, the system will cycle around the optimal slip λ^* .

5.2.1 Switching strategy

The strategy is explained with the help of Figure 5.3.

At the beginning of each phase, λ goes towards λ^* so that the tyre force evolves towards its maximum. When λ^* is crossed, the tyre force decreases and a switch to the other phase needs to take place, in order to make the brake force to increase again. The switching strategy is implemented using tyre force measurement. To get the right switching, it is important to consider only the variations of the tyre force that originates from a change of λ . However, variations on F_z , for example linked to weight transfer or road excitation, can have a large influence on the tyre force. To solve this problem, we introduce

$$F_n = \frac{F_b}{F_z} \quad (5.19)$$

where the brake force is normalized by the vertical force acting of the tyre. Depending on the sensing solution, F_z may or not be directly measured. In case of sensors placed in the tyre F_z can be assumed measured at the contact patch, while with other solutions (for example load-sensing bearings) only the force at the wheel hub is available. For generality's sake, we will assume that F_z is available. In Section 5.5, it will be shown how the algorithm can be adapted in case the direct measurement is not available.

In each phase, assumed to start at time t_s , the algorithm searches for the maximal normalized force \hat{F}_n the tyre can generate

$$\hat{F}_n(t) = \max_{t_s \leq \zeta \leq t} (F_n(\zeta)). \quad (5.20)$$

When the measured force drops of dF_n^\pm under the current maximum \hat{F}_n , one can conclude that the maximum has been exceeded and a phase switch takes place. When entering a new phase, the maximum \hat{F}_n is reset and the detection mechanism starts all over again. In case of large actuation delays, it might be necessary to delay the start of the detection mechanism, but as this is a minor detail, it is not addressed here. Computing the maximum during each phase allows the algorithm to handle changes in tyre-road friction. The use of the parameters dF_n^\pm can be compared to some kind of hysteresis. Therefore, it can be noted that, as long as dF_n^\pm are larger than zero, there will be no chattering in the controller.

The definition of dF_n require some considerations. A too large drop would lead to a longer brake distance while a too small would increase the sensitivity to noise. In practice, it can be noticed that tyres can show short but large force drops which have nothing to do with the basic characteristic. This phenomena can be observed on the top left plot of Figure 5.11. Force drops of up to 30% of the load have been observed on worn tyres. In order to avoid those drops influencing the switching strategy, a combination of large enough thresholds together with a low-pass filtering of the force measurement is employed.

5.2.2 Closed-loop control of the wheel acceleration

A way to ensure that the slip derivative is either strictly positive or negative during each phase is to control the wheel acceleration in closed-loop. The objective of the closed-loop controller is to drive the error on the wheel acceleration

$$e = \dot{\omega}_{ref} - \dot{\omega} \quad (5.21)$$

to zero as fast as possible. To this end, the closed-loop proportional control law is used

$$u = k(\dot{\omega}_{ref} - \dot{\omega}). \quad (5.22)$$

with $\dot{\omega}_{ref}$ is a tuning parameter representing the target acceleration for the current phase. To guarantee the correct slip derivative, $\dot{\omega}_{ref}$ should be positive in phase 1 and negative phase 2. The tuning is addressed in Section 5.3.2.

In the next subsections, the stability properties are analysed. Model-based design methods were considered not suitable in this case since the system (5.1)-(5.7) is non-linear, uncertain and with time delay.

If a simple version of the model is considered, it becomes possible to show that this control law together with the switching mechanism maintains the system into a bounded region of the state space. This constitutes a stability proof and gives bounds on the performances. When the more complex model with delays is considered, the following results can be extended with a linearization approach and extensive simulations to provide practical tuning tools.

5.2.3 Bounding the trajectory for a simple model

Let us consider for now the simplified model obtained neglecting the actuation delay and tyre relaxation. Due to large differences in inertia, the wheel dynamics and car body dynamics evolve on significantly different time scales, with the speed v

changing much more slowly than the wheel slip λ . v can be consequently dropped as a state variable and considered as an independent slow-varying parameter, similarly to [98, 117]. Thanks to the above assumptions the model can be written as

$$\dot{\lambda} = -\frac{r}{v} \left(\frac{rF_z f(\lambda) - T_b}{J} \right) \quad (5.23)$$

$$\dot{T}_b = -\gamma k \left(\dot{\omega}_{ref} - \frac{rF_z f(\lambda) - T_b}{J} \right) \quad (5.24)$$

Note that the brake torque T_b and the wheel acceleration $\dot{\omega}$ are linked by an algebraic equation. This means that any of the two can equivalently be used as system state. In this subsection, λ and T_b are used as states as it allows for a simplification of the equations.

Theorem 5.1. *Consider the system (5.23-5.24) for a given velocity v together with the proposed switching and acceleration control, and take an ϵ strictly positive.*

If the controller gain k is such that

$$\gamma k + \frac{r^2}{v} F_z f'(\lambda) > 0 \quad \forall \lambda : 0 \leq \lambda \leq 1$$

then

- the brake torque T_b is bounded by

$$rF_z f(\lambda) - B < T_b < rF_z f(\lambda) + B \quad (5.25)$$

with

$$B > \frac{\epsilon + \gamma k \dot{\omega}_{ref}^{abs}}{\frac{\gamma k}{J} + \frac{r^2}{vJ} F_z f'(\lambda)} \quad \forall \lambda : 0 \leq \lambda \leq 1 \quad (5.26)$$

where $\dot{\omega}_{ref}^{abs} = \max(|\dot{\omega}_{ref}^-|, |\dot{\omega}_{ref}^+|)$.

- the slip λ is bounded by

$$\underline{\lambda} < \lambda < \bar{\lambda} \quad (5.27)$$

with $\underline{\lambda}$ and $\bar{\lambda}$ implicitly given by

$$\begin{aligned} rF_z f(\bar{\lambda}) - B &= rF_z(F_{n_{max}} - dF_n^+) + B - \frac{v}{r} \gamma k (\bar{\lambda} - \lambda^+) \\ rF_z f(\underline{\lambda}) + B &= rF_z(F_{n_{max}} - dF_n^-) - B - \frac{v}{r} \gamma k (\underline{\lambda} - \lambda^-) \end{aligned}$$

where λ^+ and λ^- are defined by (5.30) and (5.31), and dF_n^+ and dF_n^- are the two tuning parameters defining the switching strategy;

and therefore the system's trajectory remains in a bounded region of the state space (λ, T_b) , which ensures stability.

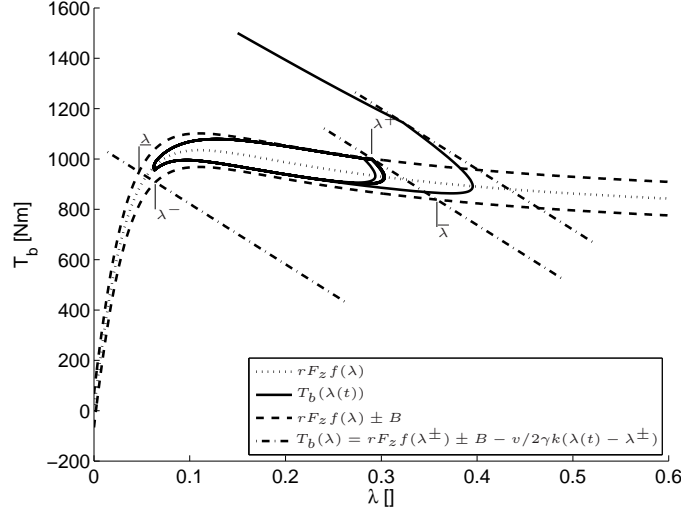


Figure 5.4: Bounds on the trajectory when the simple model (5.23)-(5.24) is considered. First the curves $rF_z f(\lambda) \pm B$ defines upper and lower bounds on T_b . Then the lines $T_b(\lambda) = rF_z f(\lambda^\pm) \pm B - \frac{v}{2}\gamma k(\lambda(t) - \lambda^\pm)$ gives upper and lower bounds on λ .

Proof. First we will show that if (5.25) holds the trajectory is attracted toward a bounded region of the state space, then we will find bounds on the size of that region in terms of maximum and minimum T_b and λ .

Let us define the region R as the region contained between $\bar{T}_b = rF_z f(\lambda) + B$ and $\underline{T}_b = rF_z f(\lambda) - B$ for all λ where B is a parameter to be defined, see Figure 5.4. From there, the region Q and S can also be defined, respectively above R : ($T_b > \bar{T}_b$); and under R : ($T_b < \underline{T}_b$).

The first step is to show that R is attractive when the initial condition is outside R . This is done using Lyapunov-like arguments.

Consider the initial condition $X_0 = (\lambda_0, T_{b_0})$ in Q . Thanks to continuity arguments, the trajectory will either remain in Q or will cross at some point the boundary \bar{T}_b . Let the function

$$V(\lambda, T_b) = T_b - (rF_z f(\lambda) + B)$$

indicate the distance of x from R along the T_b axis; as long as V is positive the trajectory will be in Q , as soon as $V = 0$ the trajectory has entered R . We will now show that it is possible to bound the time derivative of V so that the trajectory will enter R in finite time. Consider

$$\begin{aligned} \dot{V}(\lambda, T_b) &= \dot{T}_b - rF_z f'(\lambda)\dot{\lambda} \\ &= -\gamma k \dot{\omega}_{ref} + \left(\gamma k + \frac{r^2}{v} F_z f'(\lambda) \right) \frac{rF_z f(\lambda) - T_b}{J}, \end{aligned} \quad (5.28)$$

if (5.25) holds and we recall that $x \in Q$, equation (5.28) is bounded from above by

$$\dot{V}(\lambda, T_b) < -\gamma k \dot{\omega}_{ref} - \left(\gamma k + \frac{r^2}{v} F_z f'(\lambda) \right) \frac{B}{J}. \quad (5.29)$$

Depending on the phase, $\dot{\omega}_{ref}$ could be either negative or positive; as we are trying to bound $\dot{V}(\lambda, T_b)$ from above we will consider the negative one. If we chose B such that

$$B > \frac{\epsilon - \gamma k \dot{\omega}_{ref}^-}{\frac{\gamma k}{J} + \frac{r^2}{vJ} F_z f'(\lambda)} \quad \forall \lambda : 0 \leq \lambda \leq 1$$

then $\dot{V}(\lambda, T_b) < -\epsilon$ in Q with ϵ a positive value defining the speed of convergence. By the comparison lemma [69], if x starts in Q , it will enter R in finite time regardless of the switching strategy.

The same results can be shown to hold for x starting in S . In this case the Lyapunov-like function is $V_S(\lambda, T_b) = -T_b + (rF_z f(\lambda) - B)$. A similar condition on B (with the positive ω_{ref}) is obtained; by taking the $\max(|\omega_{ref}^+|, |\omega_{ref}^-|)$, B can be made unique for both cases, thus obtaining a symmetric attractive region around $rF_z f(\lambda)$.

So far, two conditions have been introduced. The first condition (5.25) on k ensures stability while the second condition (5.26) determines the size of the attractive and invariant region R .

Let us now consider the bound on λ by taking into account the switching strategy. As in this simple model there is only a static relationship between tyre slip and tyre force, the switching strategy based on forces can be implicitly rewritten in term of slip:

- switching from phase 1 to phase 2 takes place at

$$\lambda^+ = f_{\lambda > \lambda^*}^{-1} (F_{n_{max}} - dF_n^+) \quad (5.30)$$

- switching from phase 2 to phase 1 takes place at

$$\lambda^- = f_{\lambda < \lambda^*}^{-1} (F_{n_{max}} - dF_n^-) \quad (5.31)$$

where $F_{n_{max}}$ is the maximum normalized friction force. Note that, even if f is not invertible on its entire domain, f limited to either $\lambda > \lambda^*$ or $\lambda < \lambda^*$ is invertible. The objective is to find a bound on the trajectory of λ after a switch.

By combining equations (5.23) and (5.24), we can get

$$\dot{T}_b = -\gamma k \dot{\omega}_{ref} - \frac{v}{r} \dot{\lambda} \gamma k. \quad (5.32)$$

This can be integrated between the last switching time t_s and t :

$$\begin{aligned} \int_{t_s}^t \dot{T}_b dt &= - \int_{t_s}^t \gamma k \dot{\omega}_{ref} dt - \int_{t_s}^t \frac{v}{r} \dot{\lambda} \gamma k dt \\ T_b(t) - T_b(t_s) &= -\gamma k \dot{\omega}_{ref} (t - t_s) - \frac{v}{r} \gamma k (\lambda(t) - \lambda(t_s)) \end{aligned} \quad (5.33)$$

Note that since t_s is the most recent switching time before t , $\dot{\omega}_{ref}$ is constant during the interval of integration.

From (5.25) and (5.26) we know that x will enter R in finite time; once it has entered R , T_b at the time of the switch can be bounded:

- During phase 1 where $\dot{\omega}_{ref} > 0$, we have that $T_b(t_s) < rF_z f(\lambda^+) + B$ and thus

$$T_b(t) \leq rF_z f(\lambda^+) + B - \frac{v}{r} \gamma k(\lambda(t) - \lambda^+). \quad (5.34)$$

- During phase 2 where $\dot{\omega}_{ref} < 0$, we have that $T_b(t_s) > rF_z f(\lambda^+) - B$ and thus

$$T_b(t) \geq rF_z f(\lambda^-) - B - \frac{v}{r} \gamma k(\lambda(t) - \lambda^-). \quad (5.35)$$

A bound on the maximal slip, which will occur during phase 1, can be found by combining \underline{T}_b and (5.34). Equivalently, a bound on the minimal slip, which will then occur during phase 2, can be found by combining \bar{T}_b and (5.35). In particular, once the trajectory has entered R , the slip λ is bounded by

$$\underline{\lambda} < \lambda < \bar{\lambda} \quad (5.36)$$

with $\underline{\lambda}$ and $\bar{\lambda}$ implicitly given by

$$\begin{aligned} rF_z f(\bar{\lambda}) - B &= rF_z f(\lambda^+) + B - \frac{v}{r} \gamma k(\bar{\lambda} - \lambda^+) \\ rF_z f(\underline{\lambda}) + B &= rF_z f(\lambda^-) - B - \frac{v}{r} \gamma k(\underline{\lambda} - \lambda^-) \end{aligned}$$

□

The bounds $\underline{\lambda}$ and $\bar{\lambda}$ are visualized on Figure 5.4. Simulations confirm that the system trajectory is attracted by the bounded region and that once inside the bounded region the trajectory will cycle between a maximum and a minimum λ ; although derived using conservative arguments, the above bounds provide useful indications for the controller tuning. The following conclusions can be drawn from Theorem 5.1.

- The larger $\dot{\omega}_{ref}^{abs}$, the larger the cycles, since B is proportional to $\dot{\omega}_{ref}^{abs}$.
- The larger dF_n^\pm and the larger the cycles, since it makes λ^+ and λ^- to be further away from λ^* .
- The larger the controller gain k , the lower the influence of the tyre characteristic on the cycles, as $\frac{\gamma k}{vJ}$ dominates $\frac{r^2}{vJ} F_z f'(\lambda)$ in (5.26).
- The larger the controller gain k , the smaller the variation of the slip λ during 1 cycle, as it will increase the slope of (5.34).
- Equation (5.25) quantifies the effect of the friction characteristic on the stability. In particular, the critical condition is on $\left. \frac{\partial f}{\partial \lambda} \right|_{min}$. The greater the negative slope the more difficult it is to stabilize. It is however possible to find a bound on $\left. \frac{\partial f}{\partial \lambda} \right|_{min}$ that will hold for all surfaces and tune k consequently.
- Equation (5.25) quantifies the influence of the velocity v on the stability and size of the cycles. It is well known in the literature [106] that ABS regulation becomes more difficult as v decreases, and this is why most ABS stop using

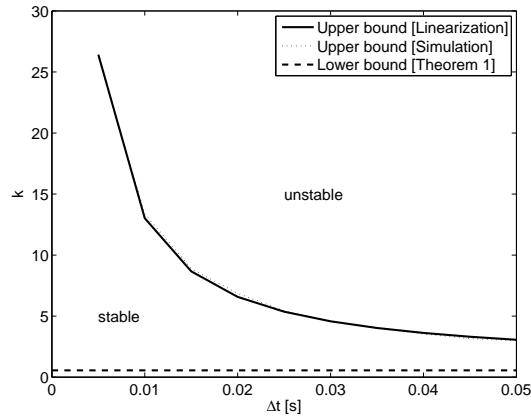


Figure 5.5: Stability region in the gain k - delay Δt space.

feedback control under a critical speed. The above results provide a useful design tool to assess in which velocity range the closed-loop system will remain stable. For any value of k , there will always be a critical speed under which the system cannot be guaranteed stable anymore. Equations (5.25) and (5.27) describe the size of the cycles as the velocity gets closer to the critical threshold.

5.3 Controller tuning

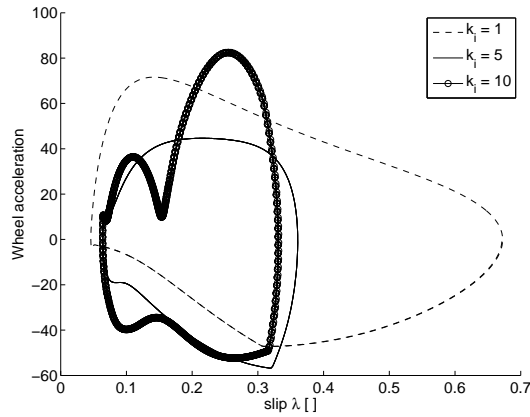
When considering the more complex system (5.1)-(5.7), the computations from Theorem 1 are not valid anymore. However, it can be shown that the main conclusions remain valid. In the next subsection, further analysis is done on the system (5.1)-(5.7) to confirm the conclusions.

5.3.1 Tuning the controller gain

In Theorem 5.1, (5.25), stability is guaranteed by imposing a lower bound on the controller gain k , which is plotted on Figure 5.5. When all the dynamics of the system are considered, including the time delay, a too large controller gain will destabilize the system. Here two approaches to determine the stability region in the gain k - delay Δt plane are proposed.

The first possibility is to run many simulations. Many combinations of delays and gains are tried and the stability region is drawn based on the outcome. A criteria is necessary to distinguish between stable and unstable simulations. Here, a configuration is classified unstable if there is no cycle or if the trajectory would require a negative torque. The stability region based on simulations is shown on Figure 5.5. It can clearly be seen that the larger the delay and the lower the controller gain has to be. Still, this brute-force method is not pleasant as it is computationally expensive and it requires a complete and precise model of the system.

The second option is to use a linearization approach and study the local stability


 Figure 5.6: Limit cycle for different controller gains k .

of the system. Linearizing (5.1)-(5.7), together with the control law (5.22), around a slip $\tilde{\lambda}$ gives the loop transfer function from reference acceleration to error:

$$L_{\tilde{\lambda}}(s) = \gamma k \frac{\tau s + 1}{J\tau s^2 + Js + F_z f'(\tilde{\lambda}) \frac{r^2}{v}} e^{-s\Delta t} \quad (5.37)$$

Figure 5.7 shows the Nyquist plots of (5.37) for different values of $\frac{\partial f}{\partial \lambda}$ and $k = 5$, $\tau = 0.01$ m, $v = 18$ m/s, $\Delta t = 0.02$ s, $\gamma = 20$ Nm/bar. It can be observed that the stability margins are rather independent from the varying parameter $\frac{\partial f}{\partial \lambda}$. For $\frac{\partial f}{\partial \lambda}$ varying between -3000 and 10000, like on Figure 5.7, the gain margin changes by less than 4% around 1.32 while the phase margin takes values between 20 and 30. The associated frequencies respectively lies in the intervals [75, 90] and [55, 70] rad/s. Similarly, the stability margins are independent of v as it appears in the same term as $F_z f'(\lambda)$ in the transfer function. Therefore, it can be concluded that the largest influence on the stability margin comes from the time delay.

Based on the gain margin of (5.37) for various time delays, the stability region is defined and plotted on Figure 5.5. Although the linearization method is valid only in the neighborhood of the linearization point, the difference between the stability regions given by both methods is extremely small. Therefore it makes sense to use a linearization approach, as it is much faster and easier to compute, and it allows for a better stability analysis. In particular, from the sensitivity analysis of the stability margins of (5.37), it can be concluded that the stability region is robust to changes in tyre parameters and in forward velocity.

The influence of k on the shape of the limit cycle is visualized on Figure 5.6. If the gain is low, the system will be quite slow and the slip excursion will be large, which means low performances. If the gain is high, the system will become oscillatory and eventually unstable.

As a conclusion, the best tuning is to take the largest controller gain k maintaining the system stable. Given the system delay, this maximum gain can easily be computed using the proposed linearization approach.

5.3.2 Tuning the acceleration levels

Two important parameters to tune in the algorithm are the reference acceleration levels $\dot{\omega}_{ref}^+$ and $\dot{\omega}_{ref}^-$. For the algorithm to work, the following conditions need to be imposed:

$$\dot{\lambda} = \frac{-r\dot{\omega}_{ref}^+ + r\omega\dot{v}}{v^2} < 0 \quad (5.38)$$

$$\dot{\lambda} = \frac{-r\dot{\omega}_{ref}^- + r\omega\dot{v}}{v^2} > 0 \quad (5.39)$$

Taking into account that $0 < r\omega < v$, the previous inequalities can be fulfilled using the sufficient conditions

$$\dot{\omega}_{ref}^+ > 0 \quad (5.40)$$

$$\dot{\omega}_{ref}^- < \frac{\dot{v}_{min}}{r} \quad (5.41)$$

where \dot{v}_{min} is the maximum deceleration achievable with a road vehicle, typically $1.2g$.

From Theorem 5.1, we can recall that the larger the $\dot{\omega}_{ref}$, the larger the limit cycle in term of slip variation. This has a large influence on performance, as will be shown using simulations. The limit cycles for different values of $\dot{\omega}_{ref}$ can be seen on Figure 5.8.

The overall performance in term of braking distance can be assessed using the simulation results presented in Figure 5.9. The case with the lowest reference levels ($\dot{\omega}_{ref} = 10 \text{ m/s}^2$) at the highest speed ($v = 150 \text{ km/h}$) is taken as reference (100 %) and the integral of the braking force, which is inversely proportional to the braking distance, is normalized. The value of $\dot{\omega}_{ref}^+$ is displayed on the x-axis while $\dot{\omega}_{ref}^-$ is taken symmetric with respect to the vehicle acceleration. As a conclusion, the reference acceleration levels should be taken as small as possible. In practice, tyre oscillations, measurement noise and wish for robustness will prevent us from taking arbitrarily small acceleration levels. The reference levels taken for experimental validation $\dot{\omega}_{ref}^+ = 30$, $\dot{\omega}_{ref}^- = -40$ decreases the performance by less than 5 % compared to the reference case with the lowest reference levels per speed.

5.4 Single-wheel validation

5.4.1 Simulation

The ABS algorithm is simulated using the model (5.1)-(5.7) where the relaxation effect of the tyre as well as the delay in actuation are taken into account. The following values are taken for the vehicle parameters: $r = 0.3\text{m}$, $J = 1.2\text{kgm}^2$, $\Delta t = 0.02\text{s}$ and $\gamma = 20\text{Nm/bar}$. The tyre curve $f(\lambda)$ is taken to match the shape of the experimental tyre curve (see Figures 5.11) with a peak force of 2800 N at a slip $\lambda^* = 0.1$. The tuning of the controller is as follows: $\dot{\omega}_{ref}^+ = 30$, $\dot{\omega}_{ref}^- = -40$, $k = 5$, $dF_n^+ = 10\%$, $dF_n^- = 7\%$.

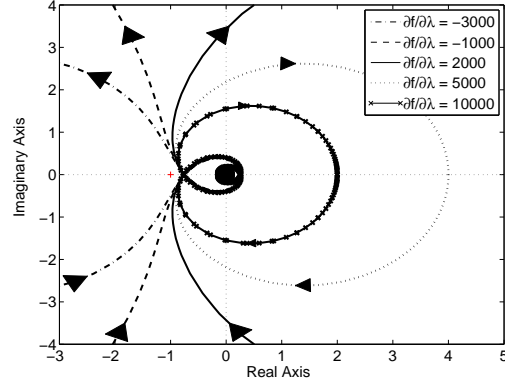


Figure 5.7: Nyquist plot of the linearized closed-loop system (5.1)-(5.7) for different values of $\frac{\partial f}{\partial \lambda}$.

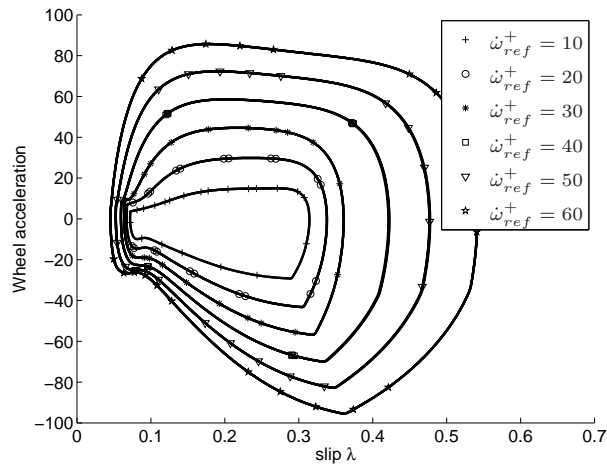


Figure 5.8: Limit cycle for different values of $\dot{\omega}_{ref}$

In the simulation presented on Figure 5.10, the single-wheel starts braking at 55 m/s and goes nearly until a full stop. The ABS cycles are clearly visible. After 5 seconds, the friction coefficient drops from 1 to 0.7; and 3 seconds after, the friction comes back to normal. The algorithm has no difficulty at all to deal with such a situation. Only the basic 2 phases are used and no extra logic is required. As the speed decreases, the ABS cycles becomes shorter. Also the influence of the actuation delay becomes relatively more important at low speed and therefore the force drop becomes slightly larger. Note that the same controller parameters are used along the whole simulation.

5.4.2 Experimental validation

The proposed algorithm has been tested on the tyre-in-the-loop experimental facility of Section 1.3.2.

The tuning is exactly like in simulation. So far, tests are performed at the constant speed of 18 m/s. In order to get a clean force signal, suitable for being used in switching mechanism, the force measurement signal is filtered with a second order filter with a cut-off frequency of 25 Hz. That frequency needs to be adapted with wheel speed. Then, the switching levels dF_n^+ and dF_n^- can easily be determined in order to contain the remaining noise level.

The results are shown on the left side of Figure 5.11. The algorithm works precisely like expected from the simulation. The brake force remains within 16% from the maximum of 3000 N.

5.4.3 Comparison with acceleration based hybrid algorithm

The deceleration-based 5-phase hybrid algorithm of Chapter 4 can serve as benchmark to compare this new ABS algorithm to. The method of Section 4.4.3 is used to deal with the actuation delay, since it leads to the best performances compared to the other methods of Chapter 4. Experimental tests of the 5-phase algorithm are recalled on the right side of Figure 5.11. The tests are done in similar conditions as for the force-based ABS: same test bench, same tyre, same loading and same speed.

From the measurements, and comparing with the left side of Figure 5.11, it can be noticed that the force-based algorithm presents some advantages:

- The force-based ABS is better at maintaining a low slip. The maximum slip during one cycle is $\lambda = 0.3$ for the force-based ABS while it is $\lambda = 0.4$ for the 5-phase ABS.
- The average brake force is larger in the case of the force-based algorithm, leading to a shorter braking distance. In particular, the 5-phase ABS let the force drop more (35%) in the stable zone than the force-based ABS (23%).
- In general, the force-based algorithm is able to detect force drops at an earlier stage and trigger more precisely the switch between phases.
- In the force-based algorithm, only 3 constant parameters need to be tuned, compared to 8 velocity-dependent parameters in the 5-phase ABS.

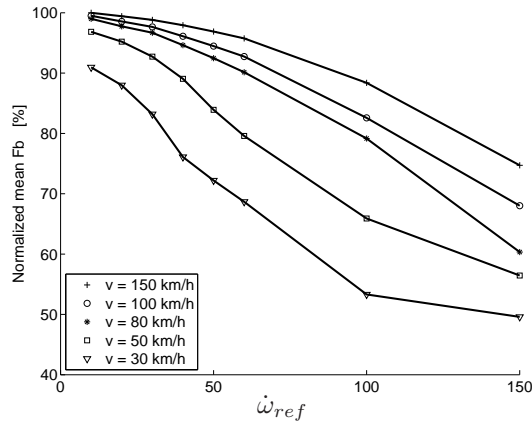


Figure 5.9: The choice of large $\dot{\omega}_{ref}$ leads to a decrease in performance, especially at lower speeds, and therefore to an increase of the braking distance.

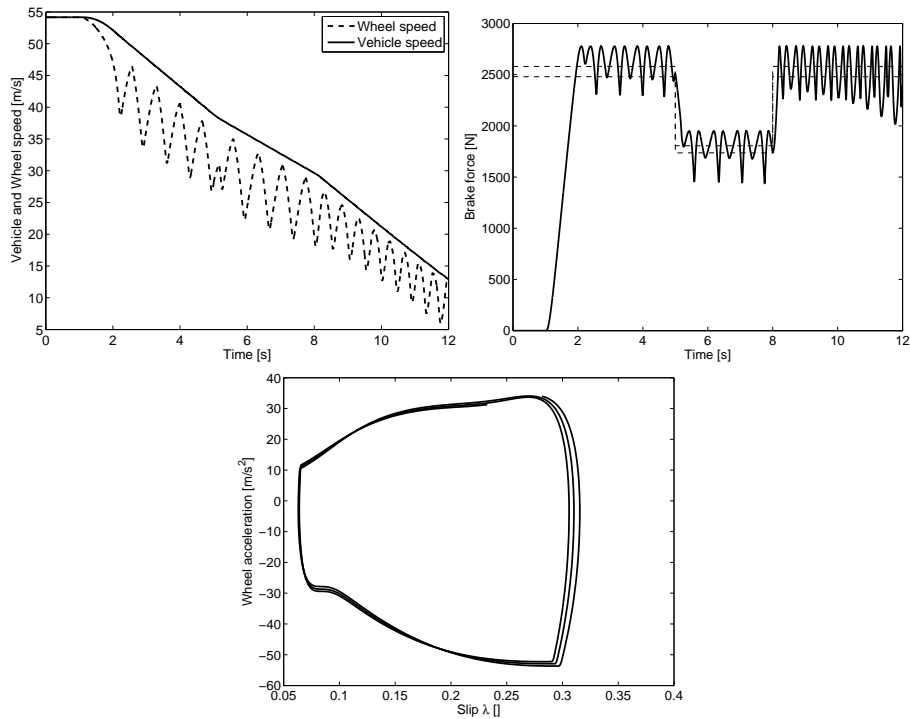


Figure 5.10: Wheel and vehicle speed, brake force and state trajectory during ABS regulation. Between the 5th and 8th second, the friction drops and the algorithm can easily handle it.

5.4. SINGLE-WHEEL VALIDATION

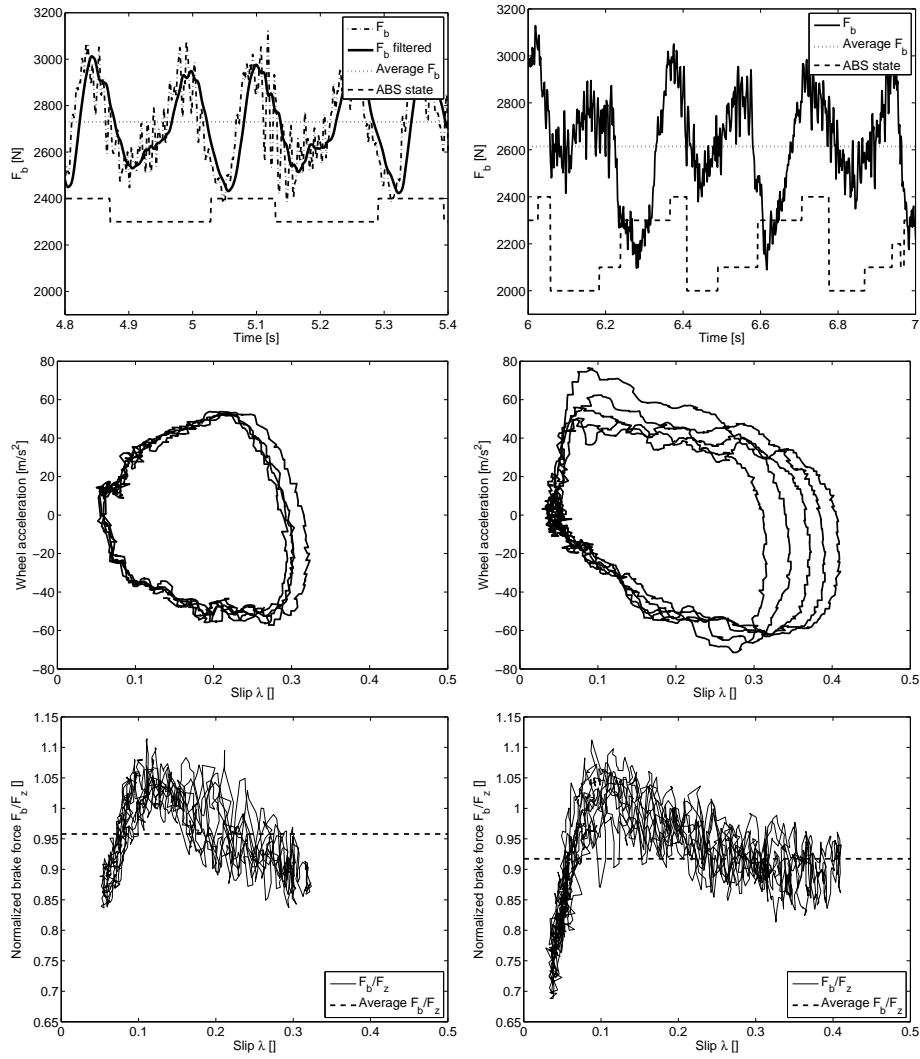


Figure 5.11: Experimental validation of the force-based ABS and comparison with the acceleration-based 5-phase algorithm. LEFT: force-based ABS. RIGHT: 5-phase ABS.

5.5 Simulation for the two-wheel vehicle

The ABS strategy is also simulated using the single-track two-wheel model (5.1)-(5.4) and (5.8)-(5.18). This scenario is realistic for a real vehicle braking in straight line as it also account for load transfer. The ABS controllers on each wheel are running separately. Forces are assumed measured via load sensing bearings. As a consequence in the algorithm implementation, equation 5.19 is modified using F_s (the vertical load on the wheel hub) instead of F_z . Both the longitudinal and vertical forces are affected by a measurement noise of 2%.

Because of the load repartition and the weight transfer, the load on the front tyre is much larger than on the rear tyre. To maintain the same performances, it is necessary to increase the brake efficiency at the front wheel, to make sure that the torque can be changed fast enough. The front brake efficiency is taken $\gamma = 40 \text{ Nm/bar}$, twice as large as in the nominal case. Accordingly, the controller gain needs to be reduced to guarantee that (5.37) remains stable. The front controller gain is taken $k = 3$.

Simulation results are shown on Figure 5.12. The vehicle starts braking at 55 m/s on dry asphalt with a friction coefficient of 1. Since the longitudinal force is normalized by the load for ABS regulation, the algorithm has no problem to handle weight transfer.

The thresholds dF_n^+ and dF_n^- used to detect force drops are large enough not to be mistriggered by measurement noise, making the algorithm robust. The difference between the vertical load F_z at the contact patch and F_s in the wheel hub remains under the 3% and it is mainly concentrated around the unsprung mass resonance (10 Hz); the difference is small enough to allow the use of one for the other in the switching strategy without affecting the overall performance.

5.6 Conclusion

A two-phase ABS algorithm has been presented. Thanks to tyre force measurement, the acceleration can be controlled in closed-loop to give a tight cycle and the switching strategy between the two phases is very precise even if simple. Stability is proven for a simple model by finding bounds on the limit cycle. When the more complex model with delays is considered, the stability results are extended with a linearization approach to provide practical and quantitative tuning tools. The best performances are achieved by using the two following tuning rules. First, the controller gain should be taken as large as possible while maintaining the stability in each phase. A linearization approach is given in order to easily compute this maximum gain for a given delay. Secondly, the reference wheel acceleration in each phase should be taken as small as possible, with a lower limit depending on the oscillations in the measurements. Furthermore, the algorithm is shown to be robust against changes in friction characteristic, vehicle speed and wheel load, without asking for extra logic or gain scheduling. An experimental tyre-in-the-loop test confirms that the algorithm is working in practice, exactly like predicted by the simulation. The algorithm is shown to perform better, while being easier to tune, compared to the 5-phase algorithm based on wheel acceleration only, implemented in Chapter 4.

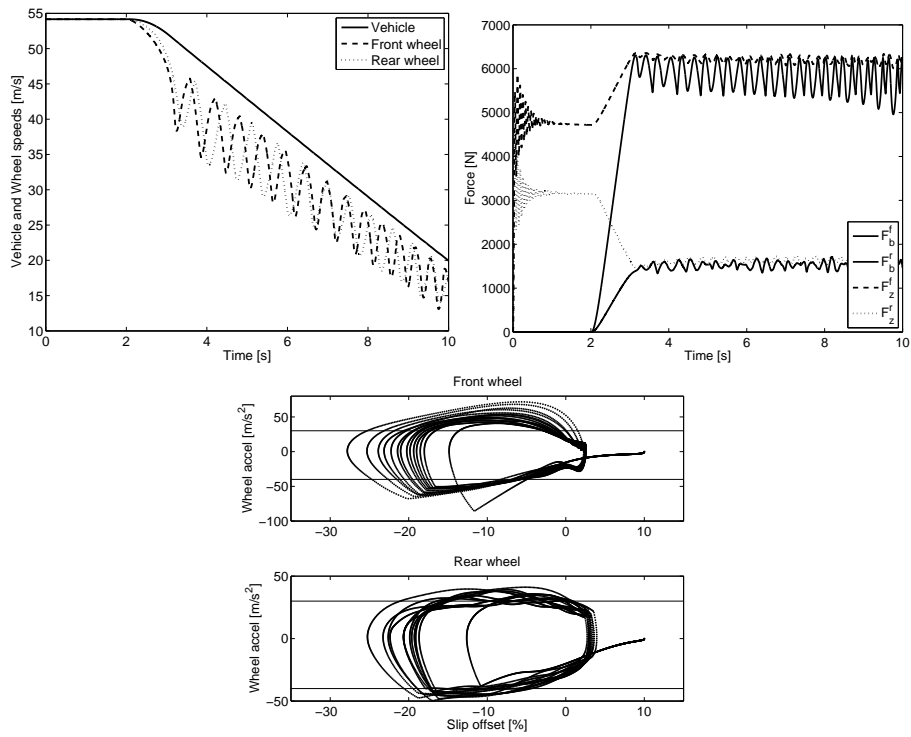


Figure 5.12: Simulation of the force-based ABS on a single-track two-wheel vehicle.



Chapter 6

ABS using Tyre Lateral Force

The main reason for implementing ABS, more important than maximizing the brake force, is to maintain a proper lateral behaviour for the vehicle during heavy braking, see Section 1.3. On one hand, the vehicle should be able to steer to avoid an obstacle, and on the other hand, the vehicle should have a stable yaw dynamics and not spin on itself. Because of the combined-slip effect, the lateral forces that the tyre is capable of producing are largely reduced when the wheel is locking, which endanger the lateral behaviour. By keeping the wheels unlocked, the ABS largely contributes to maintaining a lateral tyre potential, meaning the ability to generate lateral forces. Still, in all implementations of ABS available today, this main objective is never addressed directly.

For the class of hybrid controllers, see Section 1.3, the direct objective is to cycle around the peak of the longitudinal tyre characteristics. This maximizes the brake force and therefore minimizes the brake distance. On most surfaces, it can be expected that such a peak in the longitudinal characteristics will be present at a small slip value $\lambda \approx 0.1$, see Figure 6.1. By cycling around $\lambda \approx 0.1$, it is expected that, indirectly, a large enough tyre potential is maintained. However, there is no certainty. Furthermore, it can happen in certain conditions that the longitudinal tyre-road friction characteristics does not display a peak, see Figure 6.1. This makes all hybrid algorithms to be simply not working. In the commercial version of the Bosch algorithm, the hybrid controller is probably coupled with a slip regulator to deal with this problem.

For the class of slip regulators, see Section 1.3, the direct objective is to maintain the longitudinal slip λ at a given target λ^* . Next to the precise measurement of λ , the major difficulty resides in defining λ^* . Tyre models including non-linearities and combined-slip are clearly impossible to estimate online fast enough for ABS applications. Therefore, λ^* is always defined using rules and heuristics, with the hope that the chosen value will be a good compromise between lateral tyre potential and brake force. However, there is no guarantee, and this is one of the reason why current stability control systems have problems on road surfaces like snow.

The objective of this research is to extend the hybrid ABS algorithm developed in Chapter 5, such that the objective of maintaining a good lateral behaviour is considered directly. Requirements are set on the lateral behaviour of the front and

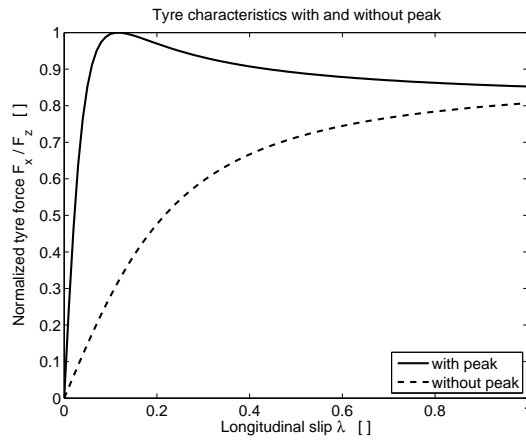


Figure 6.1: Tyre characteristics on different grounds, one with and one without a peak at a small slip.

the rear axle, and the ABS algorithm makes sure that the brake force is maximized while the lateral requirements are fulfilled. This is enabled thanks to the measurement of the lateral tyre forces.

Many different requirements could be implemented for the front and the rear axle. Sections 6.3 and 6.4 proposes 2 interesting illustrative options. As the tuning of the feel of the vehicle is extremely important for the branding, the final tuning of the algorithm is left for the car manufacturers. In both cases, a minimum lateral tyre force is computed for each axle. If the measured tyre force is lower than the minimum, actions are taken by the ABS.

Outline

The single-track vehicle model with nonlinear combined-slip tyres is described in Section 6.1. Afterwards, a simpler linear single-track model is analyzed to extract basic concepts. Section 6.2 focusses on the brake control algorithm. Finally, Sections 6.3 and 6.4 presents possible requirements for the front and rear axle, together with simulations.

6.1 Modelling

So far, only a single-wheel model was considered for ABS. Here, a vehicle model and a tyre model including the lateral dynamics are necessary. The vehicle is modelled using a single-track model. This simple model is sufficient to develop the basics of the controller. The tyres are modelled using the Magic Formula [95] that includes the combined-slip effect.

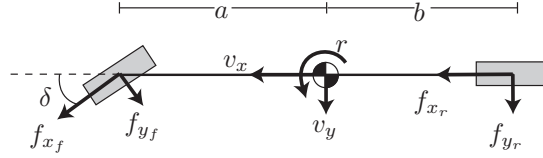


Figure 6.2: Scheme of the bicycle model.

6.1.1 Single-track model

Vehicles can be modelled with various levels of details. Large vehicle models with lots of features are definitely better in describing how a real vehicle would behave. However, for control or observation, it is definitely best practice to take reduced size models with fewer parameters that will include the main dynamics of the studied systems and lump many characteristics in a small set of general parameters.

In this research, we consider a single-track model (bicycle model) with 3 states: the longitudinal speed v_x , the lateral speed v_y and the yaw rate r . The main longitudinal and lateral dynamics are well represented. The tyre models are taken non-linear and with combined-slip effects and will be described in the next section. Effects like suspension kinematics or load transfer are not directly modelled but can be taken into account by adapting the tyre parameter. The bicycle scheme is shown on figure 6.2.

The equations of movement of the vehicle are written in the *vehicle frame*. This reference frame is attached to the centre of mass of the vehicle. The longitudinal axis lies in the symmetry plane of the vehicle and points forward while the lateral axis is directed to the left, perpendicular to the symmetry plane. Further, the tyre forces are expressed in the *tyre frame*. This reference frame is attached to the pivot point of the tyre. The longitudinal axis lies parallel to the free rolling direction of the tyre, while the lateral axis is directed to the left, perpendicular to the longitudinal axis.

The vehicle states evolves according to the following differential equations:

$$\dot{v}_x - v_y r = \frac{1}{m} (f_{x_f} \cos(\delta) - f_{y_f} \sin(\delta) + f_{x_r}) \quad (6.1)$$

$$\dot{v}_y + v_x r = \frac{1}{m} (f_{y_f} \cos(\delta) + f_{x_f} \sin(\delta) + f_{y_r}) \quad (6.2)$$

$$\dot{r} = \frac{1}{I_{zz}} (a f_{y_f} \cos(\delta) + a f_{x_f} \sin(\delta) - b f_{y_r}) \quad (6.3)$$

where f_{i_j} are the tyre longitudinal ($i = x$) or lateral ($i = y$) forces, at the front ($j = f$) or at the rear ($j = r$), m is the mass of the vehicle, I_{zz} is the inertia around the vertical axis and a and b are the distances between the centre of gravity and the front and rear axle respectively. The values of the vehicle parameters are given in Table 6.1.

Based on the vehicle states, the velocities of the front and rear tyres at the contact

m	1000 Kg	Vehicle mass
I_{zz}	1000 Kgm	Vehicle yaw inertia
a	1 m	Distance between CoG and front
b	1.5 m	Distance between CoG and rear
J	1 kg m ²	Wheel inertia
r	0.3 m	Wheel radius

Table 6.1: Vehicle parameters

patch can be written:

$$v_{x_f} = v_x \cos(\delta) + (v_y + ar) \sin(\delta) \quad (6.4)$$

$$v_{x_r} = v_x \quad (6.5)$$

$$\alpha_f = \arctan\left(\frac{v_{y_f}}{v_{x_f}}\right) = \delta - \arctan\left(\frac{v_y + ar}{v_x}\right) \quad (6.6)$$

$$\alpha_r = \arctan\left(\frac{v_{y_r}}{v_{x_r}}\right) = -\arctan\left(\frac{v_y - br}{v_x}\right) \quad (6.7)$$

$$(6.8)$$

The lateral slip α is used to represent the lateral velocity, since it is used by the Magic Formula.

6.1.2 Nonlinear Tyre Model

Tyres are extremely complex elements and in practice, a large amount of disturbing effects can be observed, which make the tyre model to deviate from a simple static friction curve. In this research, it is important to consider the longitudinal and lateral directions and include the combined-slip effect. For the sake of simplicity, the relaxation length and the vertical dynamics are omitted here. The tyre model is based on the Magic Formula [95].

The longitudinal and rotational movement of the tyre is described by the following equations:

$$J\dot{\omega}_j = -r f_{x_j} - T_{b_j} \quad (6.9)$$

$$\lambda_j = \frac{v_{x_j} - r\omega_j}{v_{x_j}} = 1 - \frac{r\omega_j}{v_{x_j}} \quad (6.10)$$

where j represents either front ($j = f$) or rear ($j = r$), ω_j is the angular speed of the wheel, v_{x_j} is the forward speed of the wheel in the *tyre frame*, λ_j is the longitudinal slip and T_{b_j} is the brake torque. The values of the parameters are given in Table 6.1. The brake torque T_{b_j} are the control inputs of the system.

In pure slip conditions, meaning that either λ or α should be equal to zero, the longitudinal and lateral tyre forces are given by:

$$f_{x_j}^0 = D_{x_j} \sin(C_{x_j} \arctan(B_{x_j} \lambda_j - E_{x_j}(B_{x_j} \lambda_j - \arctan(B_{x_j} \lambda_j)))) \quad (6.11)$$

$$f_{y_j}^0 = D_{y_j} \sin(C_{y_j} \arctan(B_{y_j} \alpha_j - E_{y_j}(B_{y_j} \alpha_j - \arctan(B_{y_j} \alpha_j)))) \quad (6.12)$$

where

Symbol	Description	Front	Rear	Rear
		without peak	with peak	without peak
K_x	Stiffness factor (long.)	20	20	20
C_x	Shape factor (long.)	0.9	1.4	0.9
D_x	Peak factor (long.)	1	1	1
E_x	Curvature factor (long.)	0	0	0
K_y	Stiffness factor (lat.)	15	25	25
C_y	Shape factor (lat.)	1.2	1.2	1.2
D_y	Peak factor (lat.)	1	1	1
E_y	Curvature factor (lat.)	0	0	0
r_{x1}	combined-slip param	15	15	15
r_{x2}	combined-slip param	15	15	15
r_{y1}	combined-slip param	15	15	15
r_{y2}	combined-slip param	15	15	15

Table 6.2: Tyre parameters for front and rear wheels, with or without peak in the characteristics, see Figure 6.1.

- C is the shape factor
- D is the peak factor
- E is the curvature factor
- $K = BCD$ is the stiffness factor

The values used for simulation are given in Table 6.2.

In case of combined-slip, when λ and α are both different from zero, there is an interaction between the longitudinal and the lateral forces modelled by:

$$f_{x_j} = G_{x_j} f_{x_j}^0 \quad (6.13)$$

$$G_{x_j} = \cos(\arctan(B_{gx_j}(\lambda_j)\alpha_j)) \quad (6.14)$$

$$B_{gx_j}(\lambda_j) = r_{x1_j} \cos(\arctan(r_{x2_j}\lambda_j)) \quad (6.15)$$

$$f_{y_j} = G_{y_j} f_{y_j}^0 \quad (6.16)$$

$$G_{y_j} = \cos(\arctan(B_{gy_j}(\alpha_j)\lambda_j)) \quad (6.17)$$

$$B_{gy_j}(\alpha_j) = r_{y1_j} \cos(\arctan(r_{y2_j}\alpha_j)) \quad (6.18)$$

where $f_{x_j}^0$ and $f_{y_j}^0$ are the longitudinal and lateral forces in pure slip and r_{x1_j} , r_{x2_j} , r_{y1_j} , r_{y2_j} are parameters, for which values are given in Table 6.2.

The changes in tyre characteristics due to combined-slip can be visualized on Figure 6.3. In particular, a large longitudinal slip λ will considerably reduce the potential for generating lateral forces. Also, the effective stiffness is largely reduced, which can lead to instability of the vehicle, as will be seen in next section.

6.1.3 Linear Analysis of the Single-Track Model

The nonlinearity of the vehicle and the tyre plays an important role for the analysis of the ABS. Still, the analysis of a simplified linear vehicle model can help quickly

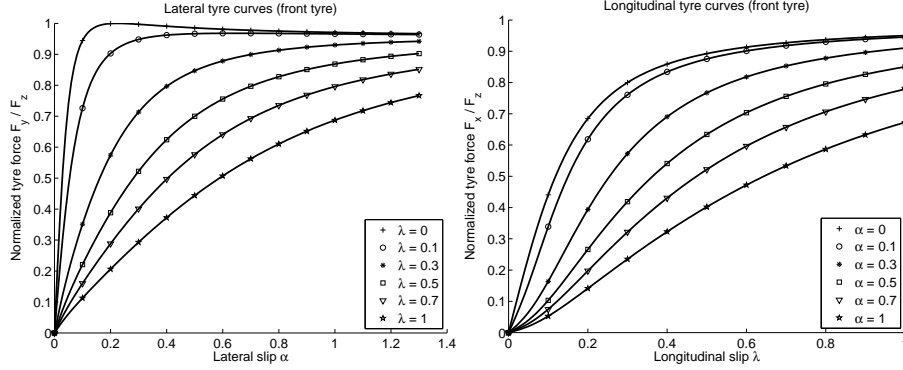


Figure 6.3: Tyre characteristics with combined-slip, lateral and longitudinal.

understanding some underlying concepts. This analysis is based on [95].

The previous nonlinear model is simplified using the following assumptions:

- The longitudinal velocity v_x is considered slowly varying and therefore taken as a parameter instead of a state. The model order is reduced to 2.
- The steering angle δ is assumed to be small.
- The lateral slip angle α is assumed to be small.
- The tyre model in the lateral direction is taken linear: $F_{y_j} = C_{y_j} \alpha_j$ where C_{y_j} is the cornering stiffness.

The equations of movement become

$$m(\dot{v}_y + v_x r) = f_{y_f} + f_{y_r} \quad (6.19)$$

$$I_{zz} \dot{r} = a f_{y_f} - b f_{y_r} \quad (6.20)$$

The slip angles are expressed by

$$\alpha_f = \delta - \frac{v_y + ar}{v_x} \quad (6.21)$$

$$\alpha_r = -\frac{v_y - br}{v_x} \quad (6.22)$$

The state equations can be written in state-space form:

$$\begin{pmatrix} \dot{v}_y \\ \dot{r} \end{pmatrix} = \underbrace{\begin{pmatrix} \frac{-C_{y_f} - C_{y_r}}{m v_x} & \frac{-C_{y_f} a + b C_{y_r}}{m v_x} - v_x \\ \frac{-a C_{y_f} + b C_{y_r}}{I_{zz} v_x} & \frac{-a^2 C_{y_f} - b^2 C_{y_r}}{I_{zz} v_x} \end{pmatrix}}_{A(C_{y_r}, v_x, \delta, C_{y_f})} \begin{pmatrix} v_y \\ r \end{pmatrix} + \begin{pmatrix} \frac{C_{y_f}}{m} \\ \frac{a C_{y_f}}{I_{zz}} \end{pmatrix} \delta \quad (6.23)$$

Linear Steady-State Cornering Solutions

When the vehicle is cornering with a constant steer angle at a constant speed, the following equations characterizes the steady-state solution.

The path curvature ($\frac{1}{R} \approx \frac{r}{v_x}$) can be computed as function of the steering angle

$$\frac{1}{R} = \frac{C_{y_f} C_{y_r} l}{C_{y_f} C_{y_r} l^2 - m v_x^2 (a C_{y_f} - b C_{y_r})} \delta \quad (6.24)$$

Introducing the understeer gradient η

$$\eta = -\frac{m g}{l} \frac{a C_{y_f} - b C_{y_r}}{C_{y_f} C_{y_r}} \quad (6.25)$$

where g is the acceleration due to gravity, we can write

$$\delta = \frac{l}{R} \left(1 + \eta \frac{v_x^2}{g l} \right) \quad (6.26)$$

It is referred to [51, 95] for details about the understeer gradient. A neutral car ($\eta = 0$) is often taken as a target for vehicle design. It can be noticed that, for a neutral car, the steady-state path curvature ($1/R$) is directly proportional to the steering angle δ .

Furthermore, the total lateral force is proportional to the path curvature

$$F_y = \frac{m v_x^2}{R} \quad (6.27)$$

Considering that, in steady-state, the front and rear forces need to balance each other

$$a f_{y_f} = b f_{y_r} \quad (6.28)$$

we can write

$$f_{y_f} = m \frac{b}{l} \frac{v_x^2}{R} \quad (6.29)$$

Stability

The local stability of the locally linearized system depending on the value of the rear cornering stiffness C_{y_r} can be assessed looking at the eigenvalues of the system matrix $A(C_{y_r}, v_x, \delta, C_{y_f})$. The maximum real part of the eigenvalues, depending on the rear cornering stiffness C_{y_r} and on the longitudinal vehicle speed v_x is shown on Figure 6.4. It can be observed that there exist a minimum cornering stiffness under which the vehicle is unstable. The larger the vehicle speed, the larger the minimum cornering stiffness need to be to ensure stability. This trend can be verified with extensive simulations on the non-linear model.

6.2 Algorithm

The algorithm provides the necessary braking action on each wheel in order to obtain the maximal brake force while ensuring that the minimum required lateral force is

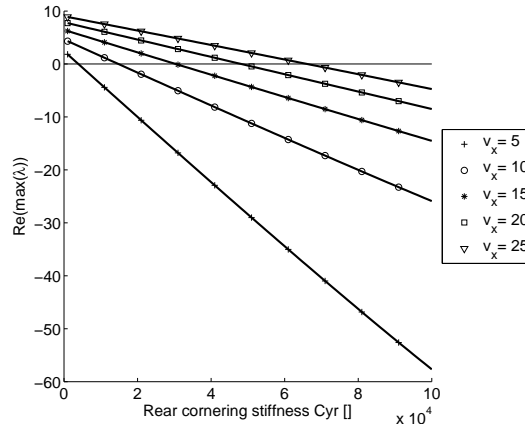


Figure 6.4: Maximum real part of the poles of the simplified and linearised model depending on the rear cornering stiffness $C_{y,r}$ and on the longitudinal vehicle speed v_x . The larger the vehicle speed, the larger the minimum cornering stiffness needs to be to ensure stability.

achieved. The algorithm is similar on both the front and the rear tyre and is running independently. Therefore references to a specific tyre are omitted in this section.

The ABS is a 3 phase hybrid algorithm extending the algorithm of Chapter 5. The automaton is depicted in Figure 6.5. Phase 1 is responsible for having the longitudinal slip to increase by providing a large enough brake torque. While in phase 1, two events can happen with the tyre:

- The longitudinal force can drop rapidly, indicating that the slip is larger than the slip providing the largest braking force.
- The lateral force can become smaller than the minimum required.

In both cases, it is necessary to decrease the longitudinal slip, either to increase the brake force or to increase the lateral force. Phases 2 and 3 are responsible for that. The different switching instants and phases are visualised on Figure 6.6.

If the longitudinal force drops of more than dF_b under it's maximum over time during the current phase \hat{F}_b , phase 2 is triggered and the slip is decreased. During each phase, \hat{F}_b at time instant k is computed as follows

$$\hat{F}_b(k) = \max(\hat{F}_b(k-1), F_b(k))$$

At the beginning of each phase, the value of \hat{F}_b is reset. This ensures that the maximal brake force is regularly adapted and that the algorithm is robust to changes in the tyre-road friction characteristic. The parameter dF_b defines how large the force drop needs to be in order to fire a phase switch. Defining the best value for this parameter is not an easy task. A too large drop will lead to a conservative algorithm giving a longer brake distance, while a too small value increases the sensitivity to noise. In practice, this parameter is often about a few hundred newtons. When the longitudinal

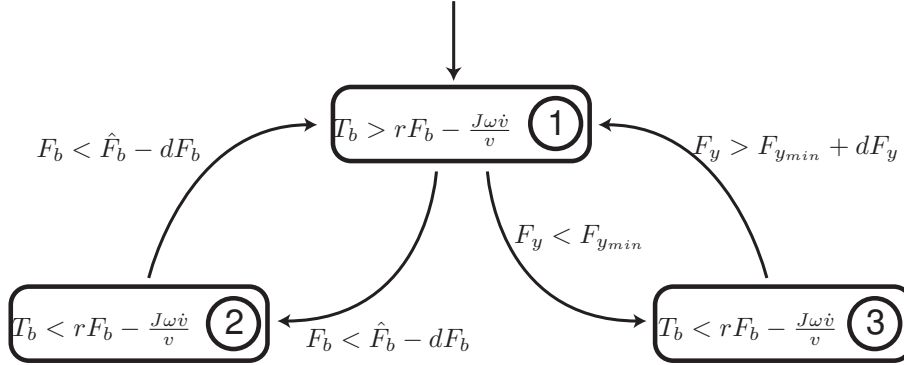


Figure 6.5: Hybrid Automaton of the 3-phase ABS algorithm. In phase 1 the slip is increased and the wheel goes towards wheel lock. In phase 2 and 3, the brake is released and the slip is decreased. A distinction is made between phase 2 and 3 depending on what reason triggered a slip decrease: drop in longitudinal force or too low lateral force; so that the algorithm knows what to look at for triggering a new slip increase.

force drops again, the maximum of the tyre curve has been passed again and phase 1 is triggered once more. This part of the algorithm is similar to Chapter 5.

If the measured lateral force F_y becomes smaller than $F_{y_{min}}$, the longitudinal slip has to be reduced and phase 3 is triggered. As soon as F_y becomes large enough, phase 1 could be triggered again. In order to avoid chattering, the parameter dF_y is added in the switching law. The choice of this parameter is not critical as it cannot make the controller to fail. It should be taken as small as possible, still maintaining a low level of chattering even in the presence of noise.

During each phase, the brake torque need to be controlled in order to get the longitudinal slip λ to evolve in the right direction. For this purpose, a method based on closed-loop control of the wheel acceleration has been developed in Chapter 5. Such method is suitable for this algorithm and could be applied. However, to reduce the complexity, a simpler method is implemented here. The brake torque T_b is assumed to be continuously controlled and, in this case, the slip derivative $\dot{\lambda}$ can be made positive or negative by setting the brake torque larger or smaller than $rF_b - \frac{J\omega\dot{v}}{v}$.

6.3 Requirement on the front axle

The objective, regarding the front axle, is to maintain a desired level of steerability. This means that the response to steering cannot be too low. Different ways to express such objective might exist. In this research, the objective is expressed in term of desired path curvature.

The path curvature ($1/R$) clearly defines the response of the car to steering action. Furthermore, it is expected that the path curvature is an instinctive measure for the driver. Therefore a minimum path curvature is required as a function of the steering angle. For any given desired understeer gradient η , the minimum path curvature

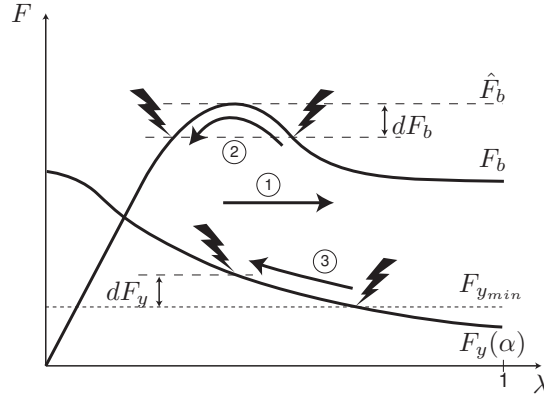


Figure 6.6: Visualization of the hybrid automaton on the longitudinal tyre curve. The lightnings represent the switching instants between the phases, while the arrows shows the direction of evolution of the longitudinal slip. F_b and F_y are the tyre forces, measured in real time by the force sensors. \hat{F}_b and $F_{y_{min}}$ are variable generated online by the controller.

can be computed using (6.26). As an example, the case of a neutral car ($\eta = 0$) is considered here and the relation is taken linear

$$\frac{1}{R} \Big|_{min} = \varphi \delta \quad (6.30)$$

From (6.29), the required minimum lateral force on the front axle is

$$f_{y_{min}} = \gamma v_x^2 \delta \quad (6.31)$$

for

$$\gamma = m \frac{b}{l} \varphi \quad (6.32)$$

6.3.1 Simulations

A simulation is performed to illustrate the functioning of the ABS. The results are shown on Figure 6.7. The vehicle is modelled using the equations of Sections 6.1.1 and 6.1.2. The vehicle is started in straight line at 30 m/s. After 2 seconds, heavy braking is performed on the front wheel only, with a requested braque torque of -2000 Nm. Because the front tyre characteristics does not present a peak, the wheel locks. At the 3rd second, a steering is initiated such that, at time 3.5 s, the steering angle is 0.1 rad. Since the wheel is locked, the lateral force is lower that the minimum required to offer the desired path curvature $\frac{1}{R} = \frac{\gamma \delta l}{m b} = 0.0083$. Therefore the ABS intervene and reduces the brake torque. f_y is increased while λ and f_x are decreased. Switching takes place to maintain f_y around the target value. It can be observed that the path curvature is just above the desired one.

Seemingly, the uncontrolled path curvature is largely depending on the longitudinal speed: the lower the speed and the larger the uncontrolled path curvature. Therefore, the control action required to maintain the desired path curvature is larger at

6.3. REQUIREMENT ON THE FRONT AXLE

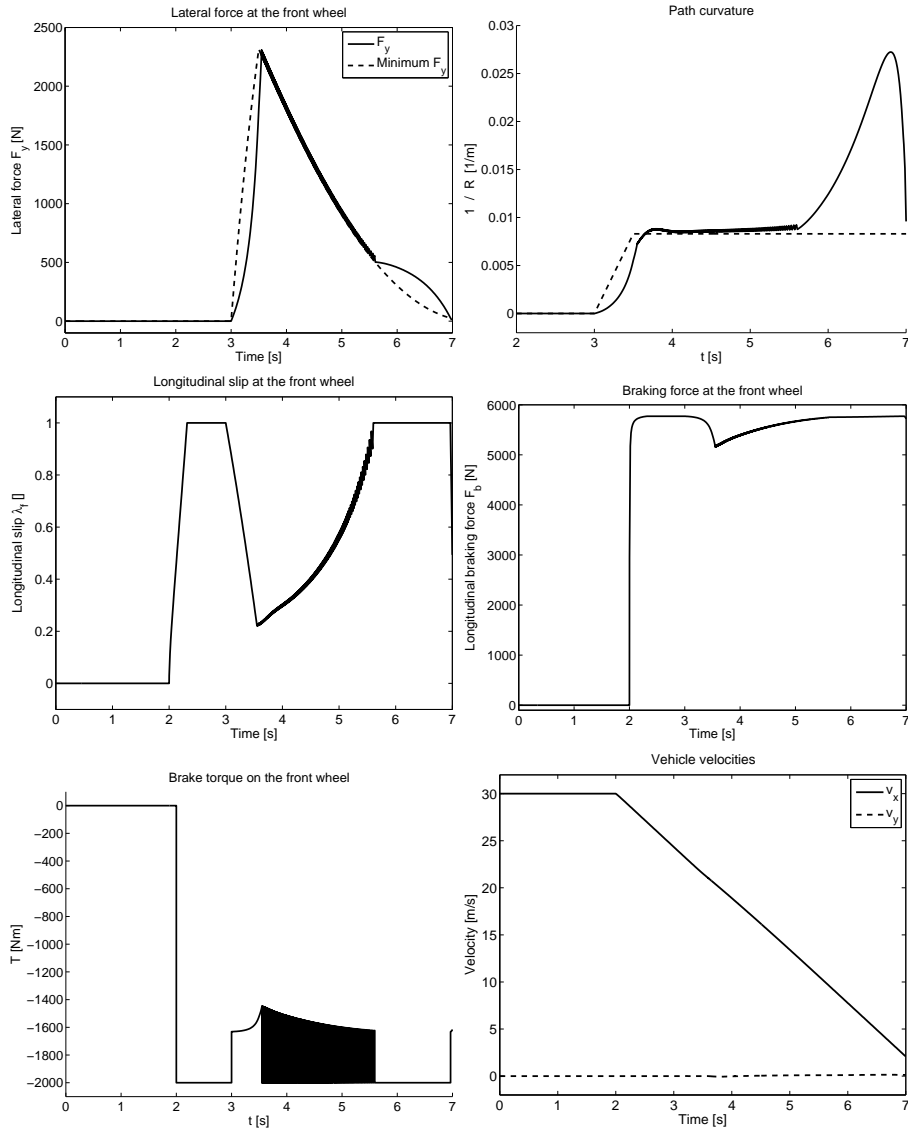


Figure 6.7: Simulation of heavy braking on the front wheel. When steering is initiated, the wheel is unlocked so that the desired cornering radius is achieved.

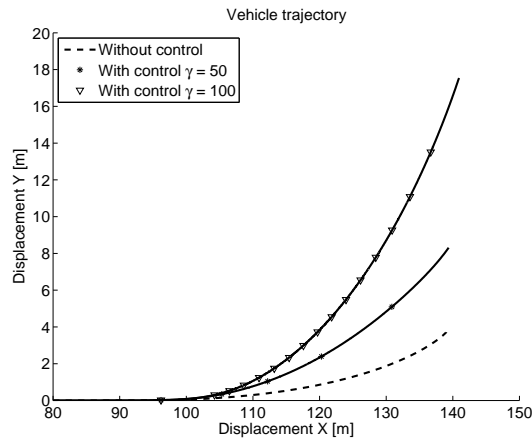


Figure 6.8: Comparison of the vehicle trajectory, with and without controller, for two different controller tuning.

high speed. In the considered simulation, for a longitudinal speed lower than 10m/s, the uncontrolled path curvature is larger than the minimum and the controller remains inactive.

Figure 6.8 shows a comparison of the vehicle trajectory, with and without controller, and for two different controller tuning. More simulations are performed to study the influence of the tuning parameter γ . The results are shown on Figure 6.9.

The left plot of Figure 6.9 shows the effective front tyre characteristics. The dotted lines illustrated the tyre characteristics in combined-slip for fixed values of λ , between 0 and 1. It can be observed that for low α , the lowest characteristics is followed, corresponding to a locked wheel; while for larger α , the characteristics is effectively given a larger slope by decreasing λ .

The right plot of Figure 6.9 shows the effective handling diagram for the vehicle. The handling diagram plots the difference between the front and the rear axle against the lateral acceleration. It is an interesting tool to evaluate the nonlinear steering behaviour of a vehicle. The local understeer/oversteer behaviour given by $\frac{\partial \delta}{\partial a_y}$ can be read from the diagram. Details about handling diagrams for a nonlinear vehicle model can be found in [95]. It can be observed that initially, the system is understeer: from (0, 0) the line goes to the left. But as soon as the controller gets active, the line goes straight towards the top. This is characteristic of a locally neutral behaviour. Note that the handling diagrams are originating from simulation data where the system is not precisely in steady-state.

6.4 Requirement on the rear axle

When it comes to the rear axle, the objective is to maintain the yaw stability of the vehicle to avoid spinning. As discussed in Section 6.1.3, the vehicle is stable as long as the cornering stiffness at the rear axle is larger than a certain minimum. The effect

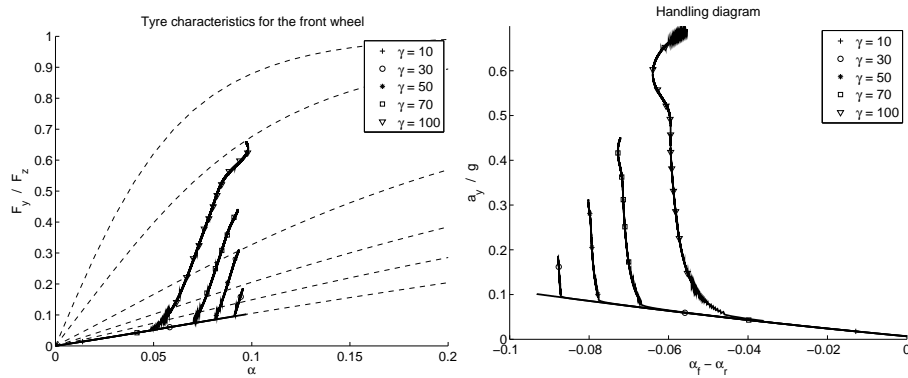


Figure 6.9: Effective front tyre characteristics and handling diagram for different values of the tuning parameter γ . Heavy braking is applied on the front wheel only.

of wheel lock is to reduce the effective cornering stiffness, which is the reason for the loss of stability. Therefore, the control objective is to maintain a minimum cornering stiffness on the rear axle.

The minimum required lateral force on the rear axle is then

$$f_{y_{r_{min}}} = C_{y_{r_{min}}} \alpha_r \quad (6.33)$$

Unfortunately, unlike for the front axle, the required lateral force cannot be implemented using only the measurement of the steering angle and an approximation of the vehicle speed. Here the lateral speed, or equivalently the side-slip angle, need to be estimated, which remains a delicate problem as discussed in Section 2.3. This constitutes a limitation regarding practical implementation, which should be addressed in future work. For example, the use of the yaw rate could be considered, similarly as in ESP systems. If an error on the minimum cornering stiffness maintained at the rear axle is tolerated, which is reasonable to assume in a certain measure, then this method can be made robust to a range of errors on the estimation of the side-slip.

6.4.1 Simulations

To illustrate the main principles, 2 simulations are performed. In both cases, the manoeuvre is the same and similar to the ones of Section 6.3.1. The initial speed of the vehicle is 15 m/s. After 3 seconds, a large brake torque reference of 1500 Nm is applied to the rear wheel only. Such brake torque is capable of making the wheel to lock. After 5 seconds, a steering angle of 6 degrees (0.1 rad) is applied on the front wheel while the braking action on the rear wheel is maintained. The manoeuvre stops when the vehicle speed has reached zero. The steering action is used here only as a way to potentially induce yaw instability, and the precise steering behavior is not looked at.

In the first simulation, the longitudinal tyre curve presents a maximum at a slip $\lambda = 0.25$. The results can be see on Figure 6.10. As soon as the braking action is triggered, the controller takes action to maintain the maximum braking force and

avoid wheel lock. As soon as the steering action is initiated, the controller realizes that the slip excursion given by the control of the brake force is too large to maintain the desired minimum cornering stiffness. Therefore, an oscillation between phases 1 and 3 will take place instead.

It can be observed that the oscillations between phases 1 and 3 are much faster than between phases 1 and 2. This has to do with the tyre dynamics and the parameters dF_b and dF_y . F_y is much more sensitive to changes in λ than F_b . Also, the parameter dF_y can be much smaller than dF_b . It should be noted that in practice, because of delays in the system and limited actuator and sensor bandwidth, the switching will be slower.

In the second simulation, the longitudinal tyre curve do not present any maximum, meaning that the maximal braking force is achieved at wheel lock. The results are presented on Figure 6.11. As soon as the braking is initiated, the wheels are locked by purpose to reach the largest braking force. At that time the vehicle is going straight and therefore no lateral potential is required from the tyre. However, as soon as the vehicle starts steering, the brake is released to come back to a more moderate slip value. Lateral potential is regained and stability is ensured.

In both simulations, the vehicle would become unstable and start spinning on itself if the controller would be disabled.

6.5 Conclusion

In this chapter, the hybrid force-based ABS of Chapter 5 has been extended to directly consider the lateral tyre behaviour during heavy braking. Only one extra phase was needed, together with the lateral tyre force measurement. The general control concept is that if the measured lateral force is smaller than a desired minimum, the longitudinal slip is reduced to regain lateral tyre potential.

The desired minimum lateral force is computed at each axle. For the front axle, this is based on a desired path curvature. For the rear axle, this should guarantee yaw stability, and could be based on a desired cornering stiffness. The investigation of other ways of computing the minimal lateral force is left for future research.

Various simulations performed on a nonlinear single track model confirms that the controller can maintain the desired steering behaviour and vehicle yaw stability in case of heavy braking. In the simulations, heavy braking is applied only to either the front or the rear axle, in order to clearly illustrate the different requirements at each axle. Combining heavy braking on all wheels at once does not bring extra complexity and no simulation is therefore shown here.

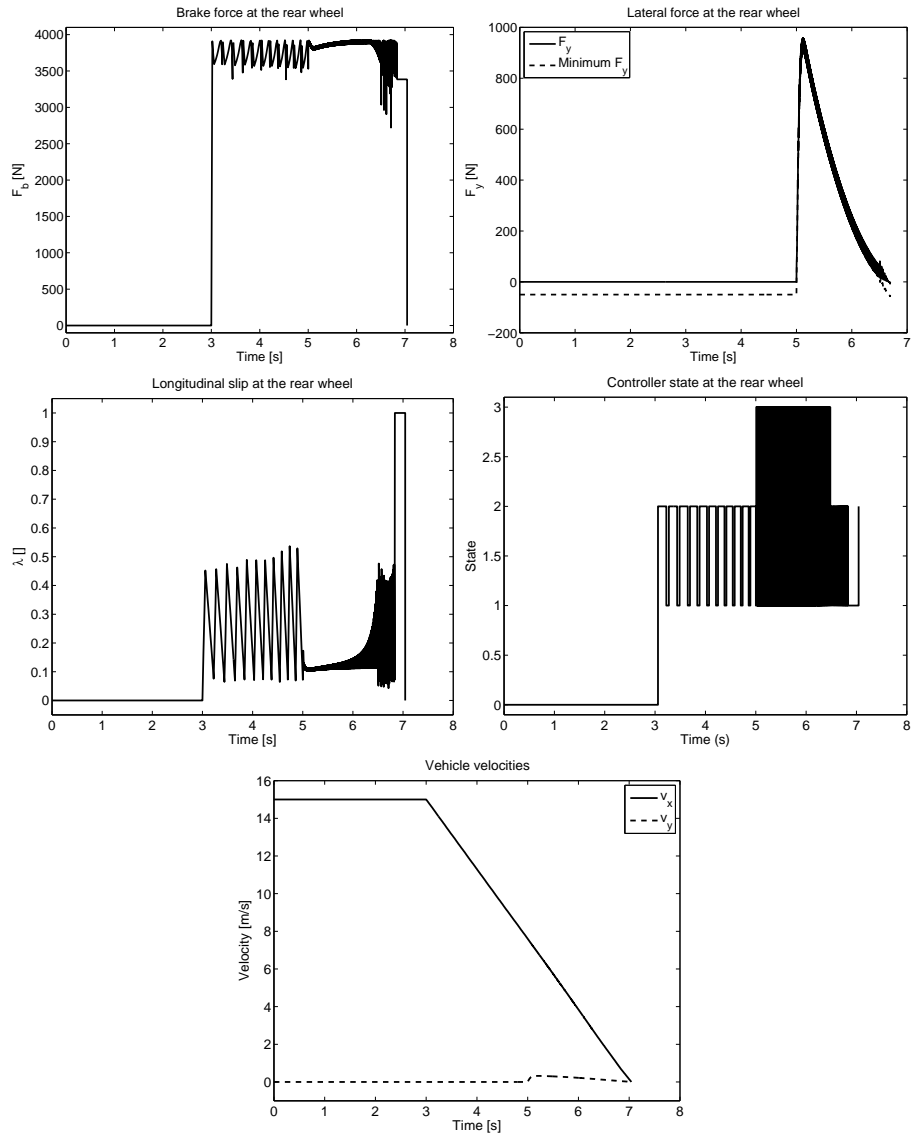


Figure 6.10: Simulation with a longitudinal tyre curve presenting a maximum at $\lambda = 0.25$. After the first 3 seconds, heavy braking is initiated at the rear axle and the controller oscillates between phases 1 and 2 to maintain the largest braking force. After 5 seconds, the front wheels are steered and a minimum cornering stiffness is imposed by the controller to maintain lateral stability.

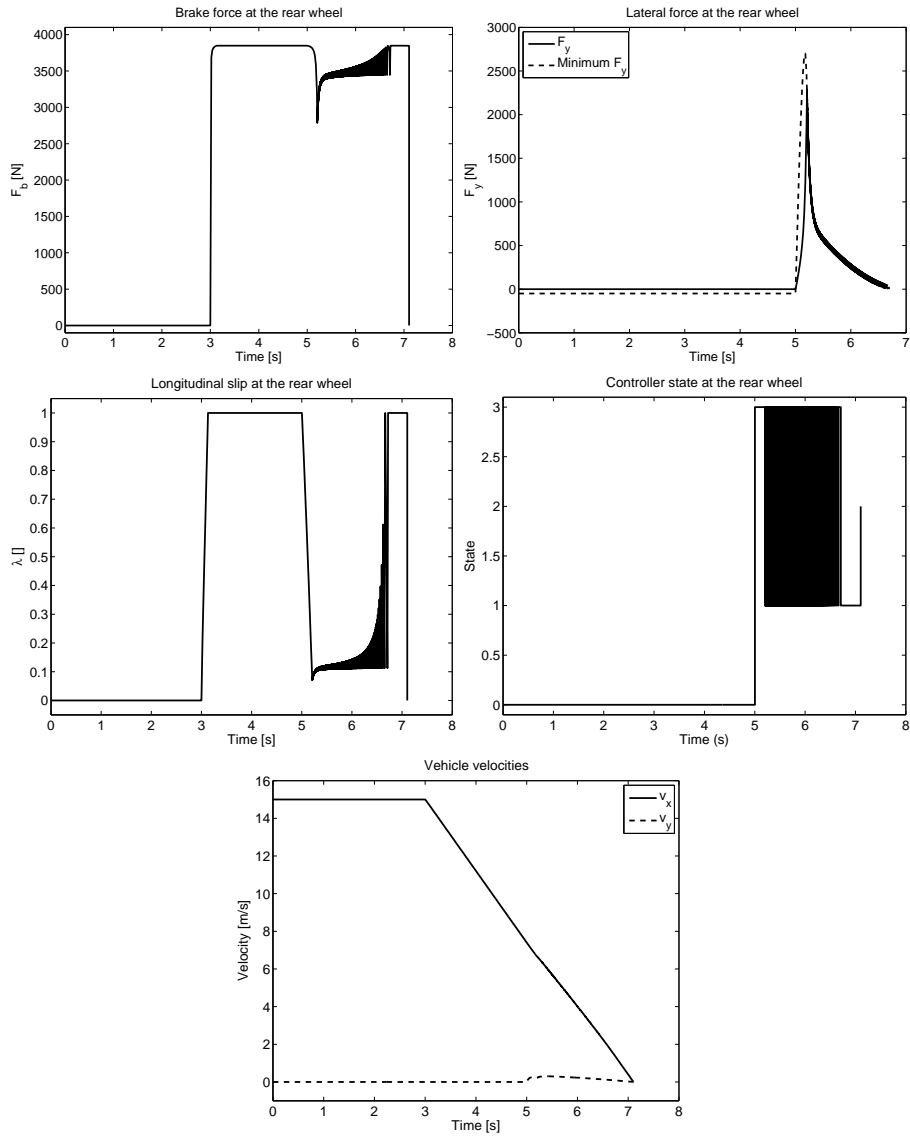


Figure 6.11: Simulation with a longitudinal tyre curve where the maximum is achieved at wheel lock. After the first 3 seconds, heavy braking is initiated at the rear axle and the wheels are locked by purpose to reach the largest braking force. After 5 seconds, the front wheel are steered and a minimum cornering stiffness is imposed by the controller to maintain lateral stability.

Chapter 7

Slip Control based on a Cascaded Approach

In collaboration with CNRS/Supelec, Paris, France.

Controlling the tyre slip λ around a given target λ^* is a popular problem, see Section 1.3. Even if the implementation of slip regulators requires the measurement of λ , which is still an open problem, see Section 2.3, they have properties complementary to hybrid ABS, which make them potentially of practical interest.

The control algorithm considered in this chapter has been introduced in [97]. This algorithm uses both wheel-slip and wheel acceleration measurement in a cascaded approach. Compared to existing approaches, the main interest of this new control algorithm are:

- it provides global exponential stability to the desired target (independently of its location in the stable or unstable region of the tyre), by taking into account the non-linear nature of the system;
- it gives precise bounds on the gains of the control law for which stability is proved mathematically;
- it contains a feedforward term, which improves the bandwidth of the closed-loop system.

The aim of this chapter is twofold. On one hand, the algorithm proposed in [97] is validated experimentally on the tyre-in-the-loop experimental facility of Section 1.3.2. On the other hand, the stability conditions proposed in [97] are relaxed, using LMI's, in order to better match with the requirements on the controller gains experienced in practice. Moreover, the theoretical results of [97] are reformulated to more conveniently fit with the control laws used in the experimental framework.

Outline

The model used for design and simulation is presented in Section 7.1. The control design and the stability proofs are discussed in Section 7.2. Section 7.3 presents

various simulations assessing performance and robustness. Finally, the tyre-in-the-loop experimental validation is performed in Section 7.4.

7.1 System modelling

The design of the control law is based on the simple single-wheel model of Section 4.1. Only the longitudinal dynamics of a single loaded wheel is considered. This model is realistic enough to include the basic phenomena related to ABS, like the nonlinear tyre characteristics and the wheel rotation dynamics, and is simple enough to allow for analytical computations, like control design and stability proof. Actuation delay and tyre relaxation are omitted in the design phase but simulations are used later on to assess the robustness, see Section 7.3.

For the states x_1 and x_2 defined as

$$\begin{aligned} x_1 &= \lambda \\ x_2 &= R\dot{\omega} - a_x^*(t), \end{aligned}$$

with a_x^* is the constant vehicle deceleration as defined in (4.7), state equations similar to (4.8) and (4.9) can be written

$$\frac{dx_1}{dt} = \frac{1}{v_x(t)} (-a_x^*(t)x_1 + x_2) \quad (7.1)$$

$$\frac{dx_2}{dt} = -\frac{a\mu'(x_1)}{v_x(t)} (-a_x^*(t)x_1 + x_2) + \frac{u}{v_x(t)}, \quad (7.2)$$

where $a = \frac{R^2}{I} F_z$ and $u = v_x(t) \frac{R}{I} \frac{dT}{dt}$.

Observe that the derivative of the torque is considered as control input. Depending the kind of technology used by the brake actuator, it might be necessary to integrate the control input in order to have a brake torque reference.

7.2 Control design

The objective is to define a control law u that drives x_1 towards a given time-dependent wheel-slip target $\lambda^*(t)$. Several steps are taken to obtain u . Firstly, the time-scale is normalized by the vehicle speed, such that the dependence on speed disappears. This is enabled by using a filtering on the target λ^* . Secondly, the convergence of x_1 is translated into a convergence of x_2 using a dynamic set-point. Two control laws are considered, one with feedback only and one with feedback and feedforward. Closed-loop stability is assessed based on Lyapunov arguments.

7.2.1 An homogeneous target filter

The following second order filter is defined for the target λ^* :

$$\begin{aligned} \frac{d\lambda_1}{dt} &= \frac{\lambda_2}{v_x(t)} \\ \frac{d\lambda_2}{dt} &= \frac{-\gamma_1(\lambda_1 - \lambda^*) - \gamma_2\lambda_2}{v_x(t)}. \end{aligned}$$

where γ_1 and γ_2 are tuning parameters.

The aim of this target filter is twofold. On one hand, it allows to have a smooth target (that one can differentiate twice) even if the original target is discontinuous (for example, piecewise constant). On the other hand, it allows to have a system for which all equations are divided by the vehicle speed. This homogeneity allows us to analyse the system in a new (nonlinear) time-scale in which the dependence on speed disappears.

Like in traditional second-order filters, the parameters γ_1 and γ_2 defines the bandwidth and the damping of the system. It is clearly necessary to choose values giving a stable filter, and desirable to have enough damping to avoid oscillations [45]. Furthermore, a large bandwidth means high performances, with a smooth target λ_1 quickly converging to the real target λ^* . However, it can be expected that a large bandwidth will ask for a large control input u .

7.2.2 A new time-scale

Since the system is homogeneous in the vehicle speed, a change of time-scale similar as in [96] can be applied. Let

$$s(t) := \int_0^t \frac{d\tau}{v_x(\tau)}$$

hence, $dt = v_x(t)ds$ and consequently, for any function $\varphi : \mathfrak{R} \rightarrow \mathfrak{R}^n$ we have

$$\frac{d\varphi}{ds} = \frac{d\varphi}{dt} \frac{dt}{ds}.$$

Therefore, defining $\dot{\varphi}(s) = \frac{d\varphi(s)}{ds}$ we have

$$\dot{x}_1 = -a_x^* x_1 + x_2 \quad (7.3)$$

$$\dot{x}_2 = -a\mu'(x_1)(-a_x^* x_1 + x_2) + u \quad (7.4)$$

$$\dot{\lambda}_1 = \lambda_2 \quad (7.5)$$

$$\dot{\lambda}_2 = -\gamma_1(\lambda_1 - \lambda^*) - \gamma_2 \lambda_2. \quad (7.6)$$

Note that, in this chapter, the dot notation refers to the derivative with respect to the new time-scale.

7.2.3 Dynamic set-point

The error on the tracking of the filtered slip target is

$$z_1 = x_1 - x_1^*$$

where $x_1^* = \lambda_1$. From (7.3), the error dynamics is

$$\dot{z}_1 = -a_x^* x_1 + x_2 - \lambda_2$$

Let us first assume that x_2 is a virtual control input. Then the control law

$$x_2 = \lambda_2 + a_x^* x_1 - \alpha z_1 + \dot{z}_1$$

with $\alpha > 0$ gives

$$\dot{z}_1 = -\alpha z_1 + z_2$$

which is exponentially stable if $z_2 = 0$. Here z_2 can be seen as the error on the wheel acceleration tracking

$$z_2 = x_2 - x_2^*$$

where

$$x_2^* = a_x^* x_1 + \lambda_2 - \alpha z_1$$

Observe that while x_1^* is only based on $\lambda_1(t)$, the set-point x_2^* is dynamic. The steady state part is $a_x^* x_1$, while the two other terms are used to decrease the error on z_1 , both using cascaded feedback $-\alpha z_1$ and feedforward λ_2 . Thanks to this dynamic set-point, the system converges to exactly the desired wheel slip irrespectively from the tyre characteristic, unlike some other mixed slip-acceleration approaches, like for example [107].

The dynamics of z_2 is given by

$$\begin{aligned} \dot{z}_2 &= \dot{x}_2 - \dot{x}_2^* \\ &= -a\mu'(\lambda)(-a_x^* x_1 + x_2) + u - (a_x^* \dot{x}_1 + \ddot{x}_1^* - \alpha \dot{z}_1) \\ &= -a\mu'(\lambda)(-a_x^* x_1 + x_2) + u - a_x^* (-a_x^* x_1 + x_2) - \dot{\lambda}_2 + \alpha(-\alpha z_1 + z_2) \\ &= -(a\mu'(\lambda) + a_x^*)(-a_x^* x_1 + x_2) - \alpha^2 z_1 + \alpha z_2 - \dot{\lambda}_2 + u \\ &\quad [\text{using } -a_x^* x_1 + x_2 = -\alpha z_1 + z_2 + \lambda_2] \\ &= \alpha z_1 (a\mu'(\lambda) + a_x^* - \alpha) - z_2 (a\mu'(\lambda) + a_x^* - \alpha) - (a\mu'(\lambda) + a_x^*) \lambda_2 - \dot{\lambda}_2 + u. \end{aligned}$$

Hence, defining

$$\eta(\lambda) := a\mu'(\lambda) + a_x^* - \alpha \quad (7.7)$$

and

$$\psi(\lambda) := -a\mu'(\lambda) - a_x^* \quad (7.8)$$

we obtain

$$\dot{z}_2 = \eta(\lambda) (\alpha z_1 - z_2) + \psi(\lambda) \lambda_2 - \dot{\lambda}_2 + u \quad (7.9)$$

The purpose of the control law u is now to drive z_2 to zero, which thanks to the dynamic set-point, ensures that z_1 converges to zero as well. Two control laws are proposed, one with feedback only and one with feedback and feedforward.

The control scheme is illustrated on Figure 7.1. The system (S) of equations (7.1) and (7.2) is controlled by both a feedback (FB) and a feedforward (FF). The dynamic set-point x_2^* is computed based on the error z_1 . The feedforward could make use of x_1 or z_1 , but this is not required.

7.2.4 Control law with proportional feedback

The first proposed control law is a linear proportional feedback on the form

$$u = -k_1 z_1 - k_2 z_2 \quad (7.10)$$

where k_1 and k_2 are two tuning parameters. This control law can be shown to stabilize the closed-loop system for suitable values of the parameters α , k_1 , k_2 , γ_1 , γ_2 . Sufficient conditions for stability are stated in the next proposition.

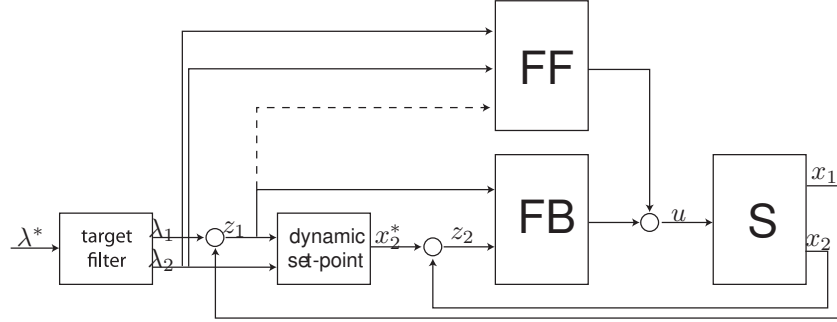


Figure 7.1: Control scheme of the cascaded wheel slip controller.

Proposition 7.1. *For a constant target λ^* , the time-varying closed-loop system obtained by introducing the control law*

$$u = -k_1 z_1 - k_2 z_2$$

into the system defined by equations (7.3)-(7.6) is globally exponentially stable and converges to $(z_1 = 0, z_2 = 0)$ if

1. *the system $\dot{z} = F_1(\lambda, z)$ with $F_1 = \begin{pmatrix} -\alpha z_1 + z_2 \\ -(k_1 - \alpha\eta(\lambda))z_1 - (k_2 + \eta(\lambda))z_2 \end{pmatrix}$, obtained when $\lambda_2 = \dot{\lambda}_2 = 0$, is globally exponentially stable,*
2. *the gains γ_1 and γ_2 are positive.*
3. *there exist a number c_μ^M such that $|\mu'(\lambda)| < c_\mu^M \quad \forall \lambda \in \mathfrak{R}$,*

Proof. Define $\tilde{\lambda}_1 := \lambda_1 - \lambda^*$. Then, with λ^* constant, the closed-loop equations are

$$\dot{z}_1 = -\alpha z_1 + z_2 \quad (7.11)$$

$$\dot{z}_2 = -(k_1 - \alpha\eta(\lambda))z_1 - (k_2 + \eta(\lambda))z_2 + \psi(\lambda)\lambda_2 - \dot{\lambda}_2 \quad (7.12)$$

$$\dot{\tilde{\lambda}}_1 = \lambda_2 \quad (7.13)$$

$$\dot{\lambda}_2 = -\gamma_1 \tilde{\lambda}_1 - \gamma_2 \lambda_2 \quad (7.14)$$

Defining $z := [z_1; z_2]$ and $\Lambda := [\tilde{\lambda}_1; \lambda_2]$ we see that the closed-loop system has a so-called cascaded form

$$\dot{z} = F_1(t, z) + G(\lambda)\Lambda \quad (7.15)$$

$$\dot{\Lambda} = F_2(\Lambda) \quad (7.16)$$

where

$$F_1(\lambda, z) := \begin{pmatrix} -\alpha z_1 + z_2 \\ -(k_1 - \alpha\eta(\lambda))z_1 - (k_2 + \eta(\lambda))z_2 \end{pmatrix}$$

$$F_2(\Lambda) := \begin{pmatrix} 0 & 1 \\ -\gamma_1 & -\gamma_2 \end{pmatrix}$$

$$G(\lambda) := \begin{pmatrix} 0 & 0 \\ \gamma_1 & \psi(\lambda) + \gamma_2 \end{pmatrix}$$

According to results for cascaded systems [80] the system (7.15)-(7.16) is globally exponentially stable at the origin if:

- (a) the origin of $\dot{z} = F_1(\lambda, z)$ is globally exponentially stable;
- (b) the origin of $\dot{\Lambda} = F_2(\Lambda)$ is globally exponentially stable;
- (c) the solutions are globally bounded uniformly in the initial conditions.

Those three conditions are ensured by the hypotheses of the theorem. Firstly, (a) is similar to the first condition of the theorem. Secondly, (b) evidently holds for any positive values of γ_1, γ_2 as the system is linear time-invariant and of second order, which is ensured by the second condition of the theorem. Thirdly, (c) holds if $G(\lambda(t))$ is bounded uniformly for all t , see [80]. The latter holds, since, thanks to the third condition of the theorem, $\psi(\lambda)$ is bounded for all $\lambda \in \mathfrak{R}$. \square

7.2.5 Stability of $\dot{z} = F_1(\lambda, z)$

It is left to show that the system $\dot{z} = F_1(\lambda, z)$ is globally exponentially stable, and to find conditions on the parameters α, k_1 and k_2 .

A first result is that, for any positive value of α and k_1 , the system $\dot{z} = F_1(\lambda, z)$ can be made stable using a large enough gain k_2 . This is shown using Lyapunov arguments.

Consider a Lyapunov function V on the form

$$V(z_1, z_2) = \frac{1}{2}\epsilon z_1^2 + \frac{1}{2}z_2^2 \quad (7.17)$$

where $\epsilon > 0$.

The total time derivative along the trajectories of $\dot{z} = F_1(\lambda, z)$ yields

$$\begin{aligned} \dot{V} &= \epsilon z_1 \dot{z}_1 + z_2 \dot{z}_2 \\ &= \epsilon z_1 (-\alpha z_1 + z_2) + z_2 (-(k_1 - \alpha\eta(\lambda))z_1 - (k_2 + \eta(\lambda))z_2) \\ &= - \begin{pmatrix} z_1 \\ z_2 \end{pmatrix}^T \begin{pmatrix} \epsilon\alpha & \frac{-\epsilon + k_1 - \alpha\eta(\lambda)}{2} \\ \frac{-\epsilon + k_1 - \alpha\eta(\lambda)}{2} & k_2 + \eta(\lambda) \end{pmatrix} \begin{pmatrix} z_1 \\ z_2 \end{pmatrix} \end{aligned}$$

Using Sylvester's criteria, the matrix is positive definite if and only if

$$\epsilon\alpha > 0 \quad (7.18)$$

$$\epsilon\alpha(k_2 + \eta(\lambda)) > \frac{(-\epsilon + k_1 - \alpha\eta(\lambda))^2}{4} \quad (7.19)$$

where the latter condition can be rewritten

$$k_2 > \frac{\epsilon^2 + k_1^2 - 2\epsilon k_1 + \alpha^2 \eta(\lambda)^2 - 2\alpha(\epsilon + k_1)\eta(\lambda)}{4\epsilon\alpha} \quad (7.20)$$

Since $\mu'(\lambda)$ is bounded, there exist two numbers $\eta_{|M|}$ and η_m such that

$$|\eta(\lambda)| < \eta_{|M|} \quad \forall \lambda \in \mathfrak{R}$$

and

$$\eta(\lambda) > \eta_m \quad \forall \lambda \in \mathfrak{R}$$

Therefore, the condition

$$k_2 > \frac{\epsilon^2 + k_1^2 - 2\epsilon k_1 + \alpha^2 \eta_{|M|}^2 - 2\alpha(\epsilon + k_1)\eta_m}{4\epsilon\alpha} \quad (7.21)$$

robustly ensures that $\dot{V} < 0$ when $(z_1, z_2) \neq (0, 0)$, which proves global exponential stability.

However, in practice, it can be observed that this bound on k_2 is conservative, since a Lyapunov function with few degrees of freedom was considered. A less conservative method for checking the stability of the system is to use a Linear Matrix Inequality (LMI) feasibility test. The system $\dot{z} = F_1(\lambda, z)$ can be considered linear with parametric uncertainties. With $\eta_m < \eta(\lambda) < \eta_M \quad \forall \lambda$, the vertices state matrices can be written

$$A_m = \begin{pmatrix} -\alpha & 1 \\ -(k_1 - \alpha\eta_m) & -(k_2 + \eta_m) \end{pmatrix} \quad (7.22)$$

$$A_M = \begin{pmatrix} -\alpha & 1 \\ -(k_1 - \alpha\eta_M) & -(k_2 + \eta_M) \end{pmatrix} \quad (7.23)$$

The LMI feasibility test is to try to find a symmetric matrix X such that

$$X > 0 \quad (7.24)$$

$$A_m^T X + X A_m < 0 \quad (7.25)$$

$$A_M^T X + X A_M < 0 \quad (7.26)$$

If X can be found, then $V = z^T X z$ is a suitable Lyapunov function that guarantees the robust stability of the system.

7.2.6 Control law with feedforward

The linear feedback controller has been shown to be able to ensure stability. However, it may be expected that it yields a relatively poor transient performance. This can be observed in the simulations of Section 7.3. Furthermore, the stability proof is not valid if the target slip λ^* is time-varying. To solve those two problems, an extended control law can be considered:

$$u = -k_1 z_1 - k_2 z_2 - \psi(\lambda)\lambda_2 + \dot{\lambda}_2 \quad (7.27)$$

The term $-\psi(\lambda)\lambda_2$ is not strictly speaking a feedforward as it is depending on the state variable λ . Still, as the main purpose is to feed changes on the target slip λ^* via λ_2 , the terminology feedforward is used. Furthermore, as $\psi(\lambda)$ is mostly uncertain, it is common in practical implementation to replace $\psi(\lambda)$ by a constant, see Section 7.2.7. In that case, the added terms in the control law are strictly speaking feedforward terms.

The stability of the closed-loop system is addressed in the following proposition.

Proposition 7.2. *For any arbitrary piecewise continuous target $\lambda^*(t)$, the time-varying closed-loop system obtained by introducing the control law*

$$u = -\gamma_1(\lambda_1 - \lambda^*) + (-\gamma_2 + a_x^* + a\mu'(\lambda))\lambda_2 - k_1z_1 - k_2z_2 \quad (7.28)$$

into the system defined by equations (7.3)-(7.6) is globally exponentially stable and converges to $(z_1 = 0, z_2 = 0)$ if

- *the system $\dot{z} = F_1(\lambda, z)$ is globally exponentially stable,*
- *there exist a number c_μ^M such that $|\mu'(\lambda)| < c_\mu^M \quad \forall \lambda \in \mathfrak{R}$,*
- *the gains γ_1 and γ_2 are positive.*

Proof. With the control law, the closed-loop system writes

$$\dot{z}_1 = -\alpha z_1 + z_2 \quad (7.29)$$

$$\dot{z}_2 = -(k_1 - \alpha\eta(\lambda))z_1 - (k_2 + \eta(\lambda))z_2 \quad (7.30)$$

$$\dot{\lambda}_1 = \lambda_2 \quad (7.31)$$

$$\dot{\lambda}_2 = -\gamma_1(\lambda_1 - \lambda^*) - \gamma_2\lambda_2 \quad (7.32)$$

where the dynamics of (z_1, z_2) and (λ_1, λ_2) are decoupled. The stability of (z_1, z_2) is the first condition of the proposition, while the stability of (λ_1, λ_2) is ensured when γ_1 and γ_2 are positive. \square

7.2.7 Feedforward with tyre uncertainties

The implementation of the feedforward requires the knowledge of the tyre characteristics $\mu'(\lambda)$, which is not the case during practical implementations. Still, it can be shown that the feedback term can maintain the system stable even if the estimates $\hat{\mu}'(\lambda)$ of $\mu'(\lambda)$ used in the feedforward is not correct.

Proposition 7.3. *For a constant target λ^* , the time-varying closed-loop system obtained by introducing the control law*

$$u = -\gamma_1(\lambda_1 - \lambda^*) + (-\gamma_2 + a_x^* + a\hat{\mu}'(\lambda))\lambda_2 - k_1z_1 - k_2z_2 \quad (7.33)$$

into the system defined by equations (7.3)-(7.6) is globally exponentially stable and converges to $(z_1 = 0, z_2 = 0)$ if

- *the system $\dot{z} = F_1(\lambda, z)$ is globally exponentially stable,*
- *$|\mu'(\lambda)|$ and $|\hat{\mu}'(\lambda)|$ are bounded for $\lambda \in \mathfrak{R}$,*
- *the gains γ_1 and γ_2 are positive.*

Proof. With the control law, and using $\tilde{\lambda}_1$ like in Proposition 7.1, the closed-loop system writes

$$\dot{z}_1 = -\alpha z_1 + z_2 \quad (7.34)$$

$$\dot{z}_2 = -(k_1 - \alpha\eta(\lambda))z_1 - (k_2 + \eta(\lambda))z_2 + a(\hat{\mu}'(\lambda) - \mu'(\lambda))\lambda_2 \quad (7.35)$$

$$\dot{\tilde{\lambda}}_1 = \lambda_2 \quad (7.36)$$

$$\dot{\lambda}_2 = -\gamma_1\tilde{\lambda}_1 - \gamma_2\lambda_2 \quad (7.37)$$

The closed-loop system has a cascaded form and the same arguments as in Proposition 7.1 can be used. \square

This result shows that the stability of the closed-loop system is robust with respect to tyre parameter uncertainties. However, the performance can be expected to be reduced if the estimate is not correct, as observed in the simulations of Section 7.3. An adaptive scheme able to adapt $\hat{\lambda}'(x_1)$ is presented in [97]. This more advanced scheme is more challenging to implement in practice and has therefore not been tested yet.

7.3 Simulation results

Simulations are performed based on the simple model of Section 7.1.

The first aim of the simulations is to observe the effects of the feedback and feedforward terms. In accordance with both intuition and theoretical study, the following phenomena can be observed :

1. When the feedback gains are equal to zero (that is, in the case of pure feedforward control), the system tracks the desired wheel slip reference only if this reference is in the tyre's stable zone ; otherwise the purely open-loop system is unstable (Figure 7.4).
2. When the feedback gains satisfy the conditions given in the proof of Proposition 7.1 and the feedforward is not used (that is, in the case of pure feedback control), the system tracks the desired wheel slip reference, but with a poorer performance during transients compared to the case with feedforward (Figure 7.5).
3. When both feedback and feedforward terms are included, with perfect system knowledge, the system follows exactly the filtered reference (Figure 7.6).

The second aim of the simulations is to observe the effects of perturbations, in order to evaluate the robustness of the control laws when both feedback and feedforward terms are used. Three cases are considered:

1. When a pure actuation delay is introduced in the control loop (take, for example, the case of a typical hydraulic actuator delay of 15 ms) the performance remains good and the system remains stable, provided that the delay is not too big (Figure 7.7).
2. When the system's parameters used in the control law do not match those of the true system (like, for exemple, a change of tyre characteristics) the system remains stable, but the performance is reduced (Figure 7.8).
3. When both pure delay and parameter uncertainties are considered, the results are quite close to the case of pure parameter uncertainties (Figure 7.9).

In order to prepare the experimental validation, the controller has also been simulated on the more complex model developed in Chapter 4. The results of the simulations are comparable to the experimental results of the next section, and are therefore skipped here.

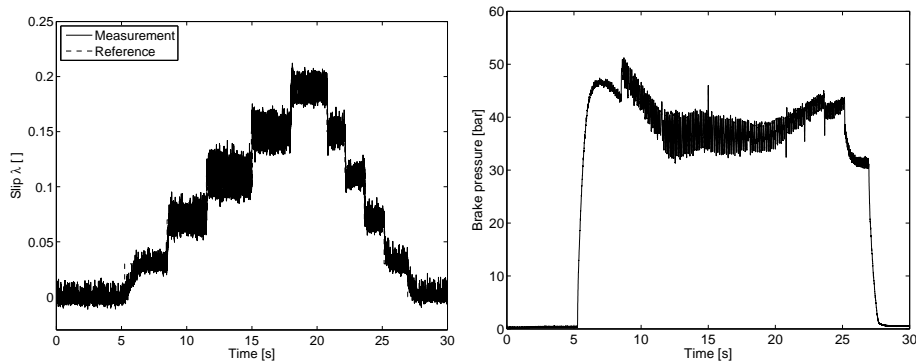


Figure 7.2: Experimental validation of the controller, when only the feedback is enabled (no feedforward). The target and measured slips are shown on the left plot while the brake pressure is shown on the right plot.

7.4 Experimental validation

The controller was implemented and tested on the tyre-in-the-loop experimental facility presented in Section 1.3.2. Two experiments have been performed on the setup, with the drum rolling at a constant speed of 18 m/s. The controller is tuned as follows: $\alpha = 250$, $k_1 = 250$, $k_2 = 1000$, $\gamma_1 = 1.6e6$ and $\gamma_2 = 2.5e3$. α , k_1 , γ_1 and γ_2 were defined experimentally in order to get the desired performances. k_2 was computed in order to ensure stability. The chosen value does not satisfy the conservative condition (7.21), but still it passes the LMI test.

During the first test, the slip reference is increased or decreased by steps of 4% from 0 up to 20% which is already in the unstable region of the tyre. The control law (7.10) with feedback only is used. The results are presented on Figure 7.2. It can be observed that the controller drives the slip precisely towards the reference value, both in the stable and unstable region of the tyre. It is interesting to note that the oscillations in the slip are larger when the slip is higher. This is linked to the fact that the damping provided by the tyre is decreasing when the brake force is approaching the saturation. The same phenomena leads to a decrease of the relaxation length at high slip, as observed in [125].

During the second test, performances with and without feedforward are compared. During the first 10 seconds, only the feedback is enabled by using the control law (7.10). Then the feedforward is turned on by switching to the control law (7.33). On Figure 7.3, it can be observed that the convergence to a new reference is much faster with the feedforward on. This is particularly noticeable at low slip, when the controller with feedback only is particularly slow.

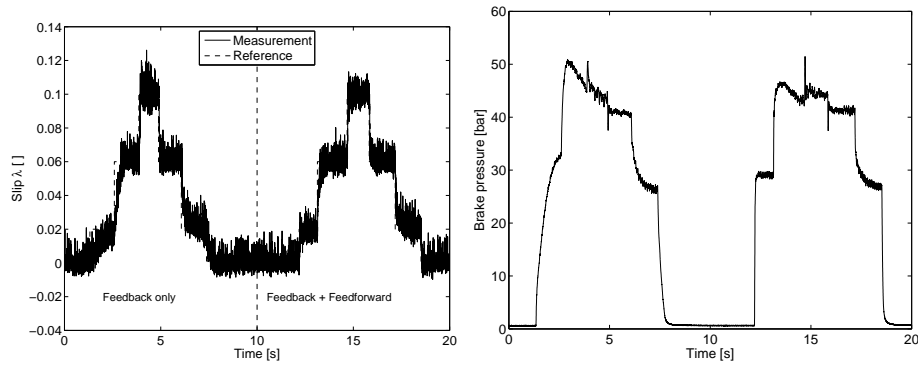


Figure 7.3: Comparison of the performances with and without feedforward. The target and measured slips are shown on the left plot while the brake pressure is shown on the right plot.

7.5 Conclusion

In this chapter, a new cascaded wheel slip control strategy based on wheel slip and wheel acceleration measurements was presented. Both a feedback and a feedforward are designed. The control laws are proven to stabilize globally and asymptotically the wheel slip around any prescribed target, both in the stable and unstable regions of the tyre, based on a simple model. Stability in case of tyre uncertainties is also shown mathematically. Simulations support the theory and assess the performance and robustness to time delays and model uncertainties. The control law is finally validated in tyre-in-the-loop experiments. The first experimental test shows the convergence of the slip towards the reference, also in the unstable zone. The second test concludes that the feedforward is significantly increasing the bandwidth, in particular in the stable zone.

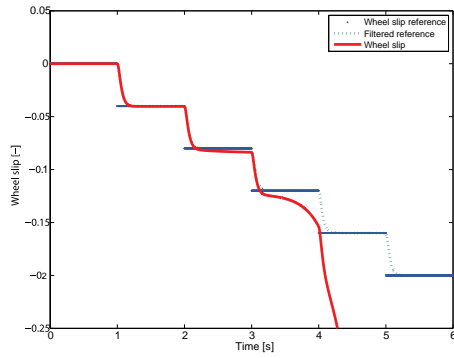


Figure 7.4: Pure feedforward control ($k_1 = 0$ and $k_2 = 0$).

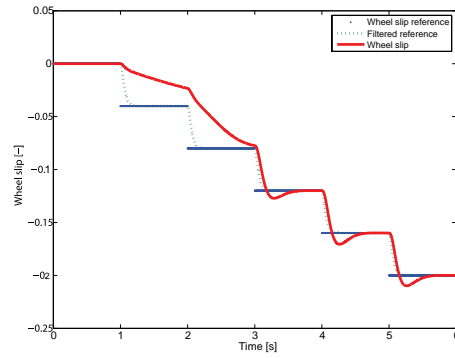


Figure 7.5: Pure feedback control.

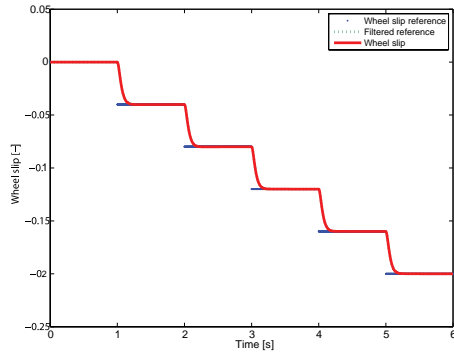


Figure 7.6: Combined feedback and feedforward control (without perturbations).

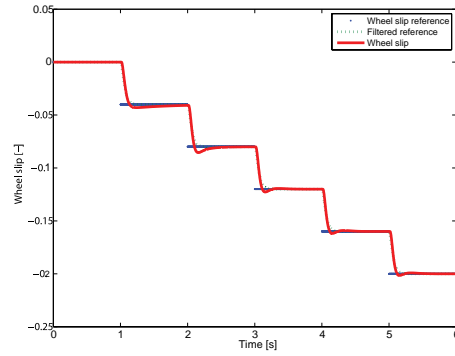


Figure 7.7: Combined control, with a delay of 15 ms.

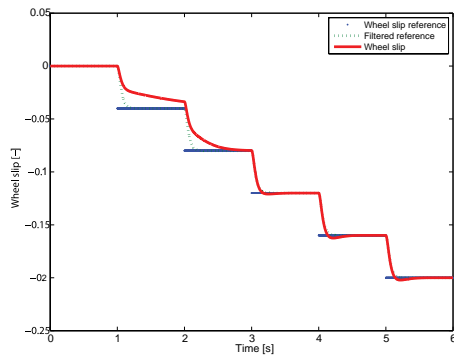


Figure 7.8: Combined control with a perturbation of $\mu(\cdot)$.

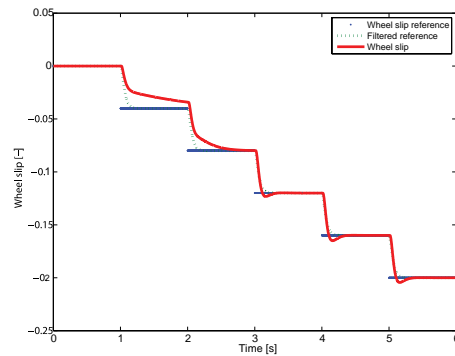


Figure 7.9: Combined control, with a delay of 15 ms and a perturbation of $\mu(\cdot)$.

Chapter 8

Conclusions and Recommendations

In this thesis, steps have been made towards simpler and more robust Global Chassis Control and Braking Control algorithms thanks to the use of force sensing, compared to currently publicly available algorithms.

In the Global Chassis Control part, a new framework extending the class of indirect allocation has been proposed. Thanks to force measurement, it becomes possible to implement simple local tyre force controllers that are intrinsically robust to tyre parameter uncertainty. This is exploited when dividing the complete problem in two levels, such that the allocation becomes convex and independent from tyre parameters. The new architecture with building blocks introduces the right number of degrees of freedom in the allocation when actuators or wheels are coupled, thus avoiding the appearance of difficult constraints.

From the analysis of the allocation problem, it can be concluded that there is a need for a continuous optimization technique. The new Hybrid Descent Method has been developed for this purpose. The force distribution is not optimized at every time step, but instead it is driven with an hybrid differential equation, similarly to a dynamical system. The main idea is to follow the steepest descent direction for the objective function in the feasible set and for the constraints in the unfeasible set. The continuous hybrid system guarantees that its trajectory enters the feasible set of the related optimization problem and next converges asymptotically to the set of optimal points.

Tyre constraints are handled in a realistic way, without the assumption that the whole tyre characteristics is known long in advance. Only when the tyre reaches its limits, a constraint, located at the currently measured operating point, is added in the allocation. While the force distribution is adapted, it is necessary to maintain the tyre at its maximal force. This necessity has driven us to further developments into ABS braking control.

In the Braking Control part, contributions in the class of hybrid controllers based on wheel deceleration and in the class of slip regulators have been made. Those are the two main classes of algorithms found in the literature. Firstly, the theoretical

hybrid 5-phase algorithm has been extended to meet the requirements for practical implementation. Secondly, a new wheel slip controller based on a cascaded approach has been reworked to better fit the practical needs. This piece of work results from a collaboration with the CNRS/Supelec, Paris, France.

Furthermore, the use of force measurement for braking control has been investigated and has led to the development of a new algorithm. The simplest version contains only 2 phases and is based on the measurement of the tyre longitudinal force and wheel acceleration. The algorithm can track the peak of the tyre characteristics without knowledge of the tyre parameters, and can handle abrupt changes in friction. When one phase is added, together with the measurement of the lateral force, the algorithm becomes able to control how much the lateral force is reduced because of combined-slip. This is the first ABS algorithm that directly maintain the lateral tyre potential during heavy braking. This should be the first objective when implementing ABS. By applying the algorithm to the front axle, a minimal path curvature is guaranteed, while by applying the algorithm to the rear axle, lateral yaw stability is maintained.

All algorithms for straight-line braking have been tested in tyre-in-the-loop experiments and have shown satisfying results. The update of the laboratory tyre measurement equipment for closed-loop ABS testing is also an achievement of this thesis.

8.1 Main conclusions

The overall conclusions of the research presented in this thesis are the following:

- Tyre force measurement allows to make the control of the tyres simpler and more robust to uncertain characteristics. However, force measurement appears to be less useful when it comes to estimating the motion states of the vehicle, since this would require the inversion of the nonlinear uncertain tyre model. Therefore, the wheel acceleration is still needed for ABS control, and the yaw-rate or the side-slip angle are still required for detecting lateral instability. It is not expected that the addition of tyre force sensors in a vehicle will allow more traditional motion sensors to be removed.
- When the right number of degrees of freedom is maintained, for example by using the building block architecture, indirect allocation can be advantageous compared to direct allocation. The allocation can be made convex and independent from uncertain tyre parameters, while the tyre uncertainties and nonlinearities can be dealt with in specific blocks. The main difficulty is the expression of the constraints. The use of roughly approximated constraints, constantly updated depending the currently measured operating point, is shown to give good results in a simulation study.
- It is possible to implement a dynamical system performing constrained continuous optimization. The Hybrid Descent Method is a suitable option for that. Control allocation can largely benefit from such method, since the allocation

can be merged with the rest of the controller and the computational complexity can be reduced.

- The delay in the braking control loop, originating for example from the brake actuator, the measurement or the lag in the tyre response, is the main performance limiter for ABS. Any new braking controller should be proven to be robust to a delay of 20ms to be of practical interest.

8.2 Recommendations and directions for future research

Based on the experience acquired during this Ph.D. research, recommendations and possible directions can be proposed for future research in global chassis control and braking control.

8.2.1 Global Chassis Control

- The Global Chassis Control framework has been developed focusing on two main objectives: “Stability and Safety” and “Ease of development”. Future research should extend the framework toward, in particular, two other important objectives: “Fault tolerance” and “Energy efficiency”. For fault tolerance, the main challenge is the detection and isolation of actuator or sensor failure. At a global level, it can be expected that actuator failures can be handled by adding constraints and reconfiguring the allocation problem online. Furthermore, making the Global Chassis Control energy efficient is of first importance today, where the necessity for limiting the world’s energy consumption is well present. The energy cost for using the different actuators should be included in the allocation cost function. Also, a good trade off should be made between energy consumption and performance. Still, it is believed that the energy factor should be considered if and only if the life of the occupant of the car is not in danger. In critical situations, the only purpose of each actuator should be avoiding an accident, and not saving or recovering energy.
- The local controllers inside the building blocks have been designed with the objective to show that a simple force feedback can perform well. Only limited tyre dynamics and no actuator dynamics were considered. This constitutes a shortcoming for practical implementation. Future research should improve the local controllers, for example using model-based design, to get a more practical and realistic solution.
- This research has shown that roughly approximated constraints are already good enough to give a first proof of concept of the method. Still, the Global Chassis Controller might benefit from a more precise expression of the constraints. Future research could investigate the opportunities in this direction.
- When humans are involved in the control loop, the performances of a controller cannot only be measured using traditional mathematical criteria, but the human

perception and acceptance should be investigated. In particular for vehicle control, the driver's feeling is a major importance. The first step for future research is the design of a driver interpreter, which can give the total forces and moment references to the allocation. This is probably complex enough for a Ph.D. research on its own. The second step is to consider the controller response, like for example the bandwidth, the delay or the overshoot, and see if it is acceptable for the driver. The use of driving simulators should be the first choice for such future research. Contributions to the development of a moving-base driving simulator have been made in the framework of this thesis [68]. Unfortunately, no tests could be performed during the time span of this thesis.

- A major difficulty related to research about Global Chassis Control is the really vague definition of the problem. By looking for a general framework, one might lose the capability of quickly applying it to a specific case. It is believed that future research about GCC could benefit from having a predefined benchmark, where all the vehicle and actuator characteristics are known. The use of the TNO Moving-Bases [99] for that purpose has been investigated during this thesis, and it is still believed that this would constitute a perfect platform. Unfortunately, tests on the Moving-Bases could not be performed during the time span of this thesis.

8.2.2 Braking Control

- The brake actuator considered in this research is an Electro-Hydraulic Brake (EHB). Future research could consider other types of brakes, and for example brake-by-wire systems. It might be of interest to modify the algorithms if the brake torque can be controlled precisely. With EHB, the brake efficiency is uncertain and the pressure rate is limited, therefore only torque increase or decrease commands are given, preferably in feedback with the wheel acceleration. If the brake torque can be controlled precisely, open-loop commands based on the measured force is expected to increase the performances.
- With the trend towards hybrid and electric vehicles, it can be expected that an electromotor will be connected to each wheel, in parallel to the brake. During normal driving, the motor can be used for regenerative braking. However, when the ABS is triggered, the motor could be used to improve the braking performances. Electromotors usually have a much larger bandwidth, a shorter actuation delay and a better accuracy than friction brakes. As time delay is the main performance limiter for ABS, the improvements brought by such motor can be substantial. However, two important issues need to be considered. Firstly, the total desired braking torque can usually not be provided by the motor alone. Secondly, the motor inertia cannot be neglected compared to the wheel inertia. Future research should consider the opportunity to apply the high-frequency component of the torque reference signal to the electromotor, and the low-frequency component to the friction brake. As a second step, ABS algorithms should be modified according to the previous point, as an electro-

8.2. RECOMMENDATIONS AND DIRECTIONS FOR FUTURE RESEARCH

motor can precisely control its torque. Finally, the algorithms should be made fault-tolerant to deal with potential failure of the actuators.

- The consideration of the suspension dynamics during ABS design might be important. Unfortunately, this could not be investigated during the time span of this thesis. Future research should look at this issue in more details. It is believed that the tyre-in-the-loop experimental facility could be a nice test environment for this, provided that the rigid frame is replaced by a conventional suspension.
- The ABS algorithm using the lateral force measurement can be considered as a first step towards the implementation of force-based ESP, in the specific case of heavy braking. The basic principle for maintaining a good lateral behavior is to ensure that the lateral force is not reduced too much because of combined-slip. Future research should investigate the benefits that tyre force measurement could bring into ESP. Furthermore, when untripped roll-over avoidance is considered [110], the inverse principle could be used. There, one objective is to reduce the tyre lateral force using heavy braking. Detection of roll-over can be done based on the vertical force measurement. Future research could therefore also investigate the benefits that tyre force measurement could bring to untripped roll-over mitigation. Finally, future research should strive at integrating the different subsystems for addressing, with a force-based approach, the longitudinal, yaw and roll instabilities.

Bibliography

- [1] D. Abbink. *Neuromuscular Analysis of Haptic Gas Pedal Feedback during car following*. PhD thesis, Delft University of Technology, 2006.
- [2] I. Ait-Hammouda and W. Pasillas-Lépine. Jumps and synchronization in anti-lock brake algorithms. In *Proceedings of the 9th International Symposium on Advanced Vehicle Control, Kobe, Japan, 2008*.
- [3] R. Anderson and D. Bevly. Estimation of slip angles using a model based estimator and gps. In *Proceeding of the 2004 American Control Conference Boston, Massachusetts, 2004*.
- [4] J. Andreasson. *On Generic Road Vehicle Motion Modelling and Control*. PhD thesis, Kungliga Tekniska högskolan, 2007.
- [5] J. Andreasson and T. Bunte. Global chassis control based on inverse vehicle dynamics models. *Journal of Vehicles Systems Dynamics*, 44:321–328, 2006.
- [6] J. Andreasson and M. Gäfvert. The vehicledynamics library — overview and applications. In *International Modelica Conference, Vienna, Austria, 2006*.
- [7] K. Åström and B. Wittenmark. *Adaptive Control*. Prentice Hall, 1994.
- [8] K. Åström and B. Wittenmark. *Computer-Controlled Systems: Theory and Design*. Prentice Hall, 1997.
- [9] G. Baffet, A. Charara, and D. Lechner. Experimental evaluation of a sliding mode observer for tire-road forces and an extended kalman filter for vehicle sideslip angle. In *Proceedings of the IEEE conference on decision and control, 2007*.
- [10] A. Bemporad. Model predictive control design: New trends and tools. In *45th IEEE Conference on Decision & Control, San Diego, CA, USA, 2006*.
- [11] A. Bemporad, F. Borrelli, and M. Morari. Model predictive control based on linear programming - the explicit solution. *IEEE Transactions on Automatic Control*, 47:1974–1985, 2002.
- [12] A. Bemporad, M. Morari, V. Dua, and E. Pistikopoulos. The explicit solution of model predictive control via multiparametric quadratic programming. In *American Control Conference, Chicago, USA, 2000*.

BIBLIOGRAPHY

- [13] D. Bertsekas. *Nonlinear Programming*. Athena Scientific, 1999.
- [14] M. Best, T. J. Gordon, and P. J. Dixon. An extended adaptive kalman filter for real-time state estimation of vehicle handling dynamics. *Vehicle System Dynamics*, 34:57–75, 2000.
- [15] A. Bhaya and E. Kaszkurewicz. *Control Perspectives on Numerical Algorithms and Matrix Problems*. Society for Industrial and Applied Mathematic, 2006.
- [16] M. Bodson. Evaluation of optimization methods for control allocation. *Journal of Guidance, Control, and Dynamics*, 25(4):703–711, July 2002.
- [17] F. Borrelli, P. Falcone, T. Keviczky, J. Asgari, and D. Hrovat. Mpc-based approach to active steering for autonomous vehicle systems. *International Journal of Vehicle Autonomous Systems*, 3(2-4):265–291, 2005.
- [18] Bosch. *Automotive Handbook*. Bentley, 2003.
- [19] J. C. Botero, M. Gobbi, G. Mastinu, N. D. Piazza, and R. Martorana. On the reformulation of the abs logic by sensing forces and moments at the wheels. In *Fifth IFAC Symposium on Advances in Automotive Control*, 2007.
- [20] BOVAG-RAI Foundation, Amsterdam. Mobility in figures - 2008/2009 cars edition, 2008.
- [21] S. Boyd and L. Vandenberghe. *Convex Optimization*. Cambridge University Press, 2004.
- [22] E. A. Bretz. By-wire cars turn the corner. *IEEE Spectrum*, 38:68–73, 2001.
- [23] B. Breuer, U. Eichhorn, and J. Roth. Measurement of tyre/road friction ahead of the car and inside the tyre. In *Proceedings of the International Symposium on Advanced Vehicle Control*, 1992.
- [24] R. Brockett. Dynamical systems that sort lists, diagonalize matrices, and solve linear programming problems. *Linear Algebra and its Applications*, 146:79–91, 1991.
- [25] D. Brück, H. Elmqvist, H. Olsson, and S. Mattsson. Dymola for multi-engineering modeling and simulation. In *Proceedings of the 2nd International Modelica Conference*, 2002.
- [26] K. Buckholtz. Reference input wheel slip tracking using sliding mode control. SAE Technical Paper 2002-01-0301, 2002.
- [27] M. Burckhardt. *Fahrwerktechnik: Radschlupfregelsysteme*. Vogel-Verlag, Germany, 1993.
- [28] E. Camacho and C. Bordons. *Model Predictive Control in the Process Industry*. Springer-Verlag, 1995.
- [29] P. J. Campo and M. Morari. Robust model predictive control. In *Proceedings of the American Control Conference*, 1987.

- [30] C. Carlson and J. Gerdes. Nonlinear estimation of longitudinal tire slip under several driving conditions. In *Proceedings of the 2003 American Control Conference*, 2003.
- [31] F. Clarke. *Optimization and Nonsmooth Analysis*. Wiley, New-York, 1983.
- [32] M. Corno. *Active Stability Control Systems Design for Road Vehicles*. PhD thesis, Politecnico di Milano, 2008.
- [33] M. Corno, S. Savaresi, and G. Balas. On Linear Parameter Varying (LPV) Slip-Controller Design for Two-Wheeled Vehicles. *International Journal of Robust and Nonlinear Control*, 19(12):1313–1336, 2009.
- [34] C. de Boor. *A Practical Guide to Splines*. Springer, 2001.
- [35] E. de Bruijn. Force sensing in wheel slip control. Master’s thesis, Delft University of Technology, 2009.
- [36] E. de Bruijn, M. Gerard, M. Corno, M. Verhaegen, and E. Holweg. On the performance increase of wheel deceleration control through force sensing. In *Proceedings of the 2010 IEEE Multi-Conference on Systems and Control*, 2010.
- [37] A. D. Dominguez-Garcia, J. G. Kassakian, and J. E. Schindall. A backup system for automotive steer-by-wire, actuated by selective braking. In *Proceedings of the 35th Annual IEEE Power Electronics Specialists Conference, Aachen, Germany*, 2004.
- [38] Economic commission for Europe, United Nations, Geneva. Statistics of road traffic accidents in europe and north america, 2004.
- [39] C. Edwards and S. Spurgeon. *Sliding Mode Control, Theory and Applications*. Taylor & Francis, 1998.
- [40] K. Eggers, M. Gerard, E. de Vries, and M. Verhaegen. Vehicle side-slip angle estimation using sliding mode observers and lateral forces. In *Proceedings of IAVSD conference, Stockholm, Sweden*, 2009.
- [41] A. Erke. Effects of electronic stability control (esc) on accidents: A review of empirical evidence. *Accident Analysis & Prevention*, 40(1):167–173, 2008.
- [42] J. Farrelly and P. Wellstead. Estimation of vehicle lateral velocity. In *Proceedings of the 1996 IEEE International Conference on Control Applications Dearborn, MI*, 1996.
- [43] A. Ferrara and C. Vecchio. Low vibration vehicle traction control to solve fastest acceleration/deceleration problems via second order sliding modes. In *Proceedings of the American Control Conference*, 2007.
- [44] A. Filippov. *Differential Equations with Discontinuous Right-hand Side*. Kluwer Academic Publishers, The Netherlands, 1988.

BIBLIOGRAPHY

- [45] G. F. Franklin, J. D. Powell, and A. Emami-Naeini. *Feedback Control of Dynamic Systems*. Prentice Hall, 2002.
- [46] P. Fritzson. *Principles of Object-Oriented Modelling and Simulation with Mod-
elica 2.1*. IEEE Press, 2004.
- [47] C. Garcia, D. Preth, and M. Morari. Model predictive control: theory and
practice - a survey. *Automatica*, 25(3):335–348, 1989.
- [48] M. Gerard. Tire-road friction estimation using slip-based observers. Master’s
thesis, Department of Automatic Control, Lund University, Sweden, 2006.
- [49] M. Gerard, A. Loria, W. Pasillas-Lépine, and M. Verhaegen. Design and experi-
mental validation of a cascaded wheel slip control strategy. In *10th International
Symposium on Advanced Vehicle Control, Loughborough, UK*, 2010.
- [50] O. Gietelink. *Design and Validation of Advanced Driver Assistance Systems*.
PhD thesis, Delft University of Technology, 2007.
- [51] T. D. Gillespie. *Fundamentals of Vehicle Dynamics*. Society of Automotive
Engineers, 1992.
- [52] M. Gipser. Ftire: a physically based application-oriented tyre model for use with
detailed mbs and finite-element suspension models. *Vehicle System Dynamics*,
43:76–91, 2005.
- [53] M. Gobbi and G. Mastinu. Wheels with integrated sensors for measuring tire
forces and moments. In *Proceedings of the 7th International Conference on
Advanced Vehicle Control*, 2004.
- [54] T. Gordon, M. Howell, and F. Brandao. Integrated control methodologies for
road vehicles. *Vehicle System Dynamics*, 40(1-3):157–190, January 2003.
- [55] F. Gustafsson. Estimation and change detection of tire-road friction using the
wheel slip. *IEEE Control Systems Magazine*, 1997.
- [56] B. Hardung, T. Kölzow, and A. Krüger. Reuse of software in distributed em-
bedded automotive systems. In *Fourth ACM International Conference on Em-
bedded Software (EMSOFT 2004), Pisa, Italy*, 2004.
- [57] O. Härkegård. *Backstepping and Control Allocation with Applications to Flight
Control*. PhD thesis, Linköping University, Sweden, 2003.
- [58] D. Harty. Brand-by-wire - a possibility? *Society of Automotive Engineers*,
(2003-01-0097), 2003.
- [59] E. Hewitt and K. Stromberg. *Real and Abstract Analysis*. Springer, 1975.
- [60] P. Ioannou and J. Sun. *Robust Adaptive Control*. Prentice Hall, 1996.
- [61] B. Jansen. Brake-by-steer concept; steer-by-wire application with independently
actuated wheels used for stopping a vehicle. Master’s thesis, Delft University
of Technology, 2010.

- [62] F. Jiang and Z. Gao. An adaptive nonlinear filter approach to the vehicle velocity estimation for ABS. In *Proceedings of the 2000 IEEE International Conference on Control Application, Anchorage*, September 25-27 2000.
- [63] T. Johansen. Optimizing nonlinear control allocation. In *IEEE Conference on Decision and Control, Bahamas*, 2004.
- [64] R. Johansson and A. Rantzer, editors. *Nonlinear and Hybrid Systems in Automotive Control*. Springer-Verlag, 2003.
- [65] M. Jonasson and J. Andreasson. Exploiting autonomous corner modules to resolve force constraints in the tyre contact patch. *Vehicle System Dynamics*, 46(7):553–573, July 2008.
- [66] T. Kamada, H. Fukudome, T. Fujita, and M. Murase. Study on abs control by measuring forces between road surfaces and tires. In *International Symposium on Advanced Vehicle Control (AVEC'04), Arnhem, The Netherlands*, 2004.
- [67] K. Kashimaa and Y. Yamamoto. System theory for numerical analysis. *Automatica*, 43(7):1156–1164, 2007.
- [68] D. Katzourakis, E. Holweg, M. Gerard, and R. Happee. Design issues for haptic steering force feedback on an automotive simulator. In *Proceedings of the HAVE conference, Lecco, Italy*, 2009.
- [69] H. Khalil. *Nonlinear Systems*. Prentice Hall, 2002.
- [70] U. Kiencke and A. Daiss. Observation of lateral vehicle dynamics. *Control Engineering Practice*, 5:1145–1150, 1997.
- [71] U. Kiencke and L. Nielsen. *Automotive Control Systems*. Springer-Verlag, 2000.
- [72] C. Knobel, A. Pruckner, and T. Bunte. Optimized force allocation - a general approach to control and to investigate the motion of over-actuated vehicles. In *4th IFAC Symposium on Mechatronic Systems, Heidelberg, Germany*, 2006.
- [73] K. Kobayashi, K. Cheok, and K. Watanabe. Estimation of absolute vehicle speed using fuzzy logic rule-based Kalman filter. In *Proceedings of the 1995 American Control Conference, Seattle, USA*, June 21-23 1996.
- [74] C. Kuo and E. Yeh. A four-phase control scheme of an anti-skid brake system for all road conditions. *IMEchE Part D: Journal of Automobile Engineering*, 206:275–283, 1992.
- [75] L. Laine. *Reconfigurable Motion Control Systems for Over-Actuated Road Vehicles*. PhD thesis, Chalmers University of Technology, 2007.
- [76] S.-H. Lee, S.-H. Chu, and C. C. Chung. Analysis and design of servomechanism and its application to disk drives. *IEEE Transactions on Control Systems Technology*, 11:233–241, 2003.

BIBLIOGRAPHY

- [77] T. Lee, C. Hsu, and S. Lee. Robust Hybrid Control for Antilock Braking Systems. In *Proceedings of the IEEE International Conference on Systems, Man and Cybernetics, Washington D.C., USA, 2003*.
- [78] R. I. Leine and H. Nijmeijer. *Dynamics and Bifurcations of Non-Smooth Mechanical Systems*, volume 18 of *Lecture Notes in Applied and Computational Mechanics*. Springer, 2004.
- [79] C. Lin and C. Hsu. Neural-network hybrid control for antilock braking systems. *IEEE Transactions on Neural Networks*, 14(2):351–359, 2003.
- [80] A. Loria and E. Panteley. *Cascaded nonlinear time-varying systems: analysis and design*. Lecture Notes in Control and Information Sciences. Springer Verlag, 2005.
- [81] T. Luck, R. Freimann, and E. Schneider. Driving dynamics and hybrid combined in the torque-vectoring. In *Proceedings of the VDI Conferene on Tires-Chassis-Road, Hannover, Germany, 2007*.
- [82] P. Lugner, H. Pacejka, and M. Plöchl. Recent advances in tyre models and testing procedures. *Vehicle System Dynamics*, 43:413–426, 2005.
- [83] J. Lygeros, K. Johansson, S. Simić, J. Zhang, and S. Sastry. Dynamical properties of hybrid automata. *IEEE Transaction on Automatic Control*, 48(1):2–17, 2003.
- [84] J. Maciejowski. *Predictive Control with Constraints*. Prentice Hall, Harlow, England, 2002.
- [85] S. Martinez, J. Cortes, and F. Bullo. Motion coordination with distributed information. *IEEE Control System Magazine*, 27:75–88, 2007.
- [86] J. P. Maurice. *Short Wavelength and Dynamic Tyre Behaviour under Lateral and Combined Slip Conditions*. PhD thesis, Delft University of Technology, 2000.
- [87] D. McRuer and H. Jex. A review of quasi-linear pilot models. *IEEE Transactions on Human Factors in Electronics*, 8:234–249, 1967.
- [88] J. Michon. *Human behavior and traffic safety*, chapter A critical view of driver behavior models: what do we know, what should we do?, pages 485–524. Plenum Press, New York, 1985.
- [89] O. Mokhiamar and M. Abe. Simultaneous optimal distribution of lateral and longitudinal tire forces for the model following control. *Journal of Dynamic Systems, Measurement, and Control*, 126(4):753–763, December 2004.
- [90] B. Olson, S. Shaw, and G. Stépán. Nonlinear dynamics of vehicle traction. *Vehicle System Dynamics*, 40(6):377–399, 2003.

- [91] E. Ono, K. Asano, M. Sugai, S. Ito, M. Yamamoto, M. Sawada, and Y. Yasui. Estimation of automotive tire force characteristics using wheel velocity. *Control Engineering Practice*, 11(6):1361–1370, 2003.
- [92] E. Ono, Y. Hattori, Y. Muragishi, and K. Koibuchi. Vehicle dynamics control based on tire grip margin. In *International Symposium on Advanced Vehicle Control (AVEC'04)*, Arnhem, The Netherlands, 2004.
- [93] R. Orend. Modelling and control of a vehicle with single-wheel chassis actuators. In *Proceedings of the 16th IFAC World Congress*, 2005.
- [94] M. Otter, H. Elmqvist, and S. E. Mattsson. The new modelica multibody library. In *Proceedings of the 3rd International Modelica Conference*, 2003.
- [95] H. B. Pacejka. *Tyre and Vehicle Dynamics*. Butterworths-Heinemann, London, 2006.
- [96] W. Pasillas-Lépine. Hybrid modeling and limit cycle analysis for a class of five-phase anti-lock brake algorithms. *Vehicle System Dynamics*, 44(2):173–188, 2006.
- [97] W. Pasillas-Lépine and A. Loría. A new mixed wheel slip and acceleration control based on a cascaded design. In *Proceedings of the 8th IFAC Symposium on Nonlinear Control Systems (NOLCOS)*, Bologna, Italy, 2010.
- [98] I. Petersen, T. A. Johansen, J. Kalkkuhl, and J. Lüdemann. Nonlinear wheel slip control in ABS brakes using gain scheduled constrained LQR. In *Proceedings of the European Control Conference*, pages 606–611, 2001.
- [99] J. Ploeg, H. E. Schouten, and H. Nijmeijer. Control design for a mobile robot including tire behavior. In *Proceedings of the 2008 IEEE Intelligent Vehicles Symposium*, 2008.
- [100] J. Plumlee, D. Bevly, and A. Hodel. Control of a ground vehicle using quadratic programming based control allocation techniques. In *American Control Conference*, Boston, USA, 2004.
- [101] J. Primbs. *Nonlinear Optimal Control: A Receding Horizon Approach*. PhD thesis, California Institute of Technology, 1999.
- [102] S. Qina and T. Badgwell. A survey of industrial model predictive control technology. *Control Engineering Practice*, 11:733–764, 2003.
- [103] Robert Bosch GmbH. From innovation to standard equipment - 30 years of safe braking with bosch abs. Presse Release, July 2008. PI6238 - www.bosch-presse.de.
- [104] J. Rossiter. *Model Predictive Control Design: New Trends and Tools*. CRC Press, 2003.
- [105] S. Sastry. *Nonlinear Systems*. Springer, 1999.

BIBLIOGRAPHY

- [106] S. Savaresi and M. Tanelli. *Active Braking Control Design for Road Vehicles*. Springer, 2010.
- [107] S. Savaresi, M. Tanelli, and C. Cantoni. Mixed slip-deceleration control in automotive braking systems. *ASME Journal of Dynamic Systems, Measurement, and Control*, 129(1):20–31, 2007.
- [108] S. Savaresi, M. Tanelli, and P. Langthaler. A method for calculating forces acting on the footprint area and apparatus for calculating said forces. European Patent Request: PCT/IT2006/000134, 2006. Applicant: Pirelli s.p.a.
- [109] S. Savaresi, M. Tanelli, P. Langthaler, and L. Del Re. Identification of tire-road contact forces by in-tire accelerometers. In *Proceedings of the 14th IFAC Symposium on System Identification, SYSID 2006*, 2006.
- [110] B. Schofield, T. Hägglund, and A. Rantzer. Vehicle dynamics control and controller allocation for rollover prevention. In *IEEE International Conference on Control Applications*, 2006.
- [111] S. Semmler, D. Fischer, R. Isermann, R. Schwarz, and R. P. Estimation of Vehicle velocity using Brake-by-Wire Actuators. In *Proceedings of the 15th IFAC World Congress, Barcelona, Spain, July, 21-26 2002*.
- [112] D. Shevitz and B. Paden. Lyapunov stability of nonsmooth systems. *IEEE Transactions on Automatic Control*, 39(9):1910–1914, 1994.
- [113] C. W. D. Silva. *Mechatronics: an integrated approach*. CRC Press, 2005.
- [114] J. Stephant, A. Charara, and D. Meizel. Evaluation of a sliding mode observer for vehicle sideslip angle. *Control Engineering Practice*, 15:803–812, 2006.
- [115] J. Svendenius. *Tire Modeling and Friction Estimation*. PhD thesis, Department of Automatic Control, Lund University, 2007.
- [116] SWOV Institute for Road Safety Research. Nota mobiliteit, 2008. www.swov.nl.
- [117] M. Tanelli, S. Savaresi, and A. Astolfi. Robust nonlinear output feedback control for brake by wire control systems. *Automatica*, 44(4):1078–1087, 2008.
- [118] P. Tøndel and T. Johansen. Control allocation for yaw stabilization in automotive vehicles using multiparametric nonlinear programming. In *American Control Conference, Portland, USA*, 2005.
- [119] M. Uchanski. *Road Friction Estimation for Automobiles Using Digital Signal Processing Methods*. PhD thesis, University of California, Berkeley, 2001.
- [120] C. Villegas and R. Shorten. State of the art of integrated chassis control. Technical report, Complex Embedded Automotive Control Systems (CEmACS), 2005.
- [121] L. Wei. Abs control on modern vehicle equipped with regenerative braking. Master’s thesis, Delft University of Technology, 2010.

- [122] T. A. Wenzel, K. J. Burnham, M. V. Blundell, and R. A. Williams. Dual extended kalman filter for vehicle state and parameter estimation. *Vehicle System Dynamics*, 44:153–171, 2006.
- [123] World Health Organization. World report on road traffic injury prevention, 2004. ISBN 92 4 156260 9.
- [124] J. Yu. A Robust Adaptive Wheel-Slip controller for Antilock brake System. In *Proceedings of the 36-th IEEE Conference on Decision and Control, San Diego California, USA*, 1997.
- [125] P. W. A. Zegelaar. *The dynamic Response of Tyres to Brake Torque Variations and Road Unevenness*. PhD thesis, Delft University of Technology, 1998.
- [126] S. Zetterström. Electromechanical steering, suspension, drive and brake modules. In *Vehicular Technology Conference (VTC 2002), Vancouver, Canada*, 2002.
- [127] J. Zuurbier and P. Bremmer. State estimation for integrated vehicle dynamics control. In *Proceedings of the International Symposium on Advanced Vehicle Control*, 2002.

SUMMARY

Summary

Global Chassis Control and Braking Control using Tyre Forces Measurement

Mobility and traffic safety is a major concern in the society today. Many accidents take place because the vehicle is not following the trajectory that the driver desires. To avoid such accidents, an increasing number of active safety systems are introduced in modern vehicles. Still, most of the time, those systems are designed independently, which can lead to non-optimal performances and unexpected interactions. To properly consider the coupling between the different actuators like the brakes and steering, coupling coming for example from the nonlinear tyre dynamics, a Global Chassis Control strategy is necessary. This thesis defines a new 2-level framework for Global Chassis Control.

At the chassis level, the distribution of the total control action to all the actuators is formulated as a constrained convex optimization problem, independent from uncertain parameters. As the driver is constantly changing his inputs to the vehicle, the solution of the optimization should be constantly updated. For that purpose, a new continuous optimization method, the Hybrid Descent Method, has been developed. This method defines a dynamical system such that its trajectory converges, first to a solution allowed by the constraints, and then to the optimum of the related optimization problem. In order to introduce the right number of degrees of freedom in the optimization, the actuators are grouped into building blocks depending on their coupling with the different tyre forces. Tyre constraints are handled in a realistic way, without the common assumption that the whole tyre characteristic is known long in advance.

At the wheel level, the control of the tyre forces is made simple and robust to uncertainties in the road conditions thanks to the use of tyre force measurement. Such tyre forces measurement is at the moment too expensive to be implemented. In current production vehicles, only sensors measuring motion are available, like accelerometers or gyroscopes. At the moment, SKF is developing a technology enabling the measurement of the load in their bearings. This technology allows the introduction of cheap force sensors in all vehicles, which will allow the implementation of new control algorithms like those presented in this thesis.

A particularly critical problem in vehicle dynamics control is to get the largest possible braking force out of the tyres while maintaining vehicle stability. This the-

SUMMARY

sis contributes to the development and experimental validation of Anti-lock Braking Systems (ABS). As a result of a collaboration with CNRS/Supelec, Paris, France, a theoretical hybrid ABS based on wheel deceleration has been improved to handle actuation delay; and a new wheel slip regulator based on a cascaded approach has been implemented. Furthermore, new algorithms using force measurement are shown to be simpler to tune, better performing and more robust to road conditions than acceleration-based alternatives. The first ABS algorithm directly considering the loss of potential to generate lateral tyre forces because of braking is an achievement of this thesis. All algorithms for straight-line braking have been validated on the tyre-in-the-loop experimental facility, which was made suitable for ABS testing during this research.

Samenvatting

Global Chassis Control en Braking Control met gebruik van bandkracht meting

Mobiliteit en verkeersveiligheid zijn van essentieel belang in de hedendaagse samenleving. Veel ongelukken vinden plaats omdat het voertuig niet het door de bestuurder gewenste traject volgt. Om dit soort ongelukken te voorkomen, is er een toenemend aantal actieve veiligheid systemen in moderne voertuigen geïntroduceerd. Toch zijn deze systemen in het algemeen onafhankelijk ontwikkeld, wat kan leiden tot niet-optimaal prestatie en onverwachte interactie. Om de koppeling tussen de verschillende actuatoren, bijvoorbeeld veroorzaakt door niet-lineaire banddynamica, goed mee te nemen in het ontwerp, is een Global Chassis Control strategie noodzakelijk. Deze strategie zoekt een globaal optimum voor het regelen van het hele voertuig. Dit proefschrift definieert een nieuw 2-laags kader voor Global Chassis Control.

Op het niveau van het voertuig, wordt de distributie van de totale regelactie over alle actuatoren geformuleerd als een convex optimalisatie probleem onder beperkende voorwaarden, onafhankelijk van onzekere parameters. Omdat de bestuurder voortdurend zijn input naar het voertuig verandert, moet de oplossing van de optimalisatie doorlopend bijgewerkt worden. Daarvoor is, een nieuwe continue optimalisatie methode, de Hybrid Descent Methode, ontworpen. Die methode definieert een dynamisch systeem zodat zijn traject eerst convergeert naar een, binnen beperkende voorwaarden toegestane oplossing en vervolgens naar het optimum van het gerelateerde optimalisatie probleem. Om het juiste aantal vrijheidsgraden te introduceren in de optimalisatie, zijn de actuatoren gegroepeerd tot bouwstenen, afhankelijk van hun koppeling met de bandkrachten. Beperkende voorwaarden ontleend aan het band-wegdek contact, zijn behandeld op een meer realistische manier: zonder de gebruikelijke aanname dat de hele bandkarakteristiek vooraf bekend is.

Op het niveau van de wiel is het regelen van de bandkrachten robuust gemaakt tegen onzekerheden in het band-wegdek contact dankzij het gebruik van bandkracht meting. In huidige productievoertuigen zijn alleen sensoren die de beweging meten, zoals versnellingsmeter of gyroscoop beschikbaar. Het bepalen van de bandkrachten is echter waardevol. Op dit moment is SKF een technologie aan het ontwikkelen waardoor het meten van de belasting van de wiellagers mogelijk wordt. Deze technologie maakt meten van de bandkrachten in productievoertuigen wellicht ook economisch haalbaar.

SAMENVATTING

Een bijzonder uitdagend probleem in het regelen van voertuigdynamica is het halen van de hoogst mogelijke remkracht uit de banden terwijl voertuigstabiliteit wordt behouden. Dit proefschrift draagt bij aan de ontwikkeling en experimentele validatie van een Anti- blokkeer Rem Systeem (ABS). Als een resultaat van een samenwerking met CNRS/Supélec, Parijs, werd een theoretisch hybride ABS algoritme, gebaseerd op wielversnelling verbeterd; en een nieuwe slip regelaar gebaseerd op de cascade benadering werd geïmplementeerd. Verder wordt getoond dat nieuwe algoritmes die gebruik maken van bandkrachtmeting simpeler, beter en robuuster tegen onzekere wegdek conditie kunnen zijn, in vergelijking van versnellinggebaseerde alternatieven. Het eerste ABS algoritme dat rechtstreeks het verlies van potentieel om laterale krachten te genereren meeweegt in de remregelaar is een resultaat van dit proefschrift. Alle algoritmes voor rechtdoor remmen zijn gevalideerd op de “tyre-in-the-loop” experimentele faciliteit, die geschikt gemaakt is voor ABS testen tijdens dit promotieonderzoek.

Résumé

Contrôle Global de Châssis et Contrôle du Freinage utilisant la mesure des forces du pneu

La mobilité et la sécurité routière sont des enjeux majeurs dans notre société d'aujourd'hui. Beaucoup d'accidents ont lieu parce que le véhicule ne suit pas la trajectoire désirée par le conducteur. Pour éviter ce genre d'accidents, un nombre croissant de systèmes de sécurité active sont introduits dans les véhicules modernes. Cependant, la plupart du temps, ces systèmes sont conçus indépendamment les uns des autres, ce qui conduit à des performances sub-optimales et des interactions inattendues. Pour prendre en compte le couplage entre les différents actionneurs comme les freins et la direction, couplage introduit par exemple par la dynamique non-linéaire des pneus, une stratégie de Contrôle Global de Châssis est nécessaire. Cette thèse définit un nouveau cadre à deux niveaux pour le Contrôle Global de Châssis.

Au niveau du châssis, la distribution de la commande totale vers les actionneurs est formulée comme un problème d'optimisation convexe sous contraintes, indépendant des paramètres incertains. Comme le conducteur change constamment sa commande au véhicule, la solution de l'optimisation doit être adaptée en permanence. A cette fin, une nouvelle méthode d'optimisation en continu, la Méthode de Descente Hybride, a été développée. Cette méthode définit un système dynamique tel que sa trajectoire converge d'abord vers une solution acceptable au regard des contraintes, et ensuite vers l'optimum du problème d'optimisation connexe. Dans le but d'introduire le bon nombre de degrés de liberté dans l'optimisation, les actionneurs sont groupés en blocs en fonction de leur couplage avec les différentes forces du pneu. Les contraintes liées au pneu sont gérées de manière réaliste, sans faire l'hypothèse classique que la caractéristique complète du pneu est connue longtemps à l'avance.

Au niveau des roues, le contrôle des forces générées par le pneu est rendu plus simple et plus robuste par rapport aux conditions de route grâce à l'utilisation de la mesure des forces du pneu. Cette mesure des forces n'est pas encore possible en raison des coûts trop importants. Dans les véhicules actuellement en production, seuls des capteurs mesurant le mouvement sont disponibles, comme des accéléromètres et des gyroscopes. En ce moment, SKF développe une technologie rendant possible la mesure de la charge appliquée sur les roulements à billes. Cette technologie permettra l'introduction de capteurs de forces à faible coût dans tous les véhicules ce qui permettra la mise en oeuvre de nouveaux algorithmes comme ceux présentés dans cette

SUMMARY

thèse.

Un problème particulièrement important en contrôle de la dynamique du véhicule est de retirer la plus grande force de freinage possible du pneu tout en maintenant la stabilité latérale. Cette thèse contribue au développement et à la validation expérimentale de systèmes de freinage anti-blocage (Anti-lock Braking System - ABS). A la suite d'une collaboration avec le FNRS/Supélec, Paris, France, un ABS hybride théorique basé sur la décélération des roues a été amélioré pour supporter un retard dans l'actionnement du frein et un nouveau régulateur de taux de glissement des roues basé sur une approche en cascade a été mis en oeuvre. De plus, il est montré que de nouveaux algorithmes utilisant la mesure des forces du pneu peuvent être plus simples à régler, meilleurs et plus robustes aux conditions de route par rapport aux alternatives basées sur l'accélération. Le premier algorithme ABS qui considère directement la réduction du potentiel du pneu à produire des forces latérales à cause du freinage est un accomplissement de cette thèse. Tous les algorithmes ayant trait au freinage en ligne droite ont été validés sur le banc d'essais "tyre-in-the-loop" qui a été adapté pendant cette thèse pour permettre des tests ABS.

Curriculum Vitae

Mathieu Gerard was born in Gosselies, Belgium, in 1983. He studied electrical engineering at the University of Liege, Belgium, and received his master degree Summa Cum Laude in 2006. During his studies, he spent one year in the department of Automatic Control of Lund University, Sweden, in the framework of the exchange program Erasmus. His master thesis topic was tyre-road friction estimation and he was advised by Prof.dr. Anders Rantzer and dr. Brad Schofield.

Between 2006 and 2010, Mathieu Gerard worked on his PhD project at Delft Center for Systems and Control, Delft University of Technology, The Netherlands. His PhD research was about global chassis control and braking control using tyre forces measurement, and was performed under the supervision of Prof.dr.ir. Michel Verhaegen. During his PhD project, Mathieu Gerard obtained the DISC certificate for fulfilling the course program requirements of the Dutch Institute for Systems and Control, and supervised a number of M.Sc. and B.Sc. students.

In 2009, Mathieu Gerard started developing mobile applications to bring conference programs into mobile phones, and co-founded Conference Compass together with dr. Jelmer van Ast. He is now Managing Director at Conference Compass B.V.

